La mer 45 : 1–13, 2007
Société franco-japonaise d'océanographie, Tokyo

Recent change in water temperature and its effect on fisheries catch of bottom gillnets in a coastal region of the Tsushima Warm Current

Aida SARTIMBUL[1], Hideaki NAKATA[2] and Ikuo HAYASHI[3]

Abstract: Effect of water temperature change in the recent decade on coastal fisheries in the Tsushima Warm Current region is discussed using monitoring data on the water temperature and fisheries catch of bottom gillnets from 1995–2005 near the Awashima Island, Niigata. Interannual change in water temperature at Awashima showed significant negative correlation with the Pacific Decadal Oscillation (PDO) index, indicating that even coastal water temperature is under the strong influence of climate events. The dominant species in the catch of bottom gillnets has changed in response to water temperature. Turban shell (*Turbo cornutus*) was most dominant in 1995–1998 and then rapidly declined responding to temperature increase, while yellowtail (*Seriola quinqueradiata*) dominated in warm years (1998–2001), followed by cod (*Gadidae* spp.) in 2001–2005. Further, flounder (*Paralichthys olivaceus*) preferred colder years as opposite to the yellowtail. It should be noted that a regime shift accompanied with ENSO in 1997/1998 could have large effect on the catch composition. The recent decline of the turban shell is closely connected with decrease of larger-sized individuals in the regional population. Reduced food availability and intensified wave due to increased winter wind could be the critical causes for this decline.

Keywords: *fisheries catch, Tsushima Warm Current region, turban shell, water temperature*

1. Introduction

Long-term change in water temperature of the Japan Sea has apparently affected the distribution and abundance of fisheries resources, including Pacific saury, chub mackerel and other small pelagic fishes (ZHANG *et al.*, 2000 ; HIYAMA *et al.*, 2002 ; TIAN *et al.*, 2004, for example). Many studies have demonstrated the relationship between climatic change and fluctuations in fisheries catch in recent decades as well ; however its relation to coastal fisheries has not been well understood partly due to high variability and lack of the monitoring data with good quality. During 1990s, it is known that ENSO occurred in 1997/1998 and possibly gave much effect on marine organisms all over the world, even in the Japan Sea (CHIBA *et al.*, 2003), while it is also reported that there could be a regime shift around 1998 in the North Pacific (MINOBE, 2002 ; TIAN *et al.*, 2004). The dynamics of water temperature and fisheries production in the coastal region of Tsushima Warm Current may have been connected with such climate events on both decadal and interdecadal scales. In addition, recent warming in this region may also give a serious effect on the fisheries production in near future (TIAN *et al.*, 2004 ; DRINKWATER, 2005).

In this paper, we discuss the effect of water temperature change, possibly due to the above

1 Graduate School of Science and Technology, Nagasaki University, 1–14 Bunkyo-machi, Nagasaki 852–8521, Japan.
2 Faculty of Fisheries, Nagasaki University, 1–14 Bunkyo-machi, Nagasaki 852–8521, Japan.
3 Japan Sea National Fisheries Research Institute, 1–5939–22 Suido-cho, Niigata 951–8121, Japan.
Corresponding author : Hideaki Nakata
Tel : 81–95–819–2816 Fax : 81–95–819–2799
E-mail : nakata@nagasaki-u.ac.jp

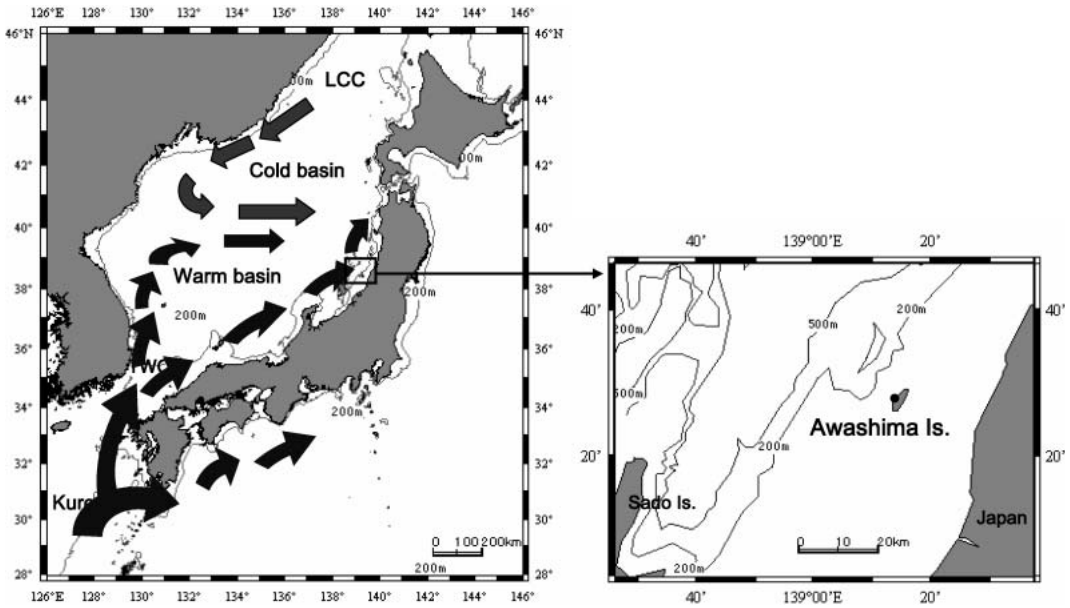

Fig. 1. The study area. Awashima Island (38°28′24.00″N and 139°14′12.23″E) is located in the coastal region of the Tsushima Warm Current (TWC).

climate events in the recent decade, on coastal fisheries in the Tsushima Warm Current region, using the data from continuous monitoring of water temperature and bottom gillnet catches at a coastal region (near Awashima Island, see Fig. 1) from 1995 to 2005. The Tsushima Warm Current (TWC) flows from south-west to north-east along the coast of the Japan Sea, and together with Liman Cold Current (LCC), TWC divides the Japan Sea into warm and cold basins with the boundary around 40° N (Senjyu, 1999). The area of this study, Awashima Island (38° 29'24.00"N and 139° 14'12.23"E), is located along the TWC path and just south of the above boundary (Fig. 1). The main objectives of this study are : (1) to identify water temperature variability in the coastal TWC region and its linkage to climate change on a larger scale ; and (2) to examine the possible effect of water temperature change on coastal gillnet fisheries, focusing on the climate event such as a regime shift in 1997/1998 accompanied by ENSO. The possible reason of recent decline of turban shell (*Turbo cornutus*), one of the dominant species for the bottom gillnet fisheries at the Awashima Island is also discussed in detail.

2. Data and Methods

We installed a set of automatic water temperature recorder, RTM–500 (Rigo Co. Ltd., Japan) on a rocky shore (about 6–7 m deep) near the Awashima Island from June 1995 to June 2005. This recorder is able to store about 65000 water temperature data covering the range between −5 to 45° C with resolution of 0.01° C and accuracy of ±0.05° C. In order to avoid over storage, the recorder was reset in every about 12 months. From the original 10 min interval data, we used ten-day and monthly means of water temperature data in this study. In addition, the Pacific Decadal Oscillation (PDO) index was used for the analysis to clarify the possible response of coastal water temperature in the TWC region to climate change. The PDO index is defined as the time coefficient of the leading EOF created from monthly Sea Surface Temperature (SST) anomalies pole-ward of 20° N in the Pacific bas in ; positive (negative) PDO indices represent the cooling (warming) phase in the central North Pacific (MANTUA and HARE, 2002). Monthly value of climatic indices (PDO) was provided by Climatic Prediction Center of NOAA for 1995 to 2005.

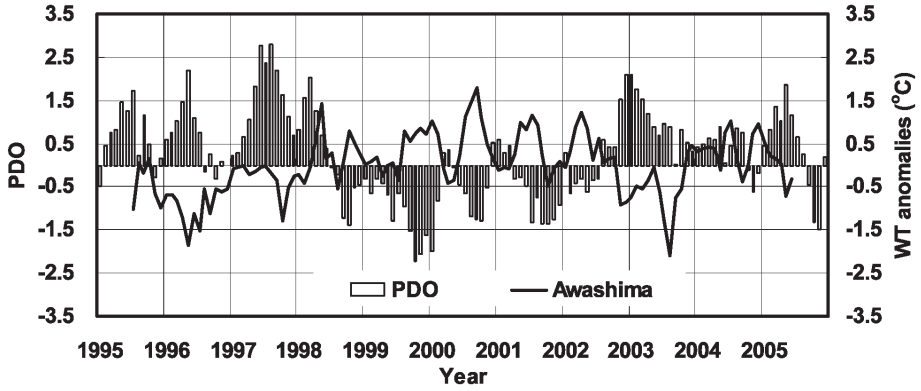

Fig. 2. Time series of water temperature anomalies at the Awashima Island (solid line) and Pacific Decadal Oscillation (PDO) index (bar).

Together with temperature data, catch data from bottom gillnet fisheries (with mesh size of about 120 mm), which has been conducted almost all year around near the Awashima Island, were collected from logbooks of fishermen of the Awashima-ura Fisheries Cooperative within the period of 1995 to 2005. As a biological time-series, these data are believed to be more reliable than other fisheries in terms of rather stable fishing efforts at mostly fixed sites. For our interest, the monthly catch data were used in this study.

Further, in order to investigate the possible factors affecting the catch of turban shell, one of the dominant species of the bottom gillnet fisheries, we analyzed annual monitoring data on the density and shell size of turban shell individuals at a wave-exposed rocky shore at the northwestern side of the Awashima Island (near the location of temperature measurement), based on the routine sampling of the areas of 42–100 m^2 at the beginning of fishing season (every June) from 1993–2006. The catch data of seaweed fisheries (from 1995–2005) at the Awashima Island were also used for the discussion, together with a time-series of winter wind (from 1995–2005) at Awashima collected from the Japan Meteorological Agency.

3. Results

Temperature variation

Figure 2 shows time series of water temperature anomalies at the Awashima Island for eleven-years (1995–2005), together with the Pacific Decadal Oscillation (PDO) index. The increase in water temperature for all the period was about 0.6℃, however prominent warming started from 1998. It is also noticeable that the change in water temperature at the Awashima Island corresponds well with the PDO indices ; positive (negative) PDO indicates the cooling (warming) event. From the time series, a regime shift between cooling (1996/1997) and warming (late 1998- early 2002) regime was detected, while another shift possibly occurred in 2002/2003 with a shorter period (one year) of cooling, followed by warming in 2004–2005. However 2004–2005 warming may not be supported by PDO indices. There is negative significant correlation between PDO indices and water temperature anomalies at the Awashima Islands ($r = -0.552$, $p < 0.001$) (Fig. 3).

Fisheries catch and its composition

Year to year change in the total catch of bottom gillnet fisheries near the Awashima Island is shown in Fig. 4 (a). The fisheries yields of about 40 tons were recorded except for 1999, 2001, and 2005 showing about twofold of the other years. The catch composition of bottom gillnet fisheries, as shown in Fig.4 (b), is dominated by migrating pelagic species such as yellowtail (*Seriola quinqueradiata*) and demersal species such as cod (*Gadidae* spp., mainly Pacific cod), coastal water species such as flounder (*Paralichthys olivaceus*) and red seabream (*Pagrus major*), and non-migrating shellfishes including turban shell (*Turbo cornutus*).

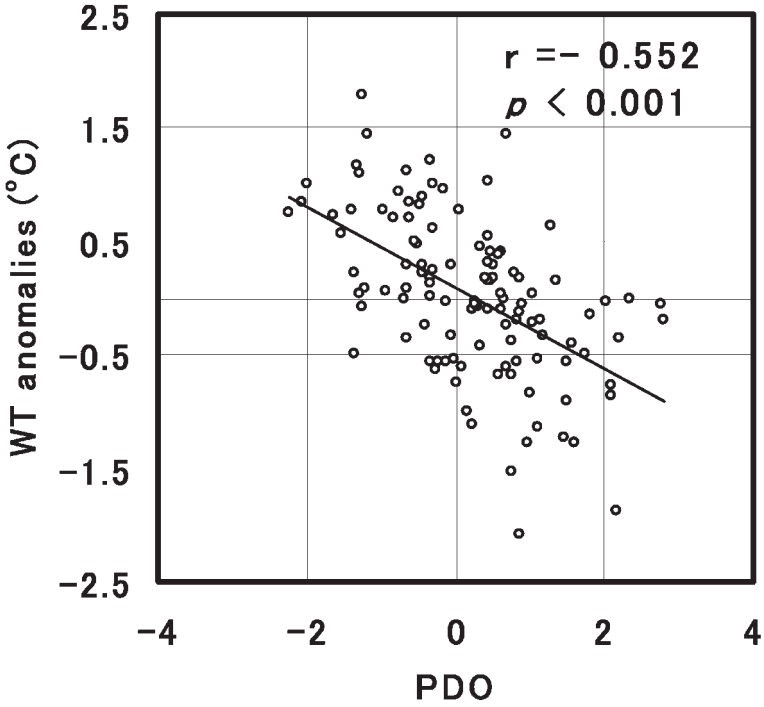

Fig. 3. Correlation between Pacific Decadal Oscillation (PDO) indices and water temperature anomalies at the Awashima Island.

From the time series, turban shell was most dominant in 1995–1998, while yellowtail in 1998–2001, followed by cod in 2001–2005. Furthermore, flounder and red seabream also contributed to the catch amount although the percentage was relatively small.

According to the Awashima-ura Fisheries Cooperative, catch data of turban shell in earlier years actually included catch yields by public diving at the opening of fishing period. However, this ceremonial catch event ceased in recent years due to rapid decline in the amount ; this is an additional evidence of abundance decline in the turban shell.

Relation between temperature variation and fisheries catch

The time changes of water temperature anomalies and fisheries yields of dominant four species (turban shell, cod, yellowtail and flounder) are demonstrated on the monthly basis in Fig. 5a-e. The catch yields of turban shell (*T. cornutus*) and cod (*Gadidae* spp.) show decreasing and increasing trends, respectively, for 11 years (Fig. 5b-c). These trends may be related in some way with warming of water temperature after a regime shift in 1997/1998 (see Fig. 2). In fact, significant negative correlation ($r = -0.706$, $p < 0.05$) between the water temperature anomalies and the catch of turban shell was obtained from cross-correlation analysis with a lag of 6 months.

On the other hand, there are more direct responses of fisheries catch to water temperature for yellowtail (*S. quinqueradiata*) and flounder (*P. olivaceus*) in an opposite way ; warm years seems favorable (unfavorable) for yellowtail (flounder) (Fig. 5d-e).

Monitoring of the density and shell size composition of turban shell

The catch yields of turban shell were high during 1995–1996 with negative anomalies of water temperature, and rapidly decreased to the lowest level in 2004–2005 without any sign of the recovery. Figure 6 demonstrates density (a) and size ratio of large (over 60 mm in shell height) and small (under 60 mm in shell

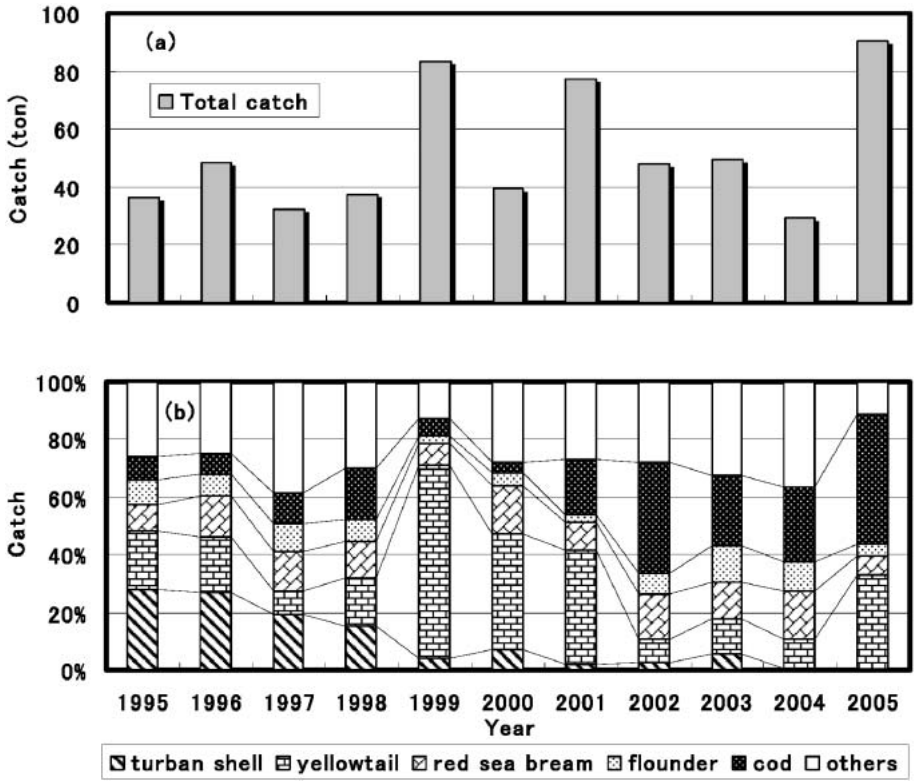

Fig. 4. (a) Interannual change in the total catch of bottom gillnet fisheries near the Awashima Island. (b) Interannual change in the catch composition of the bottom gillnet fisheries, including five dominant species : turban shell, yellowtail, red seabream, flounder, and cod.

height) individuals (b) of the turban shell, based on annual monitoring data from a rocky shore habitat of the Awashima Island in 1993–2006. It should be noted that small-sized turban shell showed remarkable increase in density, with average 3.7 individuals/ m^2 in 1998 to 2006, while large-sized one continuously decreased from about 1 individual/ m^2 in 1993–1995 to lowest levels in recent years (Fig. 6a).

The replacement of the large-sized individuals by the small-sized ones in a regional population is obvious in the time change of size composition (Fig. 6b). Since the target of the gillnet fisheries at the Awashima Island is large-sized individuals, the above change in the size composition is most critical to the fisheries yield as shown by significant negative correlations of turban shell catch with density (Fig. 7a) and size ratio (Fig. 7b) of small-sized individuals.

4. Discussion

Responses of fisheries catch to water temperature change

Figure 8 shows the standardized index of water temperature and fisheries catches of yellowtail, flounder, cod, and turban shell. All data were standardized using the formula, $(x_i - x)/sd$, where x_i denotes the original data for variable (i), and x and sd the mean and standard deviation, respectively. The catch index of turban shell starts to decline from 1997 and shows negative values after 1999. In contrast, cod shows an increasing trend with positive values after 2001. Furthermore, the catch index of yellowtail is positive during warm years (1999–2001), while that of flounder is negative during the same period.

As previously reported, regime shifts of oceanic conditions occurred in 1997/1998 (BEAMISH *et al.*, 2004 ; CHIBA *et al*, 2003) and 2002/2003

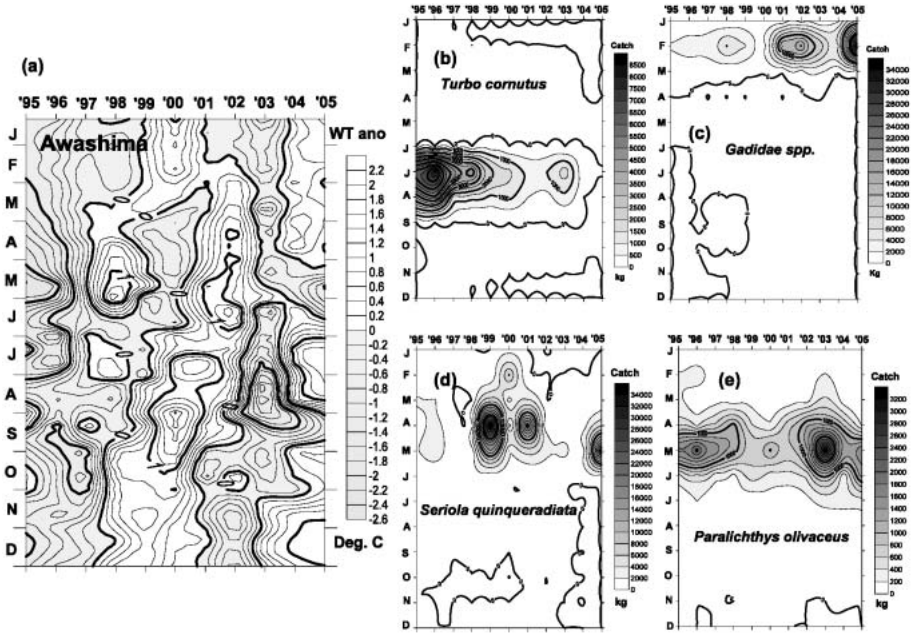

Fig. 5. Time changes of water temperature anomalies (a) and catches of dominant species (b-e) at the Awashima Island on the monthly basis.

(PICES, 2004 ; JMA, 2004). Besides the regime shifts, it is also well known that ENSO occurred in 1997/1998 (CHIBA *et al*, 2003 ; TIAN *et al*., 2004). At Awashima, the regime shift 1997/1998 could be defined as a major shift of water temperature from cold years with positive PDO to warm years with negative PDO, followed by a great change of fisheries catch as mentioned above.

From Fig. 8, we may conclude that the responses of coastal fisheries catch to water temperature change into two categories : (1) responses to warm-cold temperature change on the inter-annual scale due to El Nino-La Nina cycles, for example ; e.g. temporary shift of yellowtail and flounder catches, and (2) responses to longer-term temperature changes derived from regime shifts and/or warming trends on the inter-decadal scale ; e.g. vanishing of turban shell and increasing cod abundance in recent years.

As warm water species, yellowtail may favor warm water masses and migrate to the north in the Japan Sea. HARA (1990 a, b) reported that residence time and the period of fishery formation of yellowtail increases with warm water masses spreading into the Japan Sea coast. Furthermore during warm El Nino years like 1998, followed by a regime shift to the warm and negative PDO phase from late 1998, there was overall increase in the catch of yellowtail in the Japan Sea (TAMEISHI *et al.* ; 2005). This suggests that increased catch of yellowtail at Awashima may be caused by northward spread of yellowtail to and its prolonged residence time in the Japan Sea, following the water temperature increase due to the regime shift and ENSO in 1997/1998. However, flounder has negative response to the water temperature increase ; there is high and low catches of flounder during warm years (1999 to 2001) and cold years (before 1998 and after 2002), respectively. There has been however very little detailed information concerning temperature effect on this fish.

It is reported that Pacific cod are distributed over a wide range from North Pacific to the Japan Sea, and as a demersal cold water species, it is suggested that cold temperature regime is favorable for productivity and recruitment of Pacific cod (PFMC, 1998 ; BEAMISH *et al.*, 2004). In fact, northward shift of the Pacific

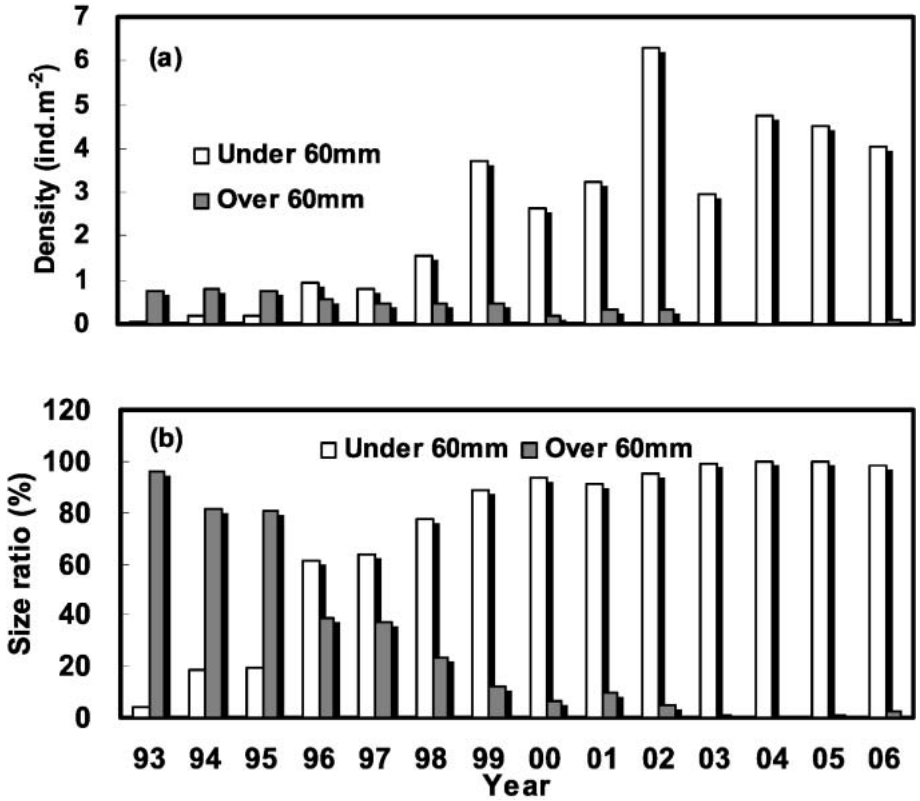

Fig. 6. (a) Interannual change in the density of turban shell (*Turbo cornutus*) at the rocky shore habitat of Awashima Island during 1993–2006. (b) Interannual change in the fraction of small-sized turban shell (under 60 mm in shell height) and large-sized one (over 60 mm in shell height).

cod distribution responding to recent warming was actually suggested in the Japan Sea, from more apparent decreasing catch yields in the southwestern Japan Sea compared to those in the north (Ishiko, unpublished data). Therefore, the reason of increase in cod catch at Awashima during warm years has remained unknown. Though the catch yields of the middle of Japan Sea including Niigata Prefecture have not yet showed any decline, relatively low temperature in the coastal regions (9.7 to 11.1 ℃ at Awashima in the period of cod fishing) could cause a spatial shift of cod distribution toward the coast, resulting in increase of cod abundance near the Awashima Island during recent warm years.

Possible factors affecting recent decline in the fisheries catch of turban shell

Remarkable decreasing of turban shell catches to the lowest level in recent years has insisted us to clarify the causal factors behind it. The first hypothesis for this incidence could be the change in food availability. It has been revealed that diets of turban shell collected from wave-exposed areas of Awashima Island are dominated by small seaweeds such as red algae (*Polysiphonia morrowii*) and brown algae (*Dictyota* spp.) (YAMAKAWA and HAYASHI, 2004). Since there was no available data on those prey biomass ; we collected the data for three types of seaweed catch, which could be a proxy of the prey biomass. The time series of seaweed catches, which are standardized in the same way as Fig. 8, is shown in Fig. 9a. It is noticeable that the period of decline of turban shell catch coincides with low seaweed catches at the Awashima Islands. The correlation between the standardized indices of the catch for turban shell and seaweeds (mean of the above

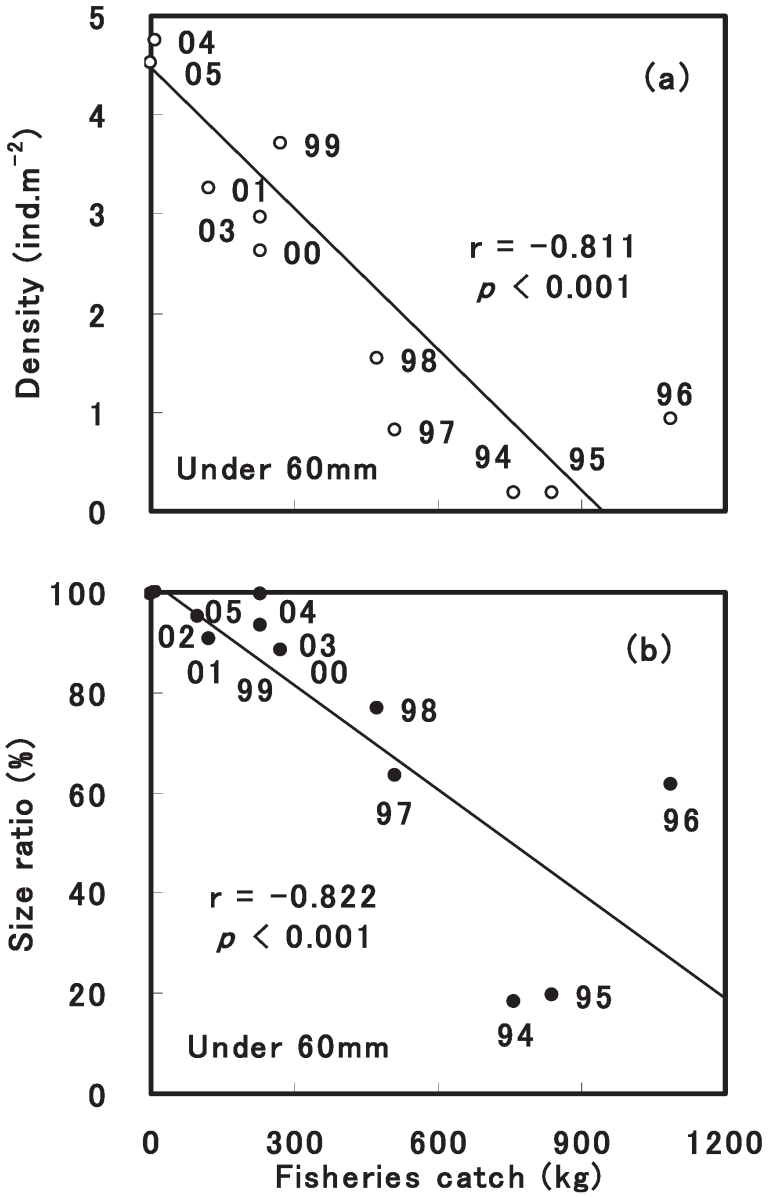

Fig. 7. Correlation of fisheries catches of turban shell with density of small-sized turban shell (a) and small-sized fraction of the turban shell (b) in the neighboring habitat.

three types of seaweed) is significant ($r = 0.739$, $p<0.01$) as seen in Fig. 9 (b). However, the above proxies are annual seaweeds and mostly grow in intertidal zones, therefore direct effect of the time change in the prey biomass on the growth of turban shell should be confirmed in another way in the future. In addition, it should be also noted that species composition of dominant seaweeds at the monitoring site has changed in recent years (HAYASHI, unpublished data) ; this suggests possible decline of food availability in the aspect of food quality.

On the other hand, increase in water temperature may lead to enhance the reproduction. In fact, density of small-sized turban shell

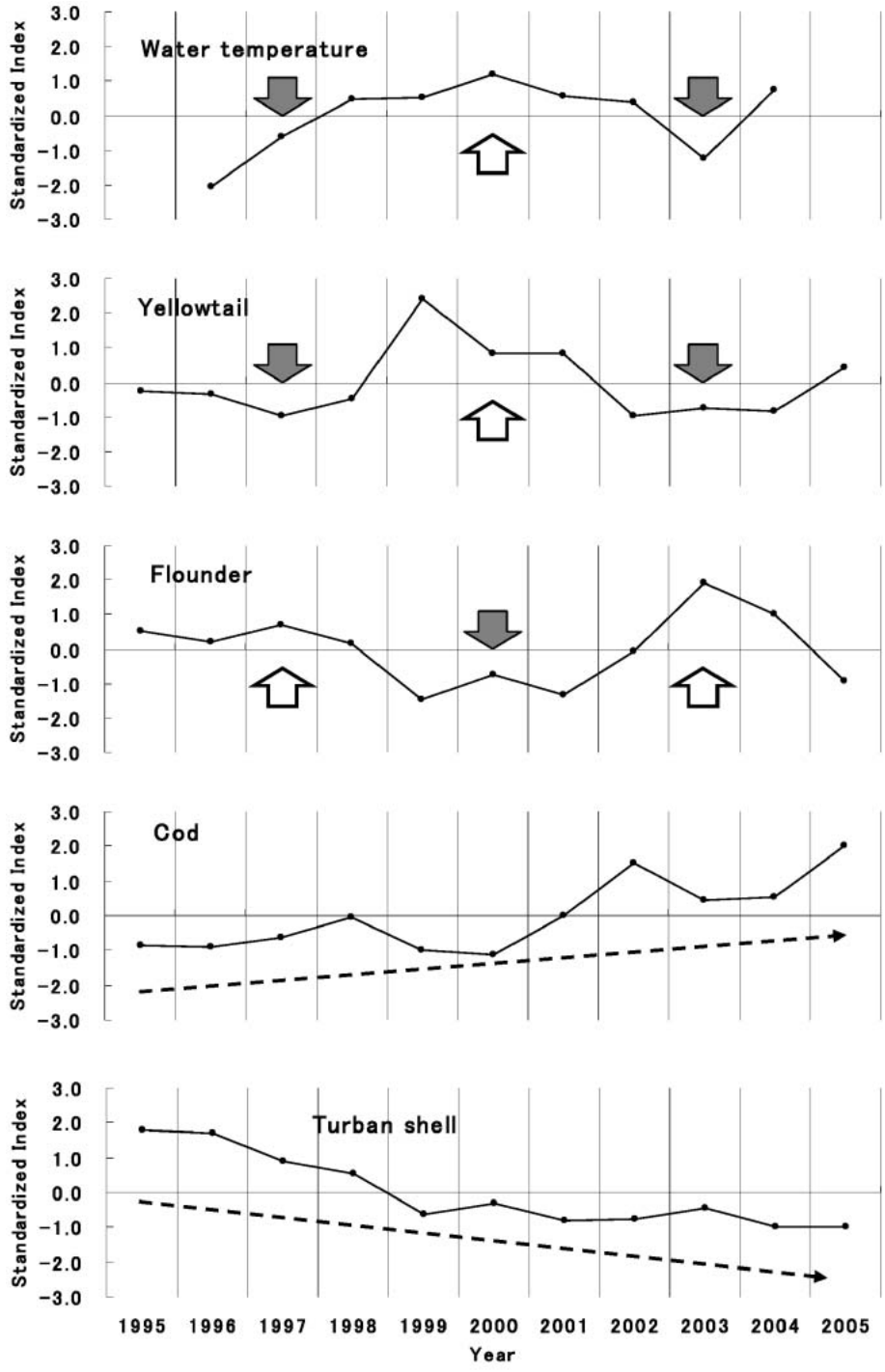

Fig. 8. Interannual change in standardized index of water temperature and fisheries catches of yellowtail, flounder, cod, and turban shell at the Awashima Island during 1995–2005. For the standardized index, see the text.

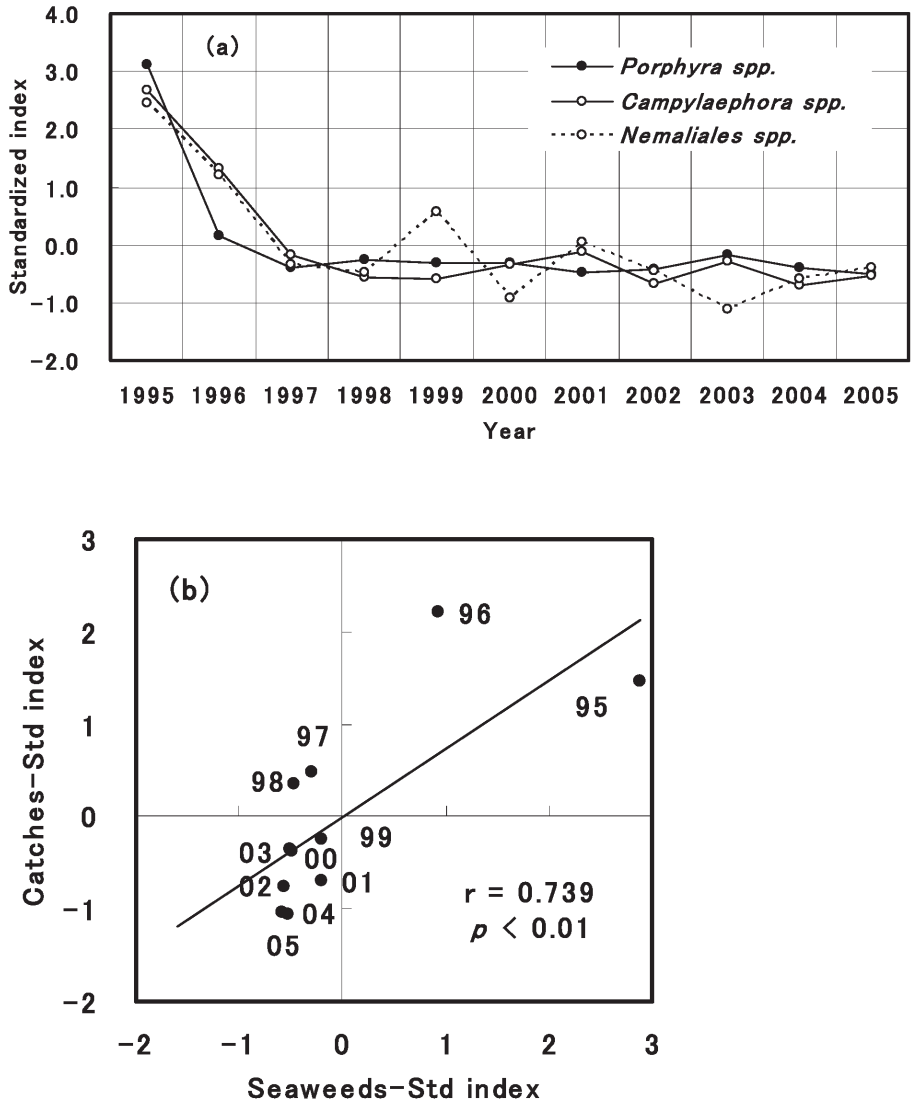

Fig. 9 (a) Interannual change in the fisheries production of seaweeds, represented by iwanori (*Porphyra* spp.), egonori (*Campylaephora* spp.) and umizomen (*Nemaliales* spp.) at the Awashima Island. The amount of production is represented by the standardized index in the same way as Fig. 8. (b) Correlation between seaweed production (mean of the above three types of seaweeds) and catch of turban shell at the Awashima Island during 1995–2005.

individuals increased to over 2 ind./m^2 after 1999 (Fig.6a). Further as seen in Fig. 7, increase in the density and ratio of small-sized turban shell (mostly the age of 2–4 years) well corresponds to the decline in the fisheries catch of commercial size turban shell (over 60 mm in shell height with the age of more than 4 years).

In addition to decline in seaweed production (Fig. 9a), density effect due to the increase in the number of small individuals may also contribute to enhance the competition among this species, resulting in further decrease in the abundance of large-sized individuals. More detailed quantitative investigation on the feeding and growth of the turban shell population in this region is necessary.

Another possible hypothesis could be physical effect of strong wind in winter when

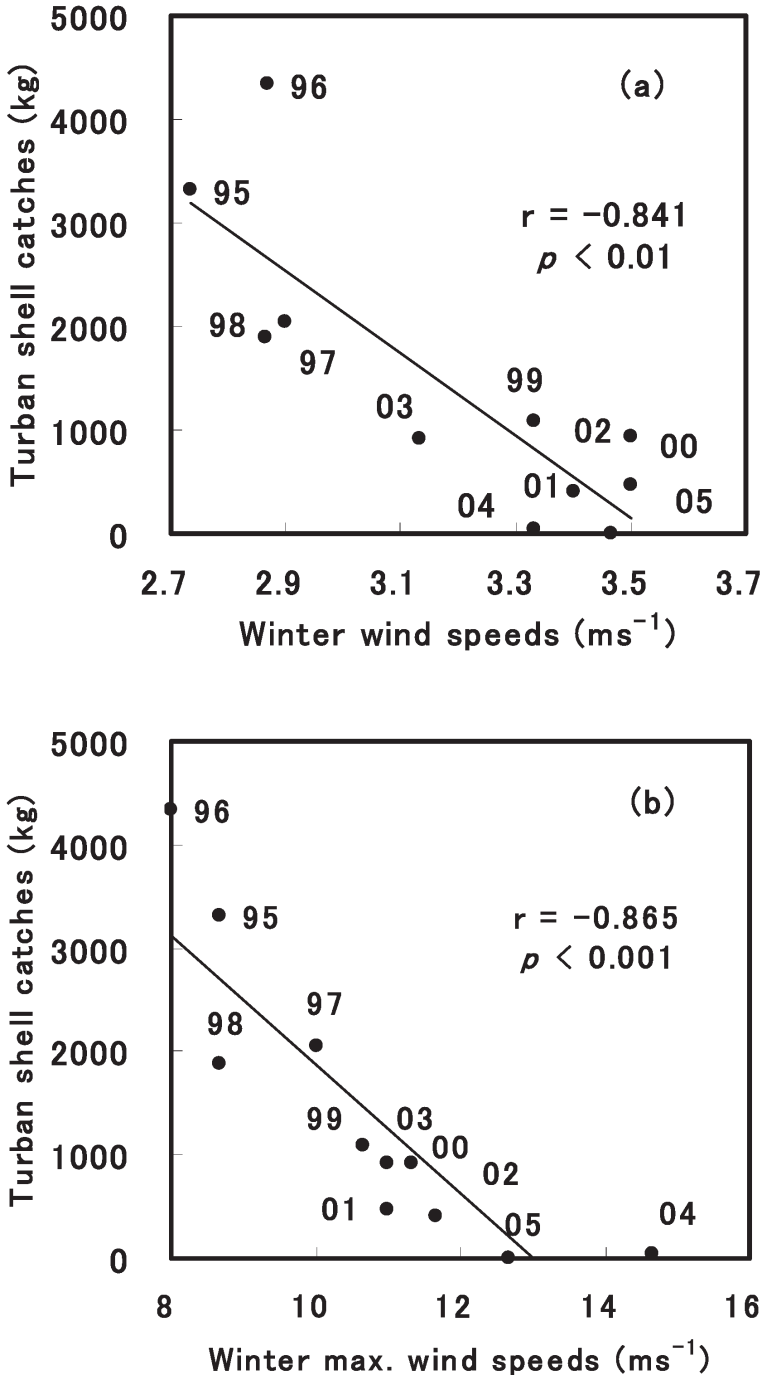

Fig. 10. Correlation of fisheries catches of turban shell with mean wind speed in winter (a) and with maximum wind speed in winter (b) at Awashima during 1995–2005.

adhesion ability of turban shell becomes weaker. Since the monitoring site of the turban shell was a wave-exposed rocky shore under the strong influence of prevailing wind in winter, strong waves generated by the strong wind may intrude the habitat of turban shell and then do damage to large-sized turban shell by washing them away from the suitable habitat, resulting in density decline in large-sized turban shell. The above statement is strengthened by the fact that there is different behavior between small and large-sized turban shell. Most of small-sized individuals tend to be hidden in the small holes and crevices among rocks to avoid from any disturbances, while large ones are on the surface of the rock where there is no place to hide away from wave action (HAYASHI, unpublished data).

Recent warming after the regime shift of 1997/1998 in the Japan Sea could have triggered high atmospheric pressure gradients between the Siberian High and the Aleutian Low, and then followed by the stronger winter wind. This hypothesis is supported by significant negative correlations between average wind speed in winter and turban shell catch ($r = -0.841$, $p < 0.01$) (Fig.10 a), and between winter maximum wind speed and turban shell catch ($r = -0.865$, $p < 0.001$) (Fig. 10 b).

In summary, our analysis suggested that water temperature change modified by climate events such as a regime shift and ENSO in 1997/1998 have remarkable effect on the coastal fisheries catch in the TWC region in the recent decade. Although the geographic location of Awashima Island, the main area of this study, could be unique as described in Fig. 1, the findings of this study strongly suggest that water temperature and associated climate events can be used as an indicator for prediction of coastal fisheries along the Tsushima Warm Current region.

Acknowledgments

We are grateful to the Awashima-ura Fisheries Cooperative for providing the valuable data of fisheries catch to this study. This study was partly supported by Global Environment Research Coordination System of the Ministry of the Environment Japan (No. 47–16).

References

BEAMISH, R.J., A.J. BENSON, R.M. SWEETING, and C.M. NEVILLE (2004) : Regimes and the history of the major fisheries off Canada's west coast. Progress in Oceanography, **60**, 355–385.

CHIBA, S. and T. SAINO (2003) : Variation in mezoplankton community structure in the Japan/East Sea (1991–1999) with possible influence of the ENSO scale climatic variability. Progress in Oceanography, **57**, 317–339.

DRINKWATER, K.F. (2005) : The response of Atlantic cod (*Gadus morhua*) to future climate change. ICES Journal of Marine Science, **62**, 1327–1337.

HARA (1990a) : An abundance index of yellowtail immigrating into the Sea of Japan and its yearly variation. Nippon Suisan Gakkaishi, **56**, 19–24 (in Japanese).

HARA (1990b) : Yearly fluctuations of yellowtail catch in set net fishery along the coastal area of the Sea of Japan. Nippon Suisan Gakkaishi, **56**, 25–30 (in Japanese).

HIYAMA, Y., M. YODA, S. OHSHIMO (2002) : Stock size fluctuations in chub mackerel (*Scomber japonicus*) in the East China Sea and Japan/East Sea. Fisheries Oceanography, **11** (**6**) , 347–353

Japan Meteorological Agency (2004) : Global climate change report. Available at http : //www.jma.go.jp/jma/indexe.html

MANTUA, N.J. and S.R. HARE (2002) : The Pacific Decadal Oscillation. Journal of Oceanography, **58,** 35–44.

MINOBE, S. (2002) : Spatial-temporal structure of pentadecadal variability over the North Pacific. Progress in Oceanography, **47**, 381–408.

Pacific Fishery Management Council (1998) : Essential fish habitat : West coast ground EFH core team for west coast groundfish, 15 June. Available online at http : //www.nwr.noaa.gov/1sustfsh/efhappendix/page1.html.

PICES (2004) : PICES special publication on Marine ecosystems of the North Pacific. North Pacific Marine Science Organization c/o Institute of Ocean Sciences, Sydney, Canada, p. 280. Also available online at www.pices.int

SENJYU, T. (1999) : The Japan Sea intermediate water : Its characteristics and circulation. Journal of Oceanography, **55**, 111–122.

TAMEISHI, H., S. FUJII and A. MAEBAYASHI (2005) : Relationship between regime-shifts of SST and condition (Spanish mackerel and yellowtail) in Japan Sea. Bulletin on Coastal Oceanography, **42** (**2**) , 125–131 (in Japanese).

TIAN, Y., Y. UENO, M. SUDA and T. AKAMINE (2004) : Decadal variability in the abundance of Pacific saury and its response to climatic/oceanic regime

shifts in the northwestern subtropical Pacific during the last half century. Journal of Marine Systems, **53**, 235–257.

YAMAKAWA, H. and I. HAYASHI (2004) : Relation between food habits of Turban shell, *Turbo* (*Batillus*) *cornustus* and algal distribution on Awashima Island, Niigata, Japan. Suisanzoshoku, **52** (1), 57–63 (in Japanese).

ZHANG, C.I., J.B. LEE, S. KIM, and J-H. OH (2000) : Climatic regime shifts and their impacts on marine ecosystem and fisheries resources in Korean waters. Progress in Oceanography, **61**, 245–265.

Received December 18, 2006
Accepted February 14, 2007

La mer 45 : 15-22, 2007
Société franco-japonaise d'océanographie, Tokyo

Structure of the upper deep current in the Melanesian Basin, western North Pacific

Kanae KOMAKI* and Masaki KAWABE

Abstract: We used velocity and echo intensity data obtained from a lowered acoustic Doppler current profiler to clarify the structure of the upper deep current at depths of 2000–3500 m over the northeastern slope of the Solomon Rise in the Melanesian Basin, western North Pacific. This current separates from the Antarctic Circumpolar Current and flows northward, carrying oxygen–rich Upper Circumpolar Water. The current comprised western and eastern cores located over the bottom slope at water depths of approximately 3000 and 4000 m, respectively. Between the double cores of the current, a thick countercurrent was observed with a width of more than 100 km. The countercurrent flowed over the bottom slope at a water depth of approximately 3500 m and carried water that is characterized by extremely high echo intensity. These observations suggest that the equatorial eastward current observed at the southern boundary of the East Caroline Basin is steered by the bottom slope and connects to the countercurrent in the Melanesian Basin, carrying equatorial water with high echo intensity.

Keywords: *LADCP, upper deep current, Upper Circumpolar Water, western North Pacific*

1. Introduction

Within the deep layer in the Pacific Ocean at depths of 2000–3500 m, hereafter termed the upper deep layer, oxygen–rich water originating from Upper Circumpolar Water (UCPW) is carried by an anticyclonic gyre in the South Pacific after leaving the Antarctic Circumpolar Current (REID, 1997). The current in the upper deep layer, hereafter termed the upper deep current, flows along the 2500 m isobath in the equatorial South Pacific, passing through the northeastern slope of the Solomon Rise in the Melanesian Basin (KAWABE *et al.*, 2003). The upper deep current in the equatorial region is located on the onshore side of the deep western boundary current in the lower deep layer below 3500 m; the deep western boundary current carries Lower Circumpolar Water (LCPW) from the Antarctic. The upper deep current enters the Philippine Sea, forming several branch currents that flow into the East and West Caroline Basins and the West Mariana Basin. The transportation of UCPW leads to elevated oxygen levels in the Philippine Sea (KAWABE, 1993; KAWABE *et al.*, 2003).

KAWABE *et al.* (2006) used moored current meters at depths of 1880–3750 m at five mooring sites (ML1–ML5) to observe the velocity of the upper deep current within the Melanesian Basin from February 1999 to February 2000. The upper deep current was recorded at depths of approximately 2000–3500 m at ML1–ML3 (3°23′N, 159°30′E to 5°07′N, 160°52′E), with the largest magnitude recorded in the middle of this layer. They also found that the structure of the upper deep current has two states and that it changes sharply between them. In the state observed during the first half of the observation period, a strong countercurrent flows at ML1 and the upper deep current flows at ML2 and ML3. In the other state observed during the second half of the observation period, the upper deep current is especially strong at ML1 and flows at ML1–ML3.

Ocean Research Institute, The University of Tokyo
1–15–1 Minamidai, Nakano–ku, Tokyo 164–8639, Japan
* Corresponding author.
Tel: +81–3–5351–6420, Fax: +81–3–5351–6418
E–mail address: kanae@nenv.k.u-tokyo.ac.jp

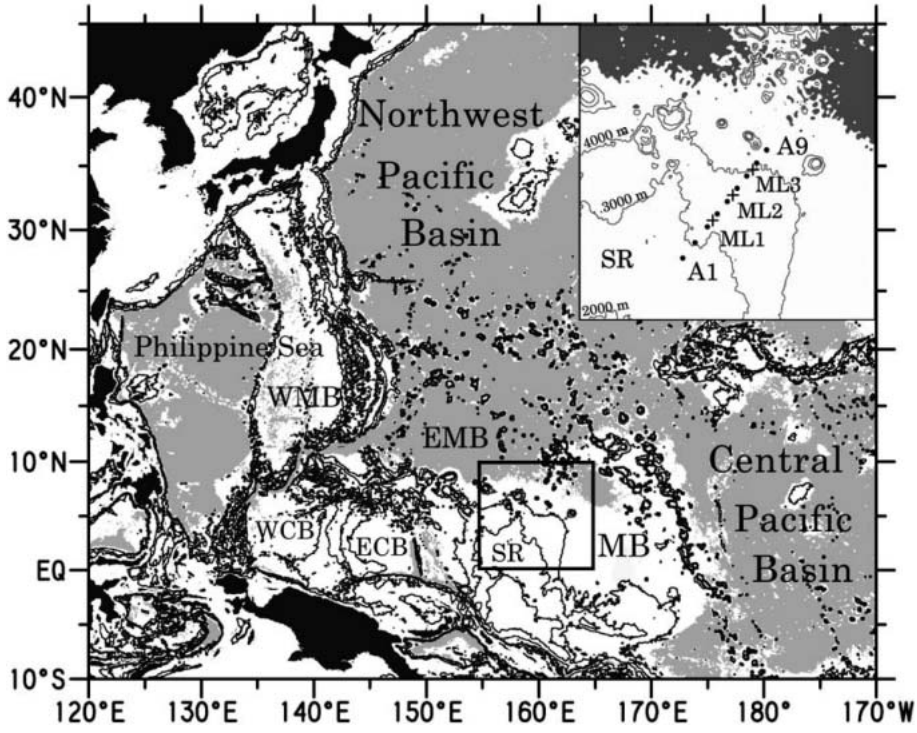

Fig. 1. Map of the western Pacific with an enlarged view (inset map; see the square on the main map for the location of the inset map) of LADCP stations A1–A9 (dots) and moorings ML1–ML3 (crosses) on the slope of the Solomon Rise within the Melanesian Basin. Contours are isobaths at 2000, 3000, and 4000 m. Shading represents areas at depths greater than 5000 m. MB, Melanesian Basin; SR, Solomon Rise; EMB, East Mariana Basin; WMB, West Mariana Basin; ECB, East Caroline Basin; WCB, West Caroline Basin.

On the basis of the distribution of dissolved oxygen and geostrophic velocity, they inferred that the upper deep current during the first half of the observation period extended to the west of ML1 and was divided into western and eastern cores by the countercurrent. This inference may be correct, but should be confirmed by direct measurement of current velocity, since oxygen data do not directly show a current, and geostrophic velocity includes an ambiguity from an assumption of a reference depth. For this purpose, velocity data from a lowered acoustic Doppler current profiler (LADCP) are suitable.

In the present paper, we confirm the double-core structure of the upper deep current in the Melanesian Basin and clarify the lateral extension of the current cores and the countercurrent by analyzing current velocity data obtained using an LADCP. Moreover, we discuss the origin of the countercurrent using data of echo intensity from LADCP, which reflects the amount of particulate scatterers and is expected to indicate the characteristics of water masses.

2. Observations and method

We used LADCP data obtained at nine stations, A1–A9, located between 2°05′N, 158°30′E and 5°46′N, 161°20′E within the Melanesian Basin (Fig. 1). The data were collected during the period 30 January-2 February 1999 on the R.V. *Hakuho Maru* KH–99–1 cruise using a 300-kHz LADCP manufactured by RD Instruments (RDI). Current velocity data obtained using the LADCP were processed following the method of Komaki and KAWABE (under review); that is, we fitted the LADCP velocity profile to current velocity at depths of 100–800 m measured using a 38-kHz RDI shipboard

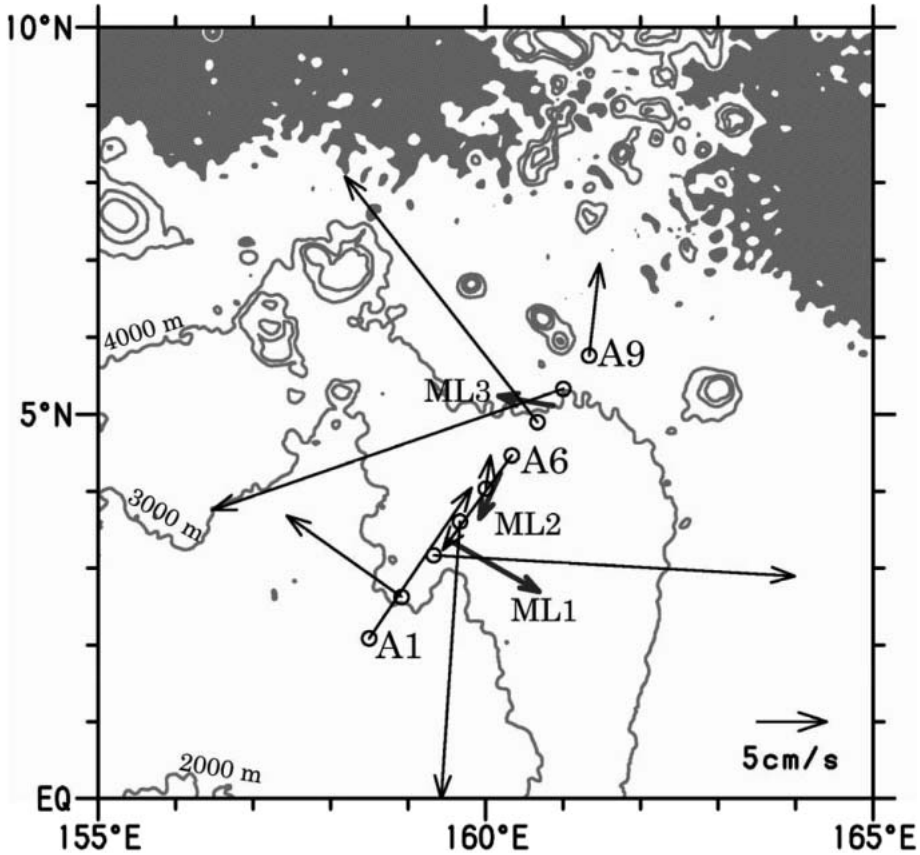

Fig. 2. Velocity vectors measured using LADCP at A1–A9 at depths of $\theta = 2.1$℃ (thin arrows) and current meters at depths of approximately 2000 m at ML1–ML3 averaged for the five-day period around the time of the LADCP observations (thick arrows). Contours are isobaths at 2000, 3000, and 4000 m. Shading represents areas at depths greater than 5000 m.

ADCP and to the bottom velocity estimated using sound pulses reflected from the sea bottom. Vertical shears of velocity were corrected to obtain a consistent profile of velocity using the fitted values. The barotropic tidal velocity estimated using the tide model of EGBERT *et al.* (1994) was removed from the processed LADCP velocity. We also used LADCP echo-intensity data reflected from the third bin (12 m below the instrument).

The upper deep current was observed at three moorings: ML1 (located between A3 and A4), ML2 (between A5 and A6), and ML3 (between A7 and A8) (KAWABE *et al.*, 2006). The velocity data obtained from three current meters stationed at depths of 2170 m (ML1), 2150 m (ML2), and 1880 m (ML3) were temporally averaged for the five-day period around the day of LADCP observations; these average values were then compared with LADCP velocity.

3. Vertical structure of the upper deep current

Figure 2 shows velocity vectors from LADCP on an isothermal surface of potential temperature, $\theta = 2.1$°C, which is close to the top of the upper deep layer at a depth of approximately 2000 m (KAWABE *et al.*, 2003). The current is eastward at A3, southward at A4, northward at A5, southwestward at A6, northwestward at A7, and southwestward at A8. The vector mean of LADCP velocity between pairs of stations is southeastward for A3 and A4, southwestward for A5 and A6, and westward for A7 and A8.

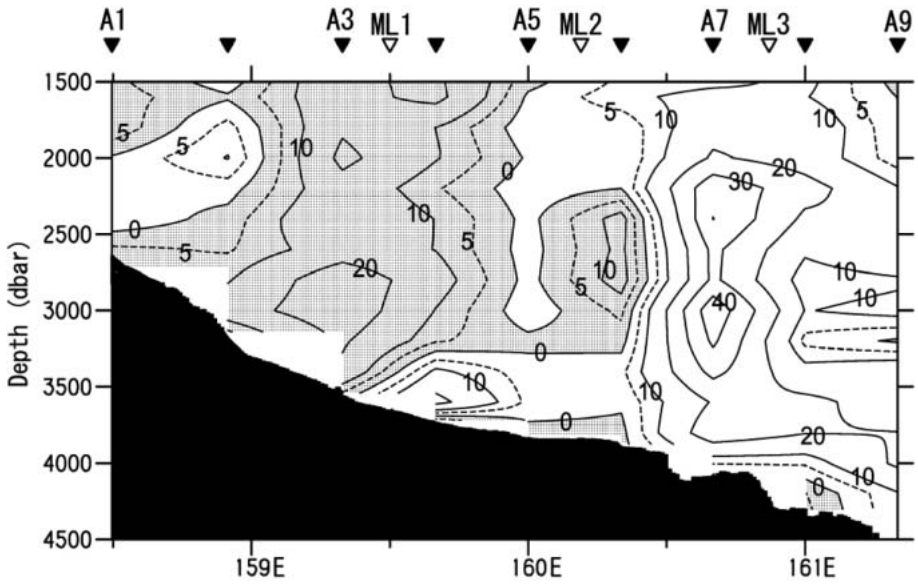

Fig. 3. Vertical sections of the velocity component (cm s^{-1}) perpendicular to the section measured at A1–A9 in the Melanesian Basin using LADCP. Shading represents a southeastward velocity. The barotropic tidal velocity estimated using the tide model of EGBERT (1994) was removed from the data. The LADCP stations are shown by solid triangles at the top of the panel. For reference, the mooring positions ML1–ML3 are shown by open triangles.

These current directions are similar to those measured using current meters at ML1, ML2 and ML3, respectively, although the amplitude of velocity is much larger. The southeastward current at ML1 and the westward current at ML3 are the countercurrent and the eastern core of the upper deep current, which continued for seven months during the first half of the mooring observation (KAWABE *et al.*, 2006). The northwestward current at A2 may represent the western core of the upper deep current inferred by KAWABE *et al.* (2006). These results demonstrate that the LADCP velocity data provide the correct direction of the velocity component perpendicular to the observation line.

The distribution of the perpendicular component of velocity (Fig. 3) indicates that the countercurrent has a great thickness at depths less than 3500 dbar and has a wide extent (159°–160°E), encompassing A3 and A4, with the maximum velocity of approximately 20 cm s^{-1} recorded at A3. The observed large vertical extent of the countercurrent is consistent with the results of mooring observations undertaken at ML1, as described by KAWABE *et al.* (2006). The width of the countercurrent spans more than two intervals between the LADCP stations, which is larger than that speculated by KAWABE *et al.* (2006). The amplitude of velocity exceeds 10 cm s^{-1} at every measurement depth and exceeds 20 cm s^{-1} at 2000 dbar and 2700–3200 dbar. These values may represent an overestimate, although such a strong current may be possible over short time periods.

West of the countercurrent, a northwestward current core exists at depths between 1600 and 2500 dbar at 158.5°–159°E (A1–A2), with a maximum velocity of 10 cm s^{-1} recorded at 2000 dbar at A2 (Fig. 3). This current likely represents the western core of the upper deep current. In contrast, the northwestward velocity at A7 represents the eastern core of the upper deep current. This may include a cyclonic eddy formed in combination with the countercurrent at A6. High velocities in excess of 30 cm s^{-1} within the eastern core may partly reflect this eddy. The cyclonic eddy (or the countercurrent at A6) was not present in the current–

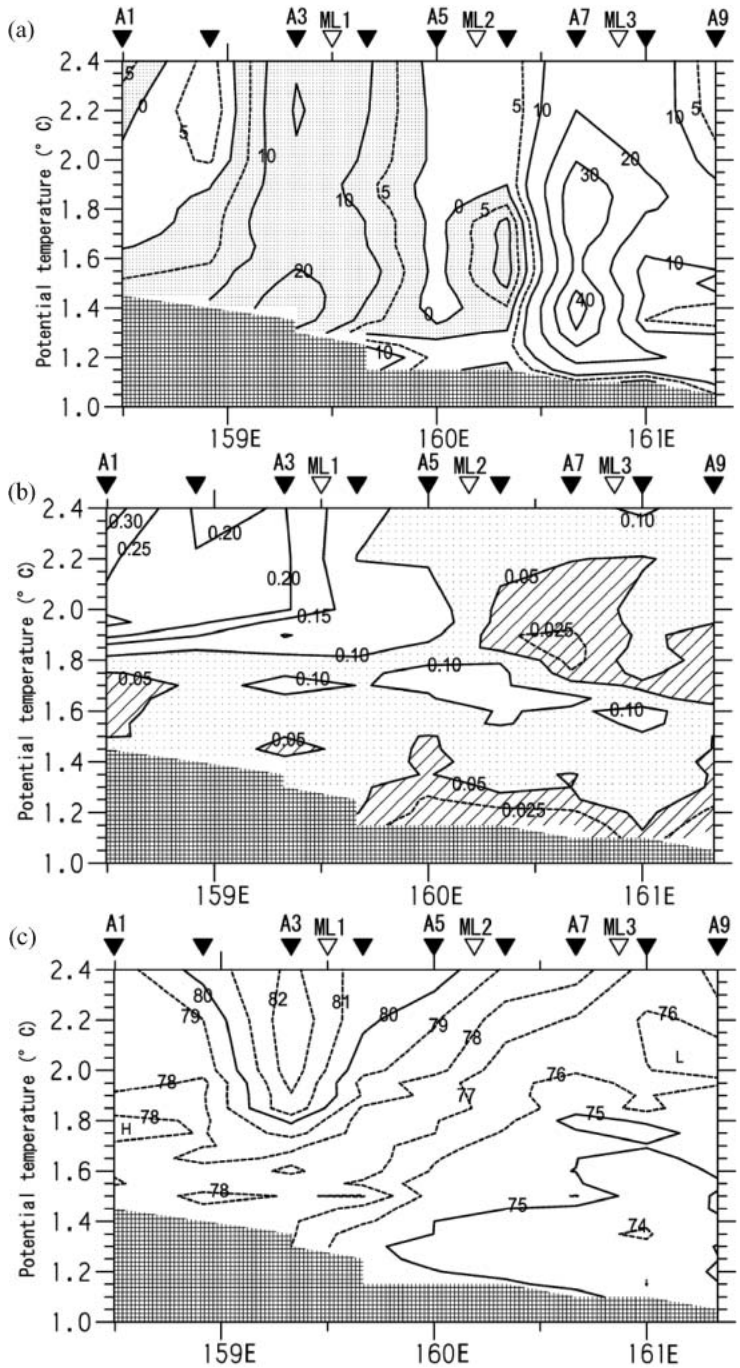

Fig. 4. Vertical sections at A1–A9 in the Melanesian Basin of the velocity component (cm s^{-1}) perpendicular to the section measured using LADCP (a), the anomaly on isotherms of dissolved oxygen (ml l^{-1}) derived from the average of values at A14–A17 (163.1°–164.3°E) as in KAWABE *et al.* (2003) (b), and echo intensity (dB) measured using LADCP (c). Potential temperature is taken as the ordinate. The hatched areas in the lower parts of (a) – (c) represent areas of no data due to the sea bottom. Shading in (a) indicates southeastward velocity. Areas of oblique lines and dotted areas in (b) indicate values of less than 0.05 and 0.10 ml l^{-1}, respectively.

meter results for the eastern core averaged during the first half of the mooring period; however, the current–meter data at 2650 m at ML2 show the countercurrent component around the time of the LADCP observation (KAWABE *et al.*, 2006). The structure of the eastern core of the upper deep current may be affected by the existence of an eddy (or small–scale countercurrent), but the location of the core is largely unaltered.

4. Characteristics of water carried by the deep currents

The western core of the upper deep current carries oxygen–rich water. This is especially pronounced in the upper part of the core above the 1.9°C isotherm, which has a large dissolved –oxygen anomaly of more than 0.20 ml l^{-1}, as determined from the averages at A14–A17 located at 8.0°–9.7°N, 163.1°–164.3°E in a small deep valley farther northeast of A9 (Fig. 4). The oxygen anomaly extends to A3, the center of the countercurrent, at depths shallower than the 1.9°C isotherm. The oxygen anomaly decreases markedly in the eastern part of the countercurrent to the east of A3. In the eastern core of the upper deep current, the anomaly is still positive but is relatively weak, occupying the upper part of the core. The oxygen anomaly in the lower part (below the 1.8°C isotherm) is almost uniformly weak in the western and eastern cores of the upper deep current and the intervening countercurrent.

Echo intensity is relatively strong in the upper part (above the 1.8°C isotherm) of the countercurrent, with the maximum intensity recorded at the center of the countercurrent. The intensity in the upper part of the countercurrent is much higher than that in the western and eastern cores of the upper deep current, being much higher than that in the eastern core. The highest echo intensity in the countercurrent and lowest in the eastern core are also seen in the lower part of the upper deep layer, although they are less pronounced than those in the upper part.

Thus, the differences in water–mass characteristics between the different currents are especially marked in the upper part of the currents (Fig. 5). The countercurrent contains

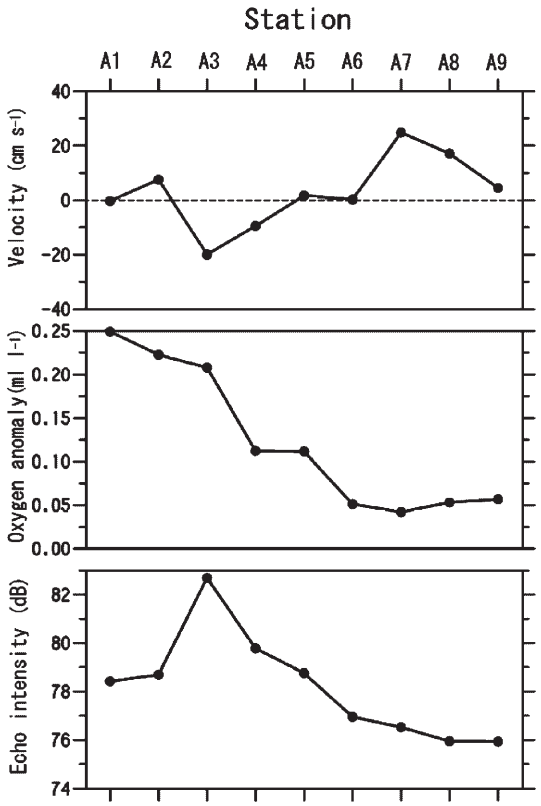

Fig. 5. Lateral distributions on an isotherm of θ = 2.1℃ at A1–A9 in the Melanesian Basin of current velocity perpendicular to the observation section measured using LADCP (upper panel), the anomaly of dissolved oxygen from A14–A17 (middle panel), and echo intensity measured using LADCP (lower panel).

an intermediate oxygen anomaly between the eastern and western cores of the upper deep current. This suggests that the countercurrent carries a mixture of the UCPW carried by the two cores of the upper deep current; however, echo intensity in the countercurrent is much higher than that in the cores. This indicates that the countercurrent carries the upstream water, which is characterized by high echo intensity. If the countercurrent flows into the Melanesian Basin by proceeding along the 3000 or 3500 m isobaths, then the countercurrent in the upstream region must flow eastward along the southern boundary of the East and West Caroline Basins near the equator, carrying water with high echo intensity peculiar to the near–equator region. During eastward

transportation, the water mixes with high–oxygen UCPW carried by the upper deep current.

FIRING *et al.* (1998) observed an eastward deep current at depths of 2000–3500 m at 0–1°S, 150°E on the southern boundary of the East Caroline Basin in August 1985 and January 1986. This eastward current may be steered into the Melanesian Basin by the bottom slope at a depth of approximately 3500 m, thereby becoming the countercurrent observed in the present study. The equatorial eastward current, however, was not found at 146°E in October 1993 (FIRING *et al.*, 1998). This may imply that the equatorial eastward current on the bottom slope is not always present. Even if the equatorial eastward current is always present, it does not detour around the Solomon Rise when it is detached from the bottom slope at the change in vertical structure. In such a case, the current probably continues eastward along the equator. The absence of the countercurrent on the Solomon Rise during the second half of the mooring observation described by KAWABE *et al.* (2006) may reflect the disappearance of the equatorial eastward current or the release of the current from topographic controls.

5. Conclusions

Current velocity and echo intensity were measured using LADCP over the northeastern slope of the Solomon Rise in the Melanesian Basin. We used these data to clarify the structure of the western and eastern cores of the upper deep current and the countercurrent at depths of 2000–3500 m. We used the echo intensity and dissolved oxygen characteristics of the water to infer the upstream pathway of the countercurrent.

The western core of the upper deep current was observed at depths of 1600–2500 dbar over the bottom slope, at water depths of approximately 3000 m, carrying UCPW with very high dissolved oxygen. The eastern core was observed in the eastern region over the bottom slope at water depths of approximately 4000 m. Between these two cores of the upper deep current, a thick countercurrent flowed with a large width of more than 100 km.

The countercurrent is located over the bottom slope at water depths of approximately 3500 m, carrying water that is characterized by extremely high echo intensity. Based on these facts, we inferred that the equatorial eastward deep current along the southern boundary of the East Caroline Basin, as observed by FIRING *et al.* (1998), is steered by the bottom slope at water depths of approximately 3500 m. This current is connected to the countercurrent within the Melanesian Basin observed in the present study.

The equatorial water carried by the equatorial eastward current mixes with high–oxygen UCPW carried by the upper deep current. This explains the fact that the water in the countercurrent has an oxygen content that is intermediate between that of the western and eastern cores of the upper deep current. Moreover, the long–time disappearance of the countercurrent in the Melanesian Basin (KAWABE *et al.*, 2006) may occur when the equatorial eastward current disappears or detaches from the bottom slope.

Acknowledgements

The authors are grateful to Captain Y. TANAKA and the crew of R.V. *Hakuho Maru* and to the scientists and technical staff who participated in cruise KH–99–1. Special thanks are extended to Dr. S. FUJIO for kindly operating the lowered and shipboard ADCPs and for helpful suggestions in terms of data processing.

References

EGBERT, G. D., A. F. BENNETT and M. G. G. FOREMAN (1994): TOPEX/Poseidon tides estimated using a global inverse model. Journal of Geophysical Research, **99**, 24821–24852.

FIRING, E., S. E. WIJFFELS and P. HACKER (1998): Equatorial subthermocline currents across the Pacific. Journal of Geophysical Research, **103**, 21413–21423.

KAWABE, M (1993): Deep water properties and circulation in the western North Pacific. *In* Teramoto, T. (Ed.) , Deep Ocean Circulation, Physical and Chemical Aspects. Elsevier Science Publishers, Amsterdam, p. 17–37.

KAWABE, M., S. FUJIO and D. YANAGIMOTO (2003): Deep–water circulation at low latitudes in the western North Pacific. Deep Sea Research Ⅰ, **50**, 631–656.

KAWABE, M., D. YANAGIMOTO and S. KITAGAWA (2006): Variations of deep western boundary currents in the Melanesian Basin in the western North Pacific. Deep Sea Research I, **53**, 942–959.

KOMAKI, K. and M. KAWABE (under review): Correction method of full–depth current velocity with lowered acoustic Doppler current profiler (LADCP). Submitted to Journal of Oceanography in 2007.

REID, J. L. (1997): On the total geostrophic circulation of the Pacific Ocean: flow patterns, tracers, and transports. Progressive Oceanography, **39**, 263–352.

Received January 20, 2007
Accepted March 28, 2007

La mer 45 : 23-34, 2007
Société franco-japonaise d'océanographie, Tokyo

Distribution and Behavior of High-turbidity Water in Shallow Water Area around Miyake-shima Island, Japan

Hisayuki ARAKAWA*, Yumiko NAKAYAMA, Tsutomu MORINAGA

Abstract: High-turbidity water was observed in the shallow water area around Miyake-shima Island, southern Japan, (latitude: 34°06′ N, longitude: 139°32′ E) , specifically, on the southwest and northeast sides of the island. On the other sides, clear ocean water was observed, which is comparable to that the Kuroshio. It was found that the localization of high-turbidity water to the northeast was caused by the Kuroshio current, which encompassed the island. This is due to the effect of the island mass. The distribution of high-turbidity water in the northeast ocean area shows a near-circular pattern with two spots at a distance of 1.0–2.0 km from the shore. The turbidity increased with the increased water depth, showing a maximum of 1.2 m^{-1} of the beam attenuation coefficient at a depth of 50 m. The content of inorganic materials in the suspended particles was very high (76%) , and they are considered to be land-based materials that originate on Miyake-shima Island. The particle size of volcanic ash on land was in a wide range between 1–2000 μm. The sediment of the seabed near the shore contained clay minerals such as smectite and chlorite, indicating that they originated from volcanic products. Moreover, the sediments did not contain particles smaller than 60 μm in size. The following process can explain these observations. When rainfall flushes out muddy water containing volcanic ash from the shore area into the coastal waters, large particles—more than 60 μm in size—immediately settle to the bottom. Particles smaller than this size are dispersed by the flow of the current and sediment; these fine suspended particles disperse 3 km offshore and intrude into the pycnocline, forming a high-turbidity water layer.

Keywords: *Turbidity distribution, Miyake-shima Island, Volcanic ash, High-turbidity water, Sediment*

1. Introduction

Mt. Oyama on Miyake-shima Island, one of the Izu islands in the North Pacific Ocean, erupted on July 8 and 14, 2000, and volcanic products (also known as volcanic ashes), were clearly visible in the atmosphere. On August 18, 2000, volcanic smoke climbed higher than 5000 m, and an enormous quantity of volcanic ash fell on Miyake-shima and its surroundings. Subsequent rainfall washed away the accumulation of volcanic ash from the coast into the surrounding sea area, causing ocean discoloration. This led to considerable concern about the effects of volcanic sediments, which originated directly from the volcanic ash that had fallen into the ocean and the ash washed away from the island, on the bountiful marine resources in the shallow water regions around Miyake-shima. These included the marine life of the surrounding ocean area such as spiny lobsters, abalones, and agar weeds.

The eruption of a marine volcano in 1974 led to the creation of Nishino-shima Shinto Island in the abovementioned ocean area. MATSUIKE *et al.* (1975) investigated the turbidity of the inner bay formed between Kyuto (the old island) and Shinto (the new island) of Nishino-shima and the turbidity of the island's surrounding ocean area. The results revealed that the water temperature of the inner bay was 8 °C higher

Department of Ocean Sciences, Tokyo University of Marine Science and Technology, Konan 4, 5-7, Minato-Ku, Tokyo, 108-8477 Japan
*Corresponding Author
Fax: 81-3-5463-0467
E-mail: arakawa@kaiyodai.ac.jp

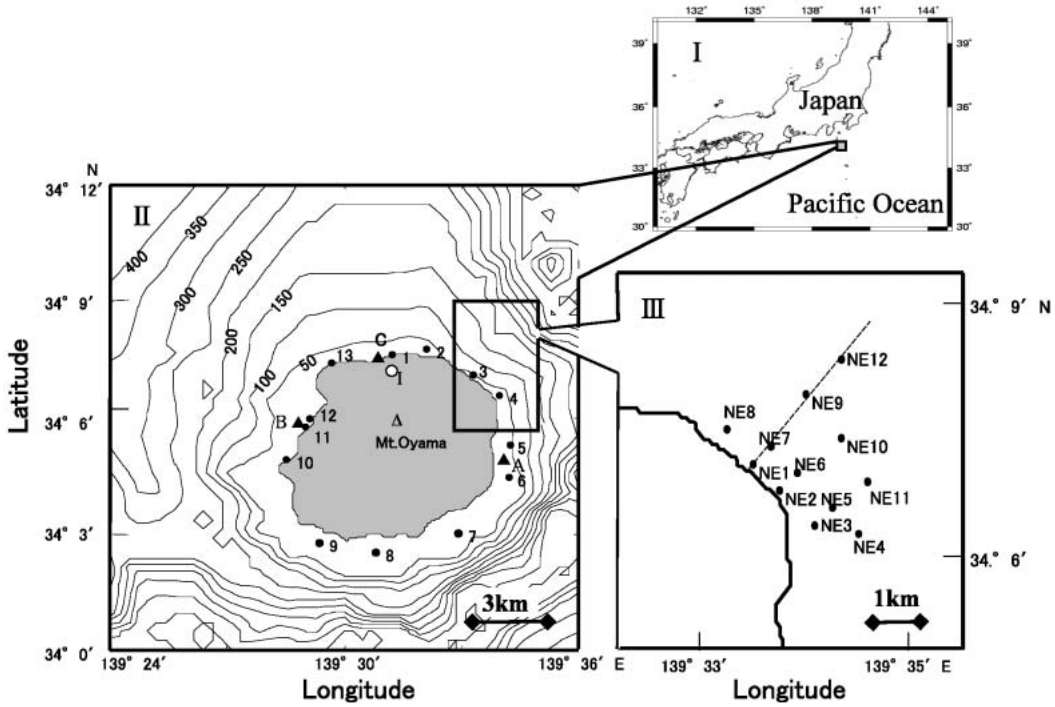

Fig. 1. Geographic location of Miyake-shima Island and the stations studied. Graph I: Geographical location. Graph II: Stations for general observation. (Sta. 1–13) . Graph III: Stations for detailed observations along the North-East direction of Miyake-shima Island. (Sta. NE1-NE12) . Stas. A, B, C, and I in Fig. 1–II indicate the locations for the collection of seabed sediments and volcanic ash, respectively.

than that of the surrounding ocean water and the amount of suspended matter was approximately 15 times higher. They also reported that a discolored ocean area, which occurred by the outflow of the inner bay water to the surrounding ocean area on surface, was observed within 0.5–0.6 nautical miles from the island.

After a period of three and four months following the Oyama eruption, ARAKAWA *et al.* (2003) investigated the turbidity distributions of the offshore area around Miyake-shima Island. They reported high-turbidity water layers at a depth of 60–90 m in the east and northwest ocean areas that are approximately 3 km offshore. More importantly, the suspended particles in the high-turbidity water layers corresponded to the terrestrial particles originating from Miyake-shima and not from phytoplankton. This conclusion was based on the high content of inorganic materials (approximately 57.7–63.4% of the total particles measured in that area) ; however, the formation process of the high-turbidity water layers remains unknown.

In this investigation, we studied the detailed turbidity distributions in the inshore areas approximately 3 km from shore. The purpose of this study was to clarify the flush-out process and the behavior of muddy water containing volcanic ash from the island.

2. Observation Methods

The oceanic observations were carried out aboard the research vessel Yashio (40 Gt) of the Oshima Branch, Tokyo Metropolitan Fisheries Experiment Station, on August 27–28, 2001. Fig. 1 illustrates the 13 observation stations (Stas. 1–13) that were set up to encompass all coastal areas around Miyake-shima (distance from the shore: 0.1–1 km). The figure also shows the 12 observation stations (Stas. NE1–NE12) that were set up in the ocean area northeast of the island (distance from the shore: 0.1–2.4 km). Sta. NE1 and Sta. NE3 correspond to Sta. 3 and Sta. 4, respectively. Measurements were performed for water tempera-

Table 1 Water color on the Forel scale and transparency in the shallow sea area for stations 1–13 around Miyake-shima.

Sta.	Water color	Transparency (m)
1	2	24
2	2	26
3	2	21
4	3	30
5	2	25
6	2	21
7	2	19
8	3	16
9	2	26
10	2	24
11	2	30
12	2	28
13	3	30

ture, salinity, turbidity, water color, and transparency. The water temperature and salinity were recorded using a CTD instrument (Ocean Sensors Inc.), and the turbidity was recorded using an *in situ* beam transmissometer (Martek Inc.; light path length: 1 m, measured wavelength: 486 nm). A continuous measurement was performed from the surface layer to the vicinity of the ocean floor. The water color was determined by the Forel-Ule scale and the transparency was determined using the Secchi disc. Using a Van Dorn sampler, the water was collected to determine the concentration of suspended solids (SS), ignition loss, concentration of chlorophyll *a*, and the particle size distribution. The concentration of suspended solids was determined by the following method: the filter cake was obtained by passing the sample water through a Millipore HA filter (pore size: 0.45 μm), dried at 60 ℃ for three days, and the residue thus obtained was weighed. To determine the ignition loss (for calculating the concentration of suspended inorganic matter), the filter cake was heated at 550 ℃ for one hour and the residue thus obtained was weighed. After the sample water filtration through a Whatman GF/F filter and chlorophyll extraction with a DMF, the chlorophyll *a* concentration was determined using a fluorometer (Turner 10AU). The fluorometric method was devised by SUZUKI and ISHIMARU (1990). The particle-size distribution was determined by freezing water samples on-site, transporting them to the laboratory, allowing the samples to thaw, and immediately analyzing them using a Coulter Counter Multisizer II in the range of 2–60 μm.

An illustration of the sampling stations for the volcanic ash on the land and for the sediment at the bottom of the ocean is included in Fig. 1. A sample of volcanic ash was taken from the parking lot (Sta. I) of the Miyake-shima Branch Office, Tokyo Metropolitan Government, immediately following the accumulation of ash on August 18, 2000. This was the day of the main Mt. Oyama eruption. On July 10, 2001, a sample of sediment from the seabed was collected from three stations and more specifically, from the east side of the island (Sta. A), west side of the island (Sta. B), and north side of the island (Sta. C). The depths of the sampling points were 7 m, 6.5 m, and 6 m, respectively, and the sampling was performed by scuba diving. The particle size distribution was determined using a particle size analyzer (LS200, Beckman Coulter Inc.), and it was found to be in the range of 0.4–2000 μm. Species and quantities of minerals were determined using an X-ray diffractometer (Rigaku Corporation, RINT2000) (SUDO *et al.*, 1961; OINUMA, 1968). To determine the density of volcanic ash, the standard method of JSF T 111–1990 (Japanese Society of Soil Mechanics and Foundation Engineering, 1990) was used.

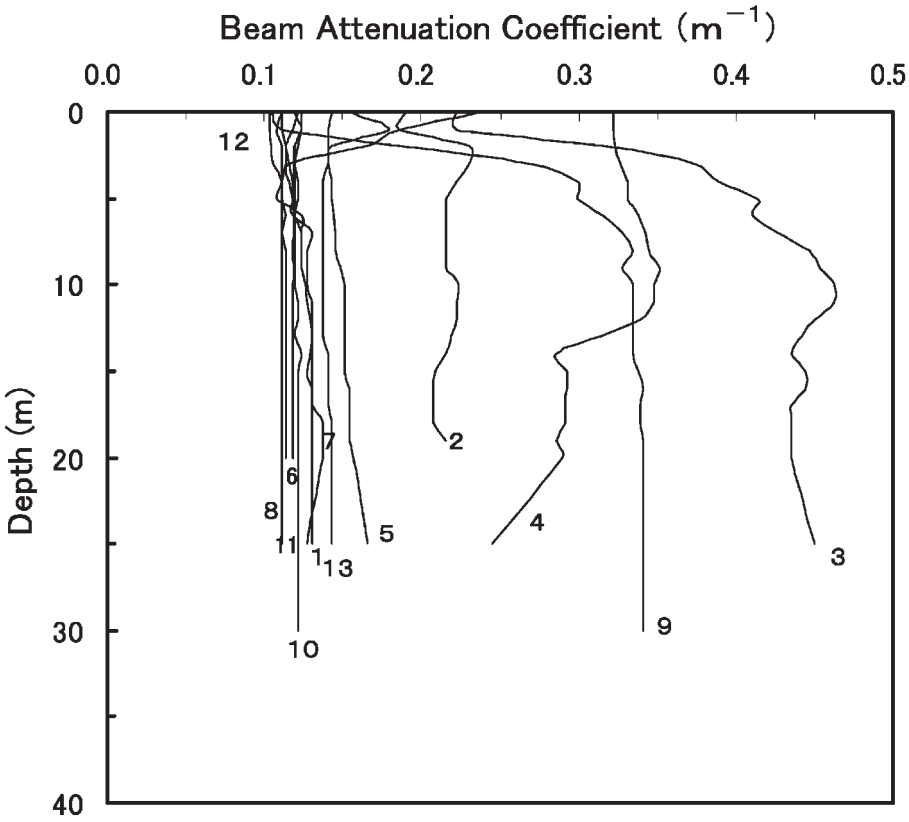

Fig. 2. Vertical profiles of turbidity in the shallow waters at Stations 1–13 in the coastal areas around Miyake-shima Island.

3. Results and Discussion

3-1 Distribution and Characteristics of High-turbidity Water in Shallow Water Areas

Over the two-day period of August 21–22, 2001, typhoon No. 11 passed over the sea and along the southern coast of Honshu Island in Japan and brought 70 mm of rain to Miyake-shima (specifically, the Tsubota district). The oceanographic observations were carried out six days after the typhoon. On that day (August 27, 2001), the Beaufort wind scale was zero to one, with very weak winds. From on board, we made naked eye observations, but we did not see any scenes of flushed-out muddy water from the shore or regions of discolored water.

Table 1 lists the water color and transparency in the shallow water areas around the island. The water color was found to be in Forel scale range of 2–3, and there was no drastic difference in the water color among the observation stations. The transparency among stations was 16–30 m, with slightly lower transparencies at Stas. 3, 6, 7, and 8.

Fig. 2 illustrates the vertical profiles of turbidity in the shallow water areas around the island. We found high-turbidity water on the southwest side (Sta. 9) and the northeast side (Stas. 2, 3, and 4) of the island, which exhibited beam attenuation coefficients between 0.20–0.46 m^{-1}. The turbidity in the other areas was 0.10–0.15 m^{-1}, which is comparable to the turbidity of the Kuroshio, which had a range between 0.1–0.2 m^{-1} (MATSUIKE and MORINAGA, 1977). This result indicates that the seawater was very clear, except on the southwest and northeast sides of the island. During the observations, the Kuroshio directly affected the sea area of Miyake-shima, causing the current to flow to the northeast around the island with a

velocity of *ca.* 1.5 knots (Quick bulletin of fisheries ocean condition on Metropolitan and 3 prefectures, No. 4068, Kanagawa Pref. Fisheries Experiment Station, 2001). With regard to the area of high-turbidity water, it was observed that the water distributed into the downstream and upstream areas of the current.

When an isolated island is directly aligned with a current's flow, a vortex is formed on the leeward side of the island by the effects of the land mass. This affects the distribution of suspended material and the underwater biological production (e.g., DOTY and OGURI, 1956; UDA and ISHINO, 1958; BARKLEY, 1972). HAMNER and HAURI (1981) reported that when a current flows against a reef or a small island, the flow of ocean water is retarded at the upstream and downstream sides and plankton accumulates in the areas of retarded flow.

In this investigation, it is not possible to clarify the vortex downstream of the island since the current was not measured. HEYWOOD *et al.* (1996) and Baines and Davies (1980) examined the conditions for vortex formation. If the radius of Miyake-shima Island is 4000 m at a depth of 50 m, the eddy viscosity is 10^2 $m^2\ s^{-1}$, and the current velocity is 0.77 $m\ s^{-1}$ (ca. 1.5 knots), then the Reynolds number (Re) is 62. Applying the results of HEYWOOD *et al.* (1996), this proves that a vortex can be formed at this time in the downstream direction of Miyake-shima Island and the island mass effect seems to act. However, we do not have results for the extent of effects of the island mass on the distribution of high-turbidity water along the northeast direction of the island. The relationship between the vortex and the accumulation of suspended particles is a subject for future examination.

Fig. 3 illustrates the horizontal distribution profiles of turbidity in the northeast ocean area. The top and bottom panels in this figure display the distributions in the surface layer and at a depth of 20 m. The turbidity distribution in the surface layer (Fig. 3, top) was 0.14 m^{-1} at Sta. NE1. With an increase in the distance from the shore, the turbidity increased, reaching 0.98 m^{-1} at Sta. NE9. Farther offshore, the turbidity decreased to 0.17 m^{-1} at Sta. NE12. The turbidity at Sta. NE6 and Sta.

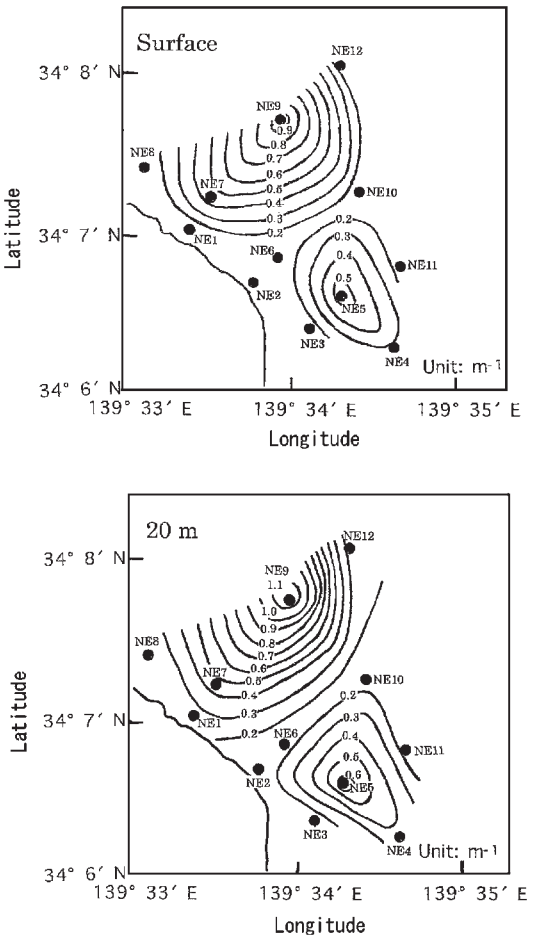

Fig. 3. Horizontal distribution of turbidity in the high-turbidity water area. The top and bottom panels show the turbidity distribution in the surface layer and at a depth of 20 m, respectively.

NE10, located 0.5–2 km from NE2, had lower values ranging between 0.11 and 0.13 m^{-1}. The turbidity at Sta. NE3 was 0.14 m^{-1}; this value increased with the distance from the shore, reaching a maximum of 0.57 m^{-1} at Sta. NE5. Farther offshore, the turbidity decreased to 0.12 m^{-1} at Sta. NE11. The distribution at a depth of 20 m (Fig. 3, bottom) showed maxima 1.11 m^{-1} and 0.63 m^{-1} at Sta. NE9 and Sta. NE5, respectively. This was also the case for the surface layer. From these observations, we can conclude that the high-turbidity water was near-circularly localized in two areas, where the maxima (beam attenuation coefficients: 0.98 and 0.57 m^{-1}), were located at a distance of

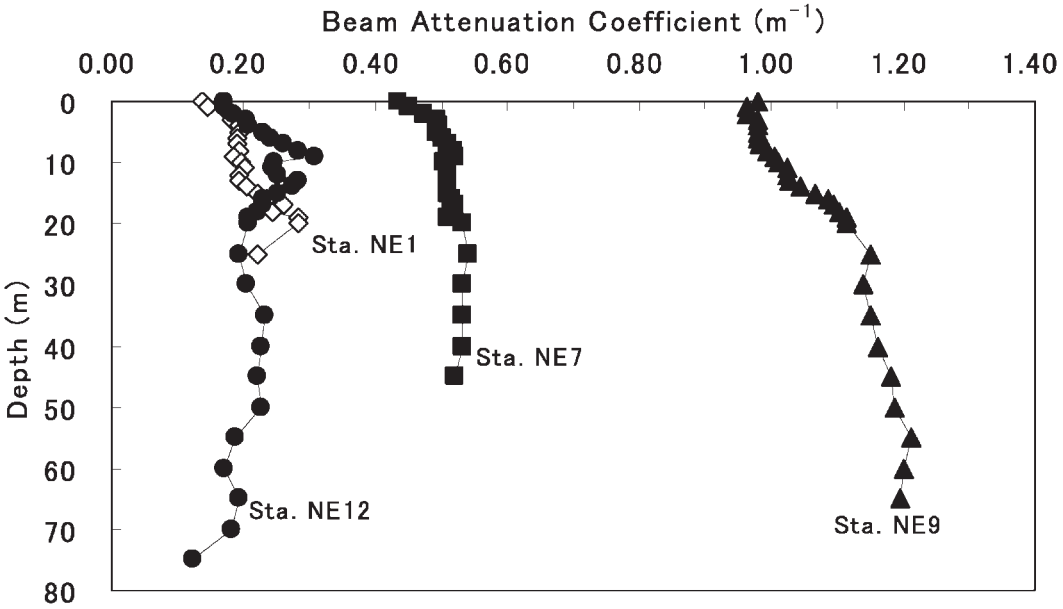

Fig. 4. Vertical distribution turbidity profiles in the high-turbidity water area, as illustrated in Fig. 1. The symbols ◇, ■, ▲, and ● represent Stas. NE1, NE7, NE9, and NE12, respectively.

Table 1 Concentration of suspended solids, inorganic matter, and chlorophyll *a* in the surface layer at Sta. NE6 and Sta. NE9.

Sta.	NE6 0m	NE9 0m
Suspended solid (mg/L)	0.38	0.70
Inorganic matter (mg/L)	0.19	0.53
Chlorophyll a (μg/L)	0.60	0.96

approximately 1.0–2.0 km from the shore.

Fig. 4 illustrates the vertical distribution of the turbidity between Stas. NE1 and NE12. The turbidity in the surface layer was highest at Sta. NE9, which was located at the center of the circular turbidity distribution. At Sta. NE9, the turbidity exceeds its value in the surface layer to a depth of 65 m and the turbidity decreases with an increase in the distance from this water column. The turbidity at Sta. NE9 increased with the depth of water, showing a maximum of 1.2 m^{-1} at a depth of 55 m.

Next, we examined the characteristics of the suspended particles distributed in this high-turbidity water. Table 2 lists the concentrations of suspended solids (SS), inorganic matter (determined from the SS and ignition loss), and chlorophyll *a*. From this table, it is seen that the surface water at Sta. NE9 has a high turbidity and the that at Sta. NE6 is relatively clear oceanic water. The SS of the high-turbidity water at Sta. NE9 was 0.70 mg L^{-1} and the concentration of the suspended inorganic matter was 0.53 mg L^{-1}. This means that approximately 76% of the suspended particles in the high-turbidity water were inorganic particles. The concentration of chlorophyll *a* at Sta. NE9 was 0.96 μg L^{-1}, which is one and a half times greater than that at Sta. NE6. This small difference in the chlorophyll *a* concentration has almost no influence on the variation of water turbidity (MORINAGA *et al.*, 1988). In other words, it was proved that the high-turbidity water had its origins in inorganic particles.

According to the observations immediately following the eruption in 2000, it was observed during a survey that the inorganic matter concentrations of the high-turbidity water of sea areas at a distance of *ca.* 3 km from the island

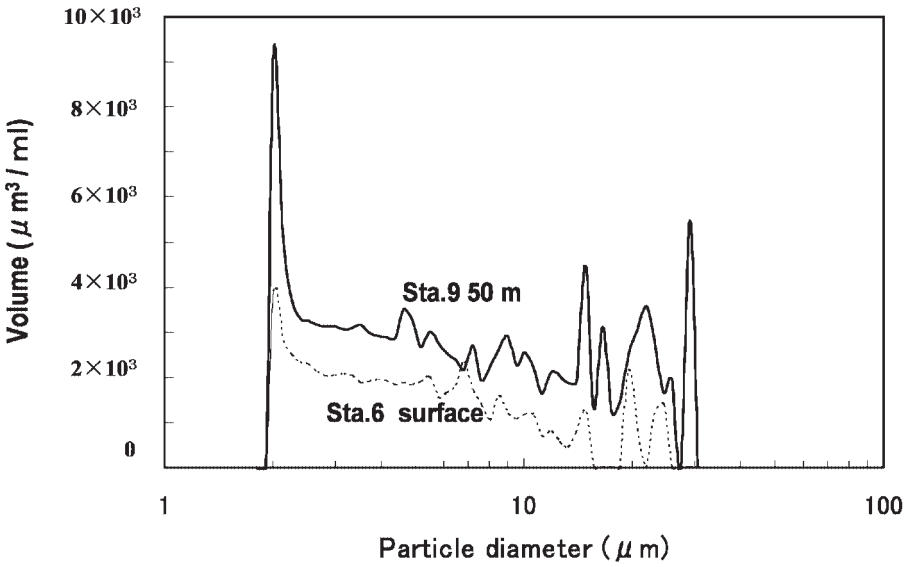

Fig. 5. Particle-size distributions in the high-turbidity water area. The solid and dotted lines indicate the distributions at a depth of 50 m at Sta. NE9 and in the surface layer at Sta. NE6, respectively.

were 57.7 % and 63.4 %. (ARAKAWA *et al.*, 2003). From this, we understood that the high-turbidity water measured in this survey contained inorganic particles more than the ratio right after the eruption.

Fig. 5 illustrates the particle-size distributions at Stas. NE6 and NE9. The suspended particle sizes in the surface layer at Sta. NE6 were in the range of 2–30 μm, and the total volume concentration was approximately 3.4×10^4 $\mu m^3\ mL^{-1}$. While the suspended particles at a depth of 50 m at Sta. NE9 also had particle sizes in the range of 2–30 μm, the total volume concentration was found to be approximately 7.0×10^4 $\mu m^3\ mL^{-1}$, which is twice that at Sta. NE6. In the offshore high-turbidity water (observed in October and November of 2000), the particle size distribution showed a prominence in the particle size range of 8–14 μm (ARAKAWA *et al.*, 2003). As a result, we can see that the particles suspended in the high-turbidity water in the shallow water area comprise a much wider range of particle sizes.

It is clear that the particles in the high-turbidity water are mainly inorganic matter and have sizes in the range of 2–30 μm.

3-2 Characteristics of Volcanic Ash on Land and Sediment at Ocean Bottom

Fig. 6 illustrates the results of X-ray diffraction for volcanic ash on land and for the sediment on the seabed. In the volcanic ash that was collected immediately following the eruption at Sta. I, a dominance of kaolinite and non-clay minerals such as quartz and feldspar was observed. The content of smectite and chlorite, which originate from volcanic material, was especially high. This trend is very similar to that of the sediment from the seabed at Stas. A, B, and C. At Stas. A and B, illite was not found, but at Sta. C, illite was found in the sediment. AOKI *et al.* (2000) collected mineral core from the Iwo Jima ridge area of the Izu islands at a depth of 3000 m and investigated the components of the clay minerals. They reported that smectite, which originates from volcanic ash, constitutes a small amount of the clay minerals in the ridge area. Based on these facts, it is evident that the particles deposited on the seabed near the shore are volcanic products. However, we cannot report in detail whether the particles are from the volcanic ash that was directly deposited following the eruption of 2000 or the volcanic ash that was indirectly deposited after being flushed-out from

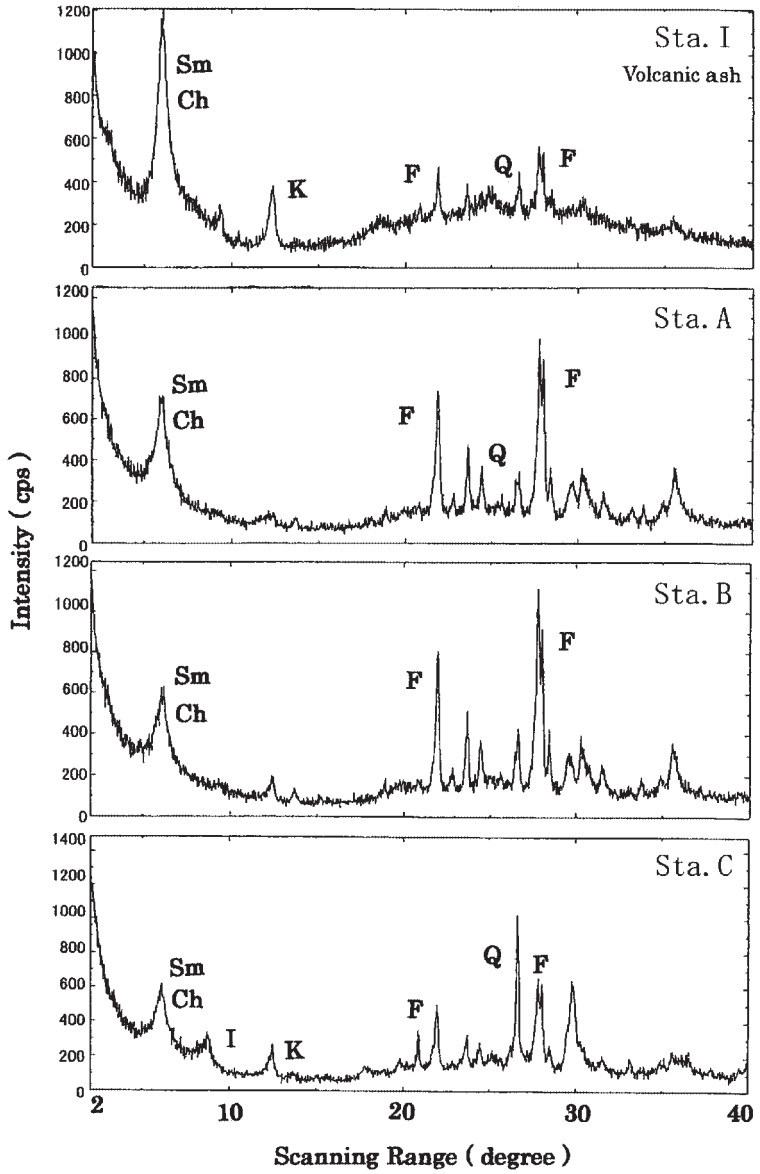

Fig. 6. X-ray diffraction analyses for volcanic ash on land and for sediment at the bottom of the ocean. Sm: smectite, Ch: chlorite, I: illite, K: kaolinite, F: feldspar, Q: quartz.

the land by rainfall.

To understand the behavior of the high-turbidity water, we need to investigate the movement of the volcanic ash that has fallen into the ocean and the ash that has been flushed out from the land as muddy water. This requires an investigation of the size of the particles that were deposited into the seabed and the size of particles that were suspended in the ocean water. This investigation was carried out by comparing the particle size distribution for the volcanic ash deposited on land as well as that deposited on the seabed. Fig. 7 illustrates the particle size distribution immediately following the eruption on August 18, 2000, for the land-deposited volcanic ash and the sediment

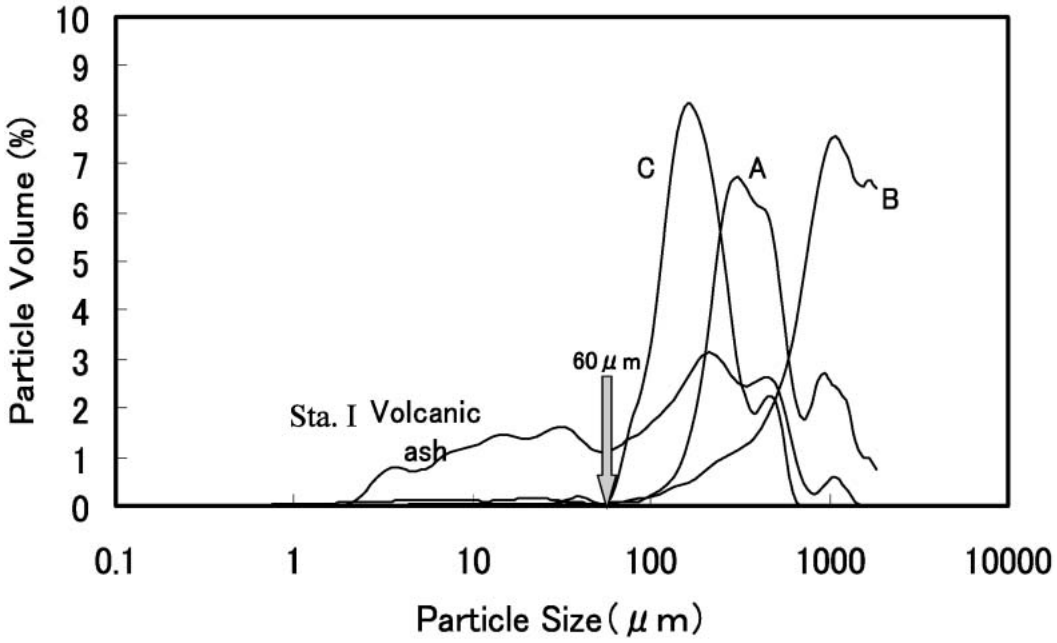

Fig. 7. Particle-size distributions for volcanic ash on land and for sediment at the bottom of the three stations. Fig. 1 shows Stas. I, A, B, and C.

from the seabed that was near the point of the muddy outflow of the deposited volcanic ash. The distribution curve for the land-deposited volcanic ash had a small peak in the range of 200–500 μm, and most particles were in the range of 1–2000 μm. At Sta. A, the distribution curve for the sediment from the seabed had a prominent peak in the range 300–350 μm; for Sta. B, the range was 1100–1200 μm; and for Sta. C, the range was 150–200 μm. Particles smaller than 60 μm were found only in a very small quantity at Sta. A, and they were not observed at the other seabed stations.

To calculate the settling velocity (ν) for the particles of size 60 μm (D), the following Stokes' equation is used:

$$\nu = \frac{1}{18} D^2 g \frac{\rho_s - \rho}{\mu},$$

where is gravitational acceleration, ρ_s is the density of the particles, ρ is the density of seawater (1.023 g cm^{-3}), and μ is the viscosity coefficient of seawater (1.0×10^{-2} dyn s cm^{-2}).

Since the specific gravity of the land-deposited volcanic ash is 2.81, the settling velocity of particles with a size of 60 μm is estimated to be approximately 3.50 mm s^{-1}. Accordingly, particles with sizes greater than 60 μm will sediment to the bottom within about 48 min after being flushed out to shallow water areas that have a depth of less than 10 m.

Judging from this, among the particles (of volcanic origin) flushed out from the island, particles with a size greater than 60 μm are expected to sediment rapidly to the seabed, and particles smaller than this size are expected to be dispersed in the suspension.

3-3 Flush-out Process of Muddy Water Containing Volcanic Ash from the Island

As mentioned previously, it is known that the suspended particles in high-turbidity water are particles of volcanic origin with sizes less than 30 μm. If we assume the average particle concentration in the water column (centered at Sta. NE9, with a radius of 1 km and depth of 50 m) is 0.5 mg L^{-1}, the total weight of the suspended particles amounts to 78,500 kg. The spouting of volcanic ash from the crater diminished from September of 2000, and no large-

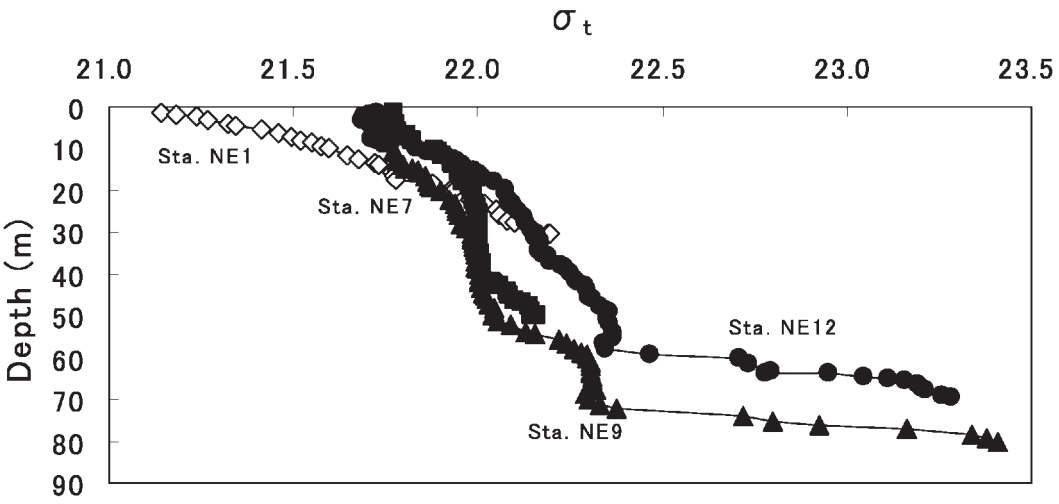

Fig. 8. Vertical distribution profiles of density in the high-turbidity water area. Symbols ◇, ■, ▲, and ● represent Stas. NE1, NE7, NE9, and NE12, respectively.

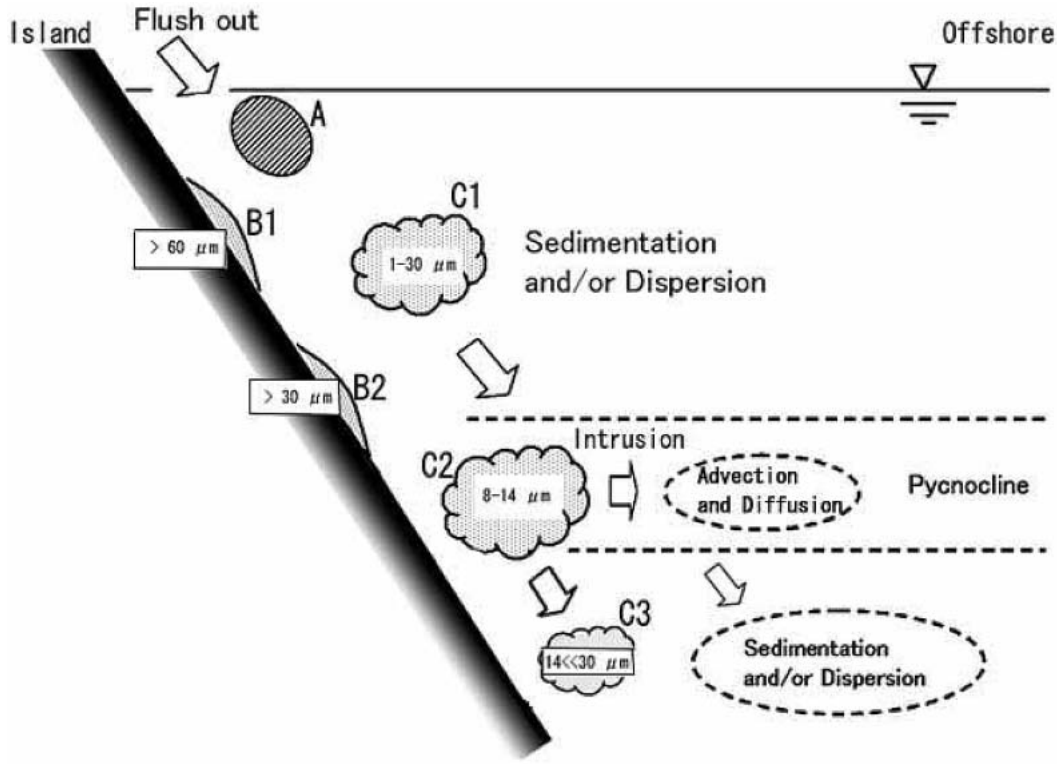

Fig. 9. Sketch of the flush-out process of volcanic ash. Numerical numbers indicate the particle diameters in μm.

scale spouting occurred until August of 2001. Therefore, the high-turbidity water observed during this period did not result from the volcanic ash that had fallen directly into the ocean from the crater.

DOI *et al.* (2005) investigated the effect of rainfall intensity on the sediment that was transported into the river on Miyake-shima Island after the eruption in 2000. They reported that some rivers on the island continue to discharge considerable volumes of sediment. Fig. 8 illustrates the vertical distribution profile of sigma-t along the line from Sta. NE1 to Sta. NE12. We see that low-density ocean water, less than 22 in sigma-t, distributes inward from the shore (Sta. NE1) to the center (Stas. NE7 and NE9) of the near-circularly localized high-turbidity water. Let us compare this with the distribution profiles for the turbidity illustrated in Fig. 4. It is clear that high-turbidity water is present at a depth of less than 70 m at Sta. NE9, where a pycnocline is observed. Therefore, we can conclude that the appearance of particles in high-turbidity water is due to muddy volcanic ash that was flushed out by rainfall that had taken place 4–5 days before the observation date.

Particles with sizes of 8–14 μm were prominent in the high-turbidity water in October and November of 2000 (3–4 months after the eruption of Mt. Oyama), and they were located in the pycnocline at a depth of 60–90 m (ARAKAWA *et al.*, 2003). We then considered how many days are required for the formation of this high-turbidity layer. To do this, we calculated the settling velocity of the particles with sizes of 8-14 μm from Stokes' equation by assuming the specific gravity of volcanic ash as 2.81, as previously mentioned. The settling velocity in the mixed layer on October and November 2000 (σ_t = *ca.* 23.5) was calculated to be 0.62×10^{-1}–1.9×10^{-1} mm s^{-1}. Therefore, particles with a diameter of 8 μm take 11.2 days to reach the pycnocline, and those that are 14 μm in size take 3.6 days.

MORIKAWA *et al.* (1996, 1997) examined the intrusion phenomenon of turbid water in Lake Biwa and explained that the intrusion of turbid water with particles that are 5-10 μm in diameter from the pycnocline resulted easily. In other words, the following should be considered: the particles discharged from the land settle in the mixed layer (requiring a period of 4–11 days), and then they intrude into the pycnocline layer; as a result, the high-turbidity layer observed in 2000 was formed.

By combining these results, we can obtain a schematic view of the flush-out process for volcanic ash particles, as illustrated in Fig. 9. When muddy volcanic ash (A) from land is flushed out by rainfall into the ocean, particles larger than 60 μm settle rapidly (B1), and smaller particles (C1) disperse and form sediments. Since the settling velocity is high, particles larger than 14 μm in the muddy water and especially those larger than 30 μm are deposited on the seabed (B2) and/or pass through the pycnocline (C3). Fine particles (C2) between 8 and 14 μm in size disperse offshore over a period of 4 to 11 days. After this period, they intrude into the pycnocline and form a high-turbidity layer. The settling velocity of the particles decreases slightly in the pycnocline. The sigma-t of the high-turbidity layer in 2000 was approximately 25, and the high turbidity-water requires more than 1.8–5.6 days to pass through the pycnocline at a depth of 60–90 m. In addition, the high-turbidity water may be adverted by entrainment into the ocean current.

In the near future, it will be possible to quantitatively estimate the damage to fishing grounds by the movement of high-turbidity water and flushed-out volcanic ash.

Acknowledgements:

This investigation is a part of the project conducted by the Tokyo University of Fisheries titled "Influence of Miyake-shima Volcanic Activity on the Fishing Environment". A part of this investigation was supported by the Research Project Fund of Tokyo University of Fisheries for the fiscal year 2001 and by a contribution from Murayama Electric Co., Ltd. Oceanographic investigation and sediment sampling from the island and from the bottom of the ocean were performed in collaboration with the Tokyo Metropolitan Fisheries Experiment Station and its Oshima Branch. X-ray diffraction measurements were performed in

collaboration with Professor Saburo AOKI of Toyo University. We express our grateful appreciation to all people involved with this study.

References

AOKI, S., N. KOHYAMA, Y. SHINOHARA (2000) : Mineralogical and geochemical study of piston cores collected from the Shichitou-Iwojima ridge area. J. Sed. Soc. Japan., **51**, 5–21.

ARAKAWA, H., A. KONISHI, S. YAMASAKI and T. MORINAGA (2003) : Turbidity distribution in the surrounding ocean area of Miyake-shima Island after the eruption of Mt. Oyama. La mer, **41** (**1**), 15–27.

BAINES, P.G. and P.A. DAVIES (1980) : Laboratory studies of topographic effects in rotating and/or stratified fluids. *In*: Oceanographic effects in planetary flows, R. Hide and P. White, editors. GARP Publ. Ser., **23**, WMO, Geneva, 233-299.

BARKLEY, R.A. (1972) : Johnston Atoll's Wake. J. Mar. Res., **30**, 201–216.

DOTY, M.S. and M. OGURI (1956) : The island mass effect. J. Conseil Perm., 22, 33–37.

DOI, Y., K. SASAHARA, T.YAMAKOSHI and H. NISHIMOTO (2005) : The effect of rainfall intensity on sediment transport in a scoria-rich river on Miyakejima Island, Japan. Sediment Budgets, 214–221.

HAMNER, W.M. and I. R. HAURI (1981) : Effects of island mass: water flow and plankton pattern around a reef in the Great Barrier Reef lagoon, Australia. Limnol. Oceanogr., 26 (6), 1084–1102.

HEYWOOD, K.J., D.P. STEVENS and G.B. BIGG (1996) : Eddy formation behind the tropical island of Aldabra. Deep-Sea Res., **43**, 555–578.

JAPANESE SOCIETY of SOIL MECHANICS AND FOUNDATION ENGINEERING (1990) : Test method for density of soil particles. *In* Manual for Soil Analysis, p 43, Doshitsu Kougaku Kai, Tokyo. (in Japanese)

KANAGAWA PREFECTURE FISHERIES EXPERIMENT STATION (2001) : Quick bulletin of fisheries ocean condition on Metropolitan and 3 prefectures dated August 27, 2001., No. 4068, Tokyo.

MATUSUIKE, K., M. HORI and T. TAKAHASHI (1975) : Oceanographic investigation of the sea area in the vicinity of Nishinoshima-shinto. J. Tokyo Univ. Fish., **61** (1−2), 49–57.

MATSUIKE, K. and T. MORINAGA (1977) : Beam attenuation and particle-size distribution in the Kuroshio area. La mer, **15** (2), 32–43.

MORIKAWA, H., K. OKUBO and H. MURAMOTO (1996) : Intrusion of turbid water in stratified lakes driven by resuspension of sediments on sloping boundaries. Proc. Hydr. Engin., **40**, 607–612.

MORIKAWA, H., K. OKUBO, H. MURAMOTO and T. EZOE (1997) : Generation of turbidity intrusion in stratified lakes. Proc. Hydr. Engin., 41, 489-494.

MORINAGA, T., T. KOIKE, K. OOTOMO and K. MATSUIKE (1988) : Response of a fish school to turbid water. La mer, **26** (1), 19–28.

OINUMA, K. (1968) : Method of quantitative estimation of clay minerals in sediments by X-ray diffraction analysis. J. Toyo Univ., General Education. (Nat. Sci.), **10**, 1-15.

SUZUKI, R. and T. ISHIMARU (1990) : An improved method for determination of phytoplankton chlorophyll using N,N-dimethylformamide. J. Oceanogr. Soc. Jap., **46**, 190–194.

SUDO T., K. OINUMA and K. KOBAYASHI (1961) : Mineralogical problems concerning rapid clay mineral analysis of sedimentary rocks. Acta Univ. Carolinae, Geologica Supply. **1**, 189–219.

UDA, M. and M. ISHINO (1958) : Enrichment pattern resulting from eddy systems in relation of fishing grounds. J. Tokyo Univ. Fish., **44**, 105–129.

Received September 20, 2006
Accepted April 24, 2007

La mer 45 : 35-46, 2007
Société franco-japonaise d'océanographie, Tokyo

愛媛県宇和海沿岸における海水温の経年変動

鈴木 怜・竹内一郎*

Inter-annual variation in seawater temperature on the Uwa Sea coast, Ehime Prefecture

Satoshi SUZUKI and Ichiro TAKEUCHI*

Abstract : Global seawater surface temperature has been rising 0.5℃/100 yr. Since the mid-1990s, in particular, The years of high temperature frequently recorded Thus, global warming is reported to have already probably influenced the fish production. Accordingly, in the present study, we analyzed seawater temperature data recorded daily on the Uwa Sea coast, Ehime Prefecture at 0.5, 2.0 and 5.0 m depths between 1981 and 2004. The coast is one of the main areas for fish and pearl oyster aquaculture. A significant trends of annual mean seawater temperature ranging between 0.032 and 0.035℃ were found for all depths. These increases occurred mainly in winter (0.059 to 0.074℃ yr^{-1}), while temperatures in summer were almost constant (0.007 to 0.022℃ yr^{-1}). In our previous study, we measured seawater salinities off Yusu in the Uwa Sea, where values were high in winter (34.47 ± 0.15) and low in summer (33.94 ± 0.27). Recently, the Kuroshio has a tendency to flow close to the southern coast of Shikoku Island. Thus, the high tempereture and salinity in winter might be caused by the inflow from the Kuroshio. On the other hand, during summer, the cold water, in a process called "bottom intrusion", derived from the Kuroshio is reported to reach the coast along the Uwa Sea. We considered that the bottom intrusion is responsible for the constancy of seawater temperatures in summer. Global warming is thought to have increased the speed of the Kuroshio Current. Therefore, the seawater temperatures at the coast of the Uwa Sea may continue to increase mainly in winter.

Keywords : *inter-annual variation, seawater temperature, Uwa Sea*

1. 緒言

二酸化炭素などの温室効果ガス濃度の上昇に伴って，海水温の上昇がオーストラリアグレートバリアリーフ等の熱帯域をはじめヨーロッパ等の世界各地の温帯域沿岸でも観測されている（COLES and BROWN, 2003; HAWKINS *et al.*, 2003; JOKIEL and BROWN, 2004; SHEPPARD and RIOJA-NIETO, 2005; WOEHRLING *et al.*, 2005）。気象庁の解析でも地球温暖化等の影響によって全球の年平均海面水温は，長期的には100年あたり0.5℃の割合で上昇しているが，特に1990年代中頃以降，高温となる年が頻出していることが報告されている（気象庁, 2006）。日本沿岸では，1985年から2003年にかけて，南西諸島から日本海で0.01–0.06℃ yr^{-1}，東海沖や関東東方沖では0.1℃ yr^{-1}を超える上昇率を示している（気象庁, 2004）。しかし，同一海域でも海水温上昇の規模やスピードには局所的に差が存在することも報告されている（SHEPPARD and RIOJA-NIETO, 2005）。また，海水温と海面水位には比較的良い相関が存在する（岩崎ら, 2002）。日本沿岸の平均的な海面水位の変動をみると，一様な上昇傾向となっておらず，1950年前後に極大がみられ，また，約20年周期の変動が繰り返されている。過去約100年にわたる日本沿岸の海面水位は統計的に有意な上昇を示していないが，1980年代半ば以降海面水位は上昇を続け，

愛媛大学農学部生態系保全学研究室, 790–8566 愛媛県松山市樽味 3－5－7
Department of Life Environment Conservation, Faculty of Agriculture, Ehime University, 3－5－7 Tarumi, Matsuyama, Ehime, 790–8566, Japan
*Corresponding author. Email: takeuchi@agr.ehime-u.ac.jp; TEL/FAX: 089–946–9899

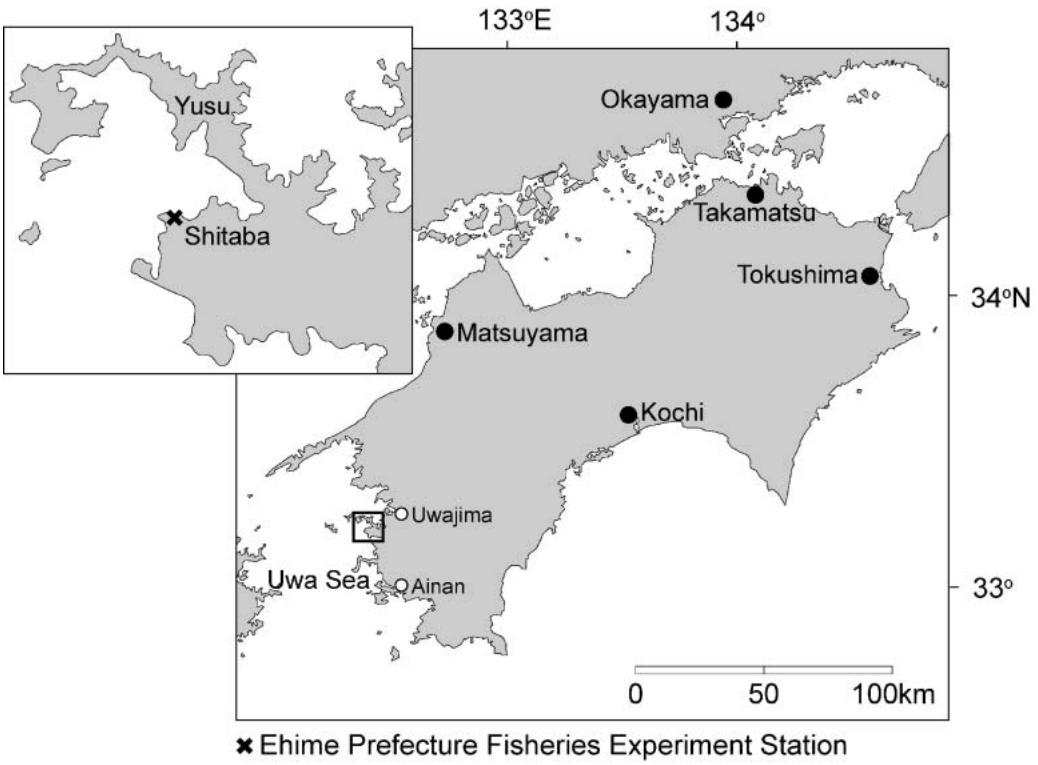

Fig. 1. Location of the study site.

近年は1950年前後とならんで過去100年でもっとも高い状態にある（気象庁, 2005）。海面水位の上昇は，特に西日本で顕著であり，過去約30年の変動は2.4 mm yr^{-1} であった（岩崎ら, 2002）。過去の変動の周期性から類推すると，1990年代半ばに海面水位の極大値，2000年代半ばに極小値がみられることが期待されるが，5年移動平均でみた観測結果からは，海面水位は低下することなく現在まで上昇を続けている（気象庁, 2005）。したがって，近年の海面水位の上昇には1960–1990年頃の海面水位の変動とは別の要因（海水温の上昇による熱膨張など）が加わっていると考えられる。

近年，地球環境変化とりわけ地球温暖化は，すでに魚類生産に影響を及ぼしている可能性も報告されるようになった（友定, 2002）。しかし，その確たる証拠は未だ見出されていない。よって，現在，その影響が検出されていないとしても，地球環境変化と魚類生産等の関係を明らかにすることは差し迫った重要課題である。海洋の変化を検出するには長期間にわたるデータの蓄積およびそれらデータの有効利用が重要であるが，日本における長期的な海洋観測は水産試験場等の限られた試験研究機関によって行われており，なかでも沿岸域における長期データは極めて少ないのが実情である。そこで，本研究では日本の南西部に位置し，魚類養殖やアコヤガイ養殖が最も盛んな地域の一つである愛媛県宇和海，特に，生物生産量が高い沿岸域における24年間の海水温の経年変動に解析した結果について報告する。

2. 資料と方法

海水温データは，愛媛県水産試験場により1981年1月から2004年12月にかけて愛媛県宇和島市下波に位置する同水産試験場地先（Fig. 1）の深さ0.5，2.0および5.0 mで1日ごとに測定されたデータを用いた。なお，測定は午前8時半から9時の間に行われている。全ての深さにおいて年間100日前後のデータ欠落が存在しているが（Table 1），それぞれの年における海水温データの欠落は，1981年を除いて各月にほぼ均等に分布している（Fig. 2）。1981年のデータに関しては冬季のデータ数（n=28）が夏季のデータ数（n=73）と比較して少なく，年平均海水温が過大評価される危険性があった為，年変動の解析においては使用しなかった。また，深さ2.0 mの海水温データに関しては1996年1月から1997年1月にかけての約1年間にわたって欠落している。

海水温の年変動の解析は，年ごとに平均値を求め，Stat View ver. 5.0（SAS Institute Inc. 1992–1998）を

Table 1 Number of samples collected annually by depth.

	1981	1982	1983	1984	1985	1986	1987	1988	1989	1990	1991	1992
0.5m	198	267	290	316	342	323	269	264	252	224	241	247
2.0m	192	268	291	317	342	325	273	263	252	225	241	246
5.0m	191	268	292	316	342	319	266	264	251	224	241	246
	1993	1994	1995	1996	1997	1998	1999	2000	2001	2002	2003	2004
0.5m	228	264	269	281	316	326	304	310	314	316	315	291
2.0m	235	266	269	0	264	323	304	310	307	316	314	289
5.0m	228	265	269	279	318	326	309	311	313	316	314	289

Table 2 Increase of annual mean seawater temperature at 3 depths between 1982 and 2004.

Depth (m)	Increase (℃ yr^{-1})
0.5	0.032
2.0	0.032
5.0	0.035

Table 3 Increase of minimum and maximum seawater temperatures in each year from 1981 to 2004.

Depth (m)	Increase (℃ yr^{-1})	
	Minimum	Maximum
0.5	0.078	−0.015
2.0	0.079	−0.012
5.0	0.067	0.005

用いて単回帰分析を行った。最高・最低水温の変動の解析は，月ごとに平均値を求め，それぞれの年における最高・最低水温を記録した月の水温を単回帰分析した。また，各月の水温変動も，月ごとに平均値を求め，単回帰分析を行った。

3. 結果

3.1. 年平均水温の変動

愛媛県宇和島市下波の年平均海水温は，深さ0.5 mでは19.5±4.2℃（平均±標準偏差）（1991年）から20.8±3.6℃（1998年）の間で変動した（Fig. 2）。また，深さ2.0 mに関しては19.1±3.5℃（1993年）から20.8±2.9℃（1997年），深さ5.0 mに関しては19.2±4.0℃（1991年）から20.5±3.4℃（1998年）の間であった（Fig. 3）。各年で比較すると，1997年を除くすべての年で深さ0.5 mの海水温が最も高く，深くなるにつれ海水温は低下した。各年の平均海水温を平年値との偏差で表すと（1982年から2004年にかけての各深さでの平均海水温を0とした），全て深さにおいて1982年から1993年にかけては主にマイナスで推移し，1994年から2004年にかけては主にプラスで推移していた（Fig. 4）。すべての深さで有意な年平均海水温の上昇傾向が示され（$p<0.05$），1982年から2004年にかけての水温上昇速度は0.032℃ yr^{-1}（深さ0.5 m），0.032℃ yr^{-1}（深さ2.0 m）および0.035℃ yr^{-1}（深さ5.0 m）であった（Table 2）。

3.2. 海水温の季節変動

愛媛県宇和島市下波における24年間にわたる海水温の季節変動は，最低平均水温は0.5 m，2.0 mおよび5.0 mの全ての深さで2月に記録し，最高平均海水温は8月に記録した（Fig. 5）。海水温の変動（最高平均海水温（8月）と最低平均海水温（2月）との差）は，深さ0.5 mでは11.5℃，2.0 mでは11.0℃，5.0 mでは10.6℃であり，浅い深度で最も変動が大きく，深くなるにつれ変動が小さくなる傾向が見られた。

各年の月平均最低海水温は，深さ0.5 mでは12.7±0.6℃（1981年）から15.7±0.6℃（1998年），深さ2.0 mでは12.8±0.3℃（1981年）から15.7±0.6℃（1998年），深さ5.0 mでは12.9±0.4℃（1981年）から15.8±0.6℃（1998年）の間で変動し（Fig. 6），全ての深度において主に2月（1981年は1月；1987，1993，1994，1995および2001年は3月）に記録した。また，各年の月平均最高海水温は，全ての深さにおいて主に8月（2002年のみ9月）に見られ，深さ0.5 mでは24.7±0.8℃（1993年）から27.3±1.1℃（1986年），深さ2.0 mでは24.2±0.8℃（1993年）から26.9±1.1℃（1986年），深さ5.0 mでは24.0±1.4および24.0±0.7℃（1982年および1993年）から26.6±0.9℃（1994年）の間で変動した（Fig. 6）。年間変動（最高−最低）は深さ0.5 mでは9.9℃（1998年）から14.4℃（1986年），2.0 mでは9.5℃（1997年）から13.7℃（1986年），5.0 mでは9.3℃（1995年）から13.3℃（1986年）であり，深さ0.5 mにおける変動幅が大きく，反対に，深さ5.0 mにおける変動幅は小さかった（Fig. 6）。月平均最低海水温の上昇速度は，深さ0.5 mでは0.078℃ yr^{-1}，2.0 mでは0.079℃ yr^{-1}，5.0 mでは0.067℃ yr^{-1}であり（Table 3），全ての深さで有意な上昇傾向を示した（$p<0.05$）。月平均最高海水温の上昇速度は，深さ0.5 mでは-0.015℃ yr^{-1}，2.0 mでは-0.012℃ yr^{-1}，5.0 mでは0.005℃ yr^{-1}であり（Table 3），深さ0.5 mおよび2.0 mは有意ではないが低下傾向，深さ5.0 mは有意ではないが僅かな上昇傾向が見られた。そして，全ての深さで最低海水温の上昇速度が最高海水温の上昇速度を大きく上回っていたため，年間変動の幅は1981年から2004年にかけて有意に小さくなった（Fig. 6；$p<0.05$）。

各月の平均海水温を平年値との偏差で表すと（1981年から2004年にかけての各月，各深さの平均海水温を

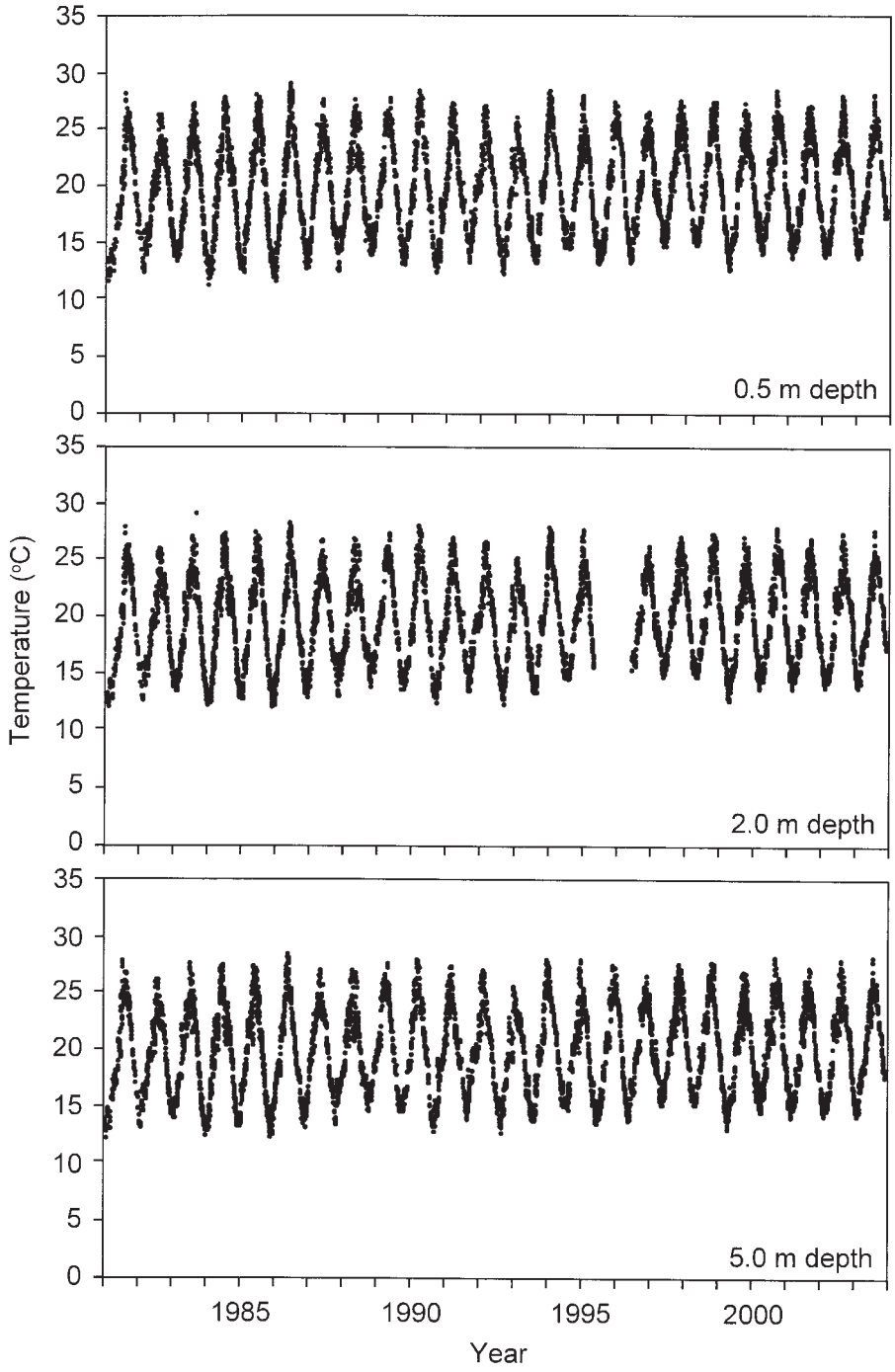

Fig. 2. Time series of original temperature data at Shitaba, Uwajima along the coast of Uwa Sea between 1981 and 2004.

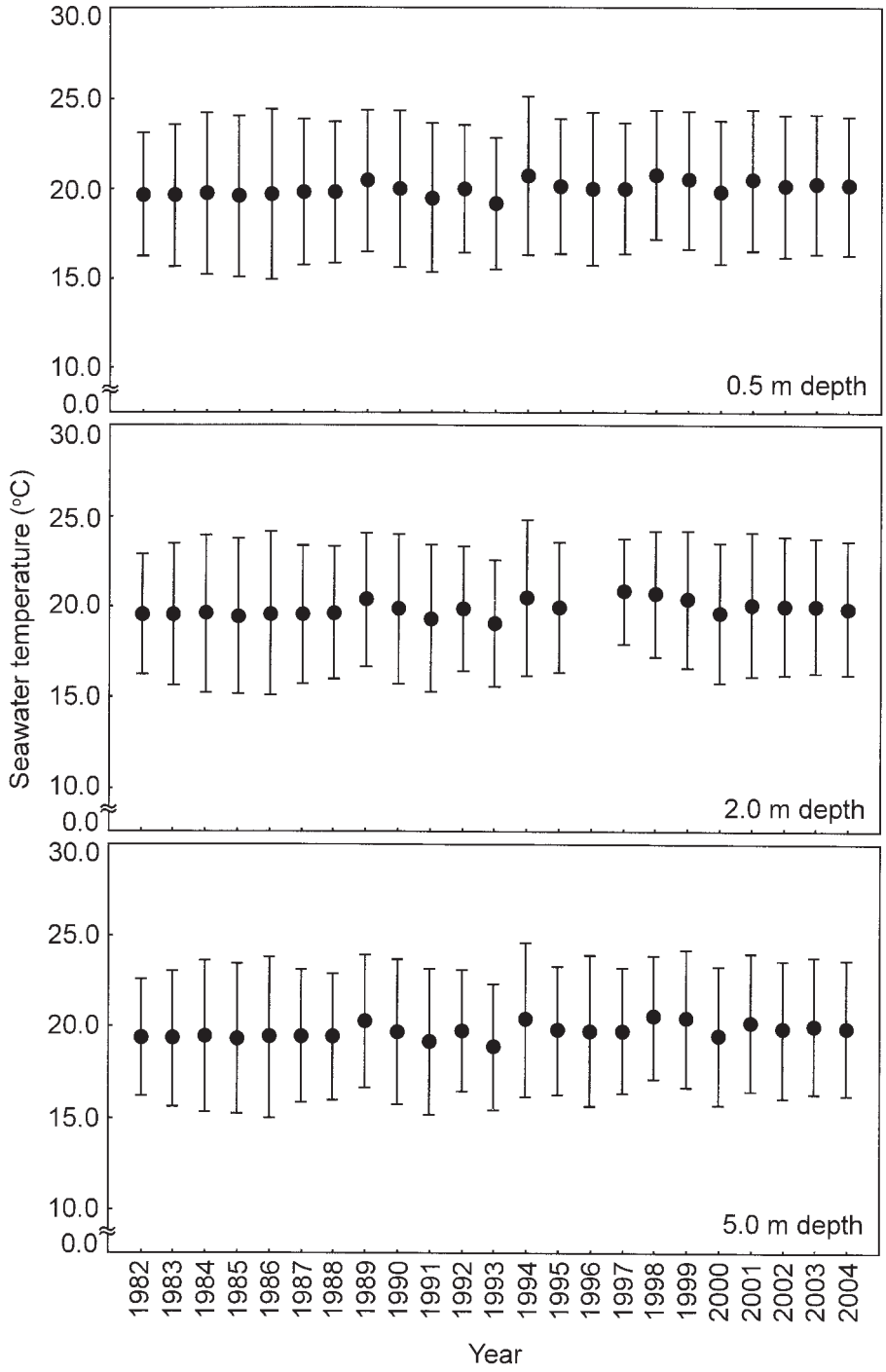

Fig. 3. Annual mean seawater temperature at Shitaba, Uwajima along the coast of Uwa Sea between 1982 and 2004. Vertical lines indicate standard deviations.

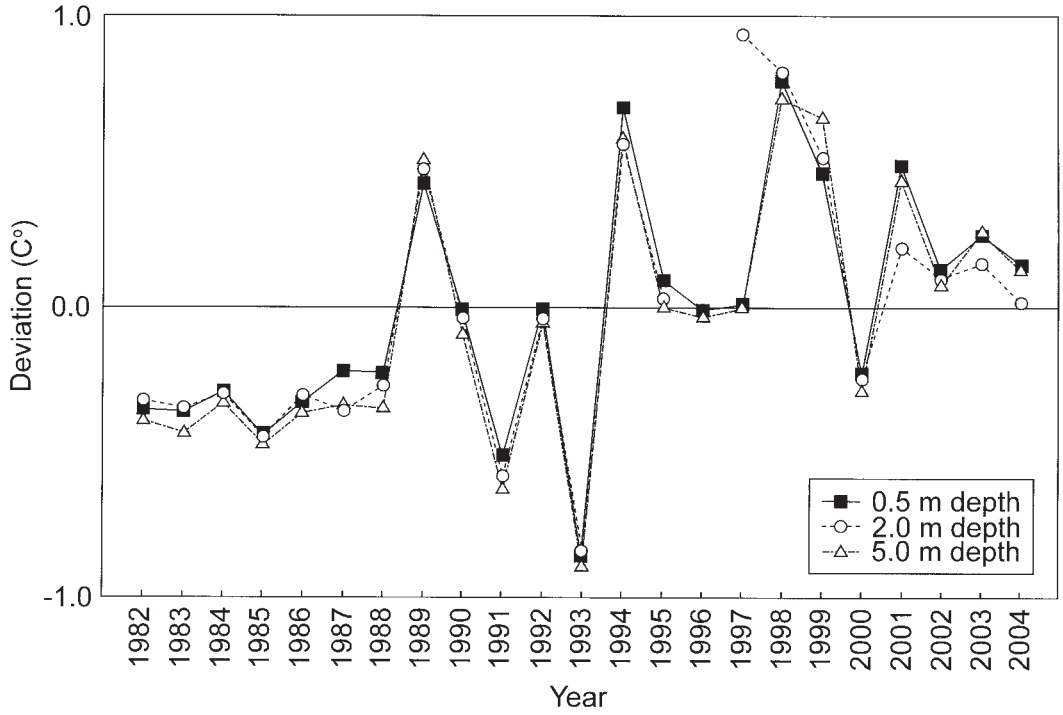

Fig. 4. Deviation in mean annual seawater temperature at Shitaba, Uwajima along the coast of Uwa Sea between 1982 and 2004. The mean from 1982 to 2004 has been set to zero.

0とした），全ての深さで冬季（12月，1月および2月）の海水温上昇が顕著であり，夏季（6月，7月および8月）はほとんど上昇が見られなかった（Fig. 7）。冬季の海水温はすべての深さで有意に上昇しており（$p<0.05$），その上昇速度は，深さ0.5 mで0.074℃ yr^{-1}，深さ2.0 mで0.064℃ yr^{-1}，深さ5.0 mで0.059℃ yr^{-1}であった。夏季の上昇速度は，有意ではないが深さ0.5 mで0.013℃ yr^{-1}，深さ2.0 mで0.007℃ yr^{-1}，深さ5.0 mで0.022℃ yr^{-1}であり，特に8月に関しては全ての深さで低下傾向を示した（Table 4）。

以上より，愛媛県宇和島市下波における海水温は，全ての深さにおいて年平均レベルでも上昇傾向を示しているが，特に冬季の海水温上昇が著しく，夏季はほぼ一定で推移しているという傾向が見られた。

4. 考察

地球温暖化によると考えられる海水温の上昇は世界各地で報告されており，カリブ海の大部分の地域では1980年頃から，インド洋から太平洋にかけては1970年代頃から海水温上昇が確認され始めた（Sheppard and Rioja-Nieto, 2005）。熱帯域では，1998年以降，オーストラリアのグレートバリアリーフ等の広範囲な海域で水温上昇がおこり，グレートバリアリーフでは大規模なサンゴ礁の白化が観測されている（Berkelmans and Oliver, 1999）。温帯域でも，北大西洋沿岸のフランス北部のGravelinesでは1990年以降，冬季の最低海水温および夏季の最高海水温が以前と比較して高く推移し（Woehrling *et al.*, 2005），また，イギリス南部のPlymouthでは1990年以降急激な海水温上昇が確認されるようになった（Hawkins *et al.*, 2003）。

本研究では，愛媛県宇和島市下波における1981年か

Table 4 Increase of mean seawater temperature in each month from 1981 to 2004.

Depth (m)	Increase (℃ yr^{-1})											
	Jan.	Feb.	Mar.	Apr.	May	Jun.	Jul.	Aug.	Sept.	Oct.	Nov.	Dec.
0.5	0.081	0.070	0.052	0.021	0.024	0.035	0.002	−0.016	0.049	0.037	0.038	0.072
2.0	0.066	0.067	0.052	0.024	0.017	0.040	0.0004	−0.019	0.050	0.036	0.028	0.060
5.0	0.070	0.057	0.046	0.024	0.032	0.055	0.019	−0.007	0.060	0.038	0.027	0.050

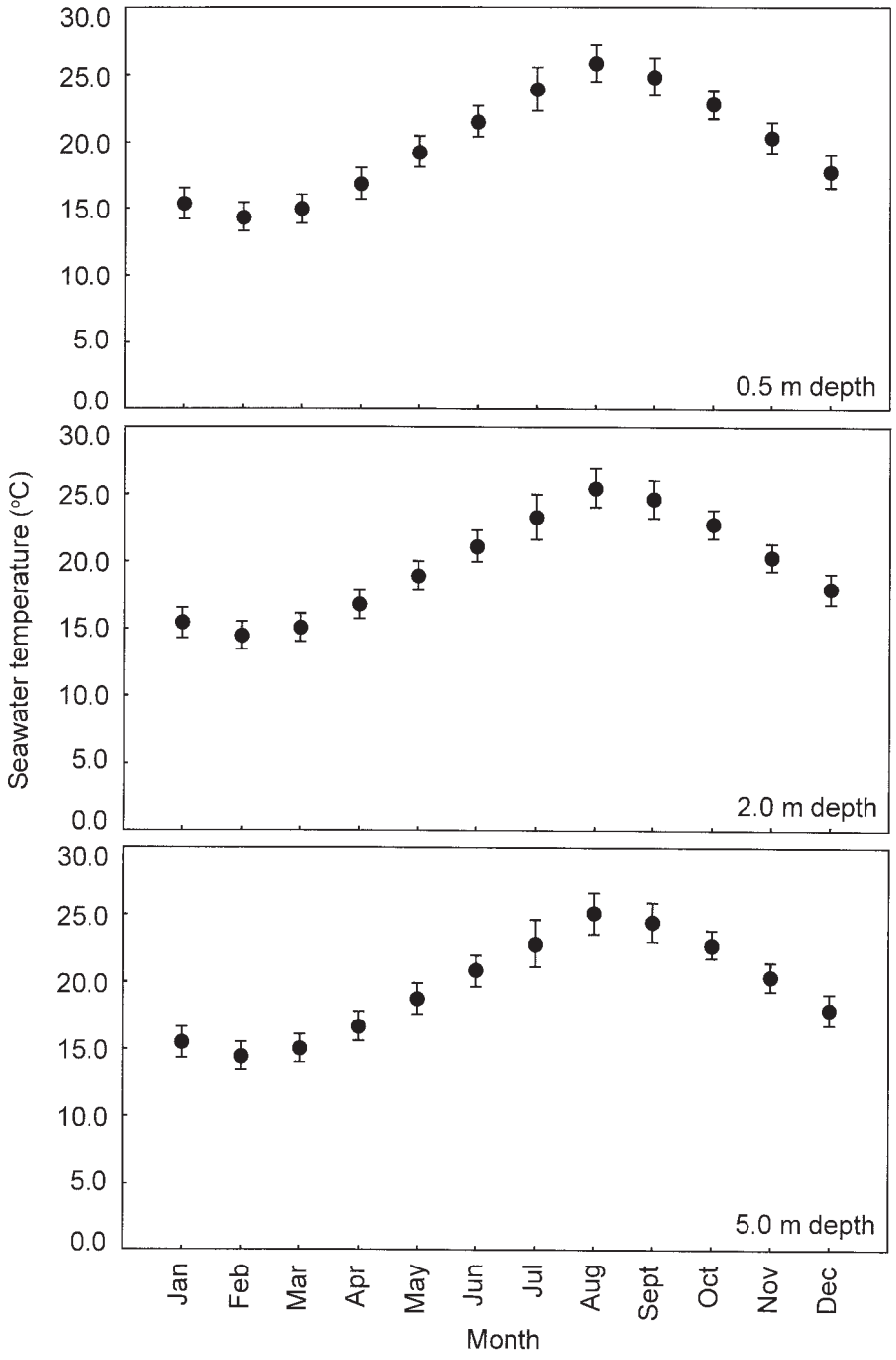

Fig. 5. Seawater temperatures averaged each month over 24 yr at Shitaba, Uwajima along the coast of Uwa Sea. Vertical lines indicate standard deviations.

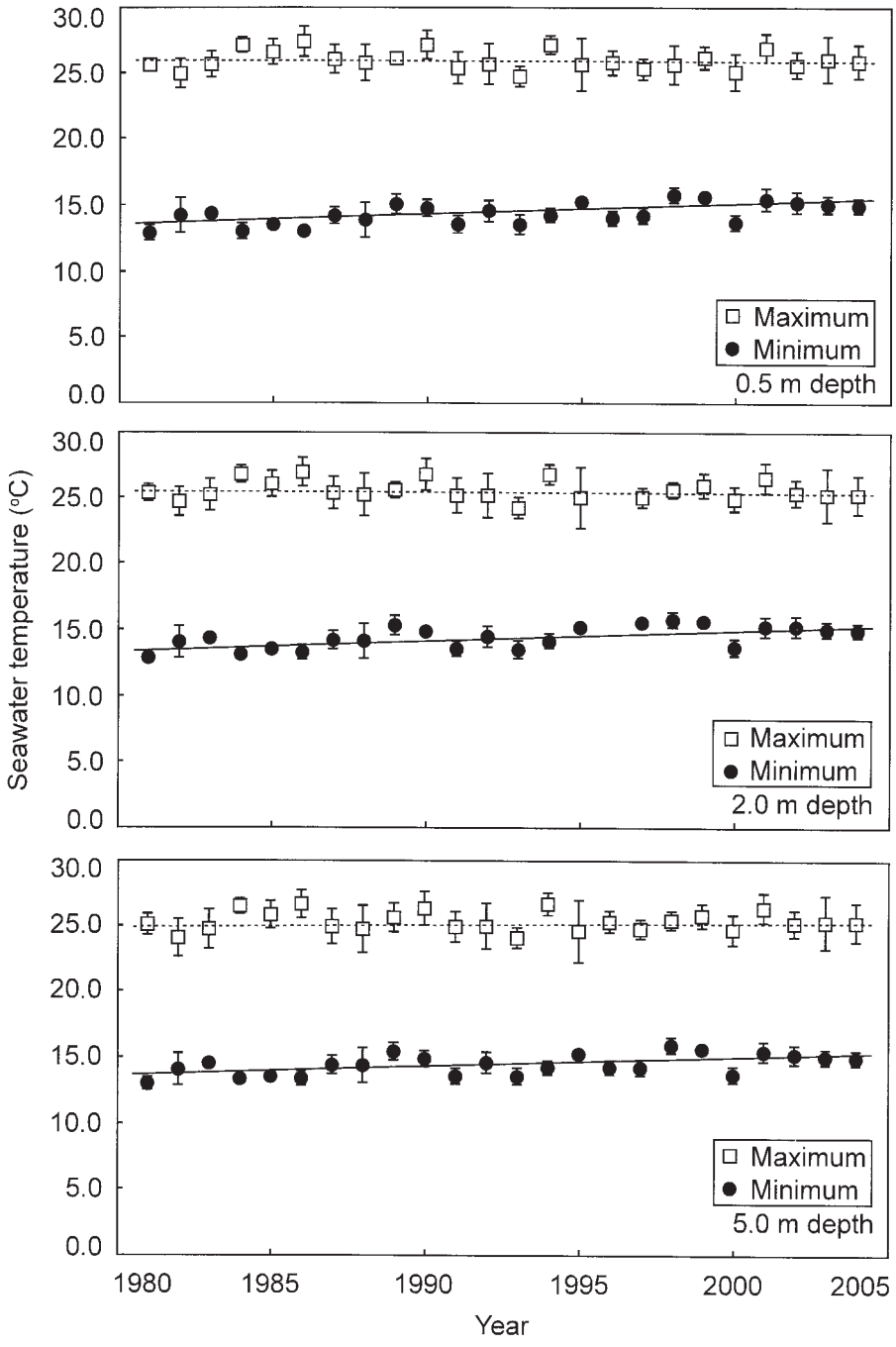

Fig. 6. Monthly average maximum and minimum seawater temperatures in each year at Shitaba, Uwajima along the coast of Uwa Sea coast from 1981 to 2004. Vertical lines indicate standard deviations.

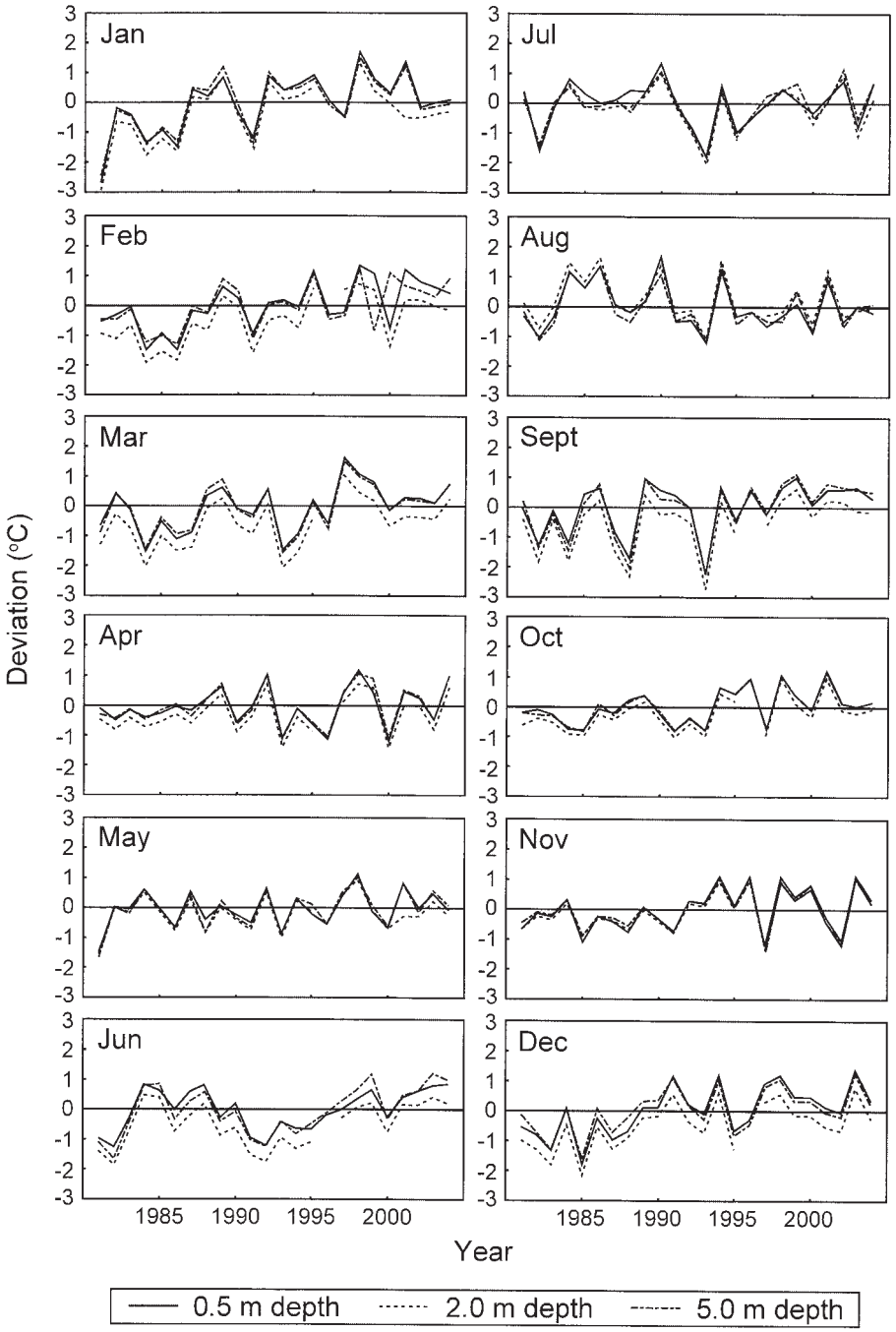

Fig. 7. Deviation in mean monthly seawater temperature at Shitaba, Uwajima along the coast of Uwa Sea between 1981 and 2004. The mean at each month from 1981 to 2004 has been set to zero.

ら測定されている海水温データを解析したが，海水温上昇は24年間（年平均水温に関しては23年間）を通して直線的であり，北大西洋沿岸などで報告されたような（Hawkins *et al.*, 2003; Woehrling *et al.*, 2005），1990年前後の海水温上昇の傾向が変化する顕著な点（変節点・変曲点）は確認されなかった。気象庁（2006）は，全球平均の海面水温は地球温暖化等の影響によって毎年0.005℃の割合で上昇し，特に1990年代中頃以降，高温となる年が頻出していると報告している。それぞれの地域における海水温の上昇率は，Plymouthでは1980年から2000年にかけての20年間で約0.9℃（Hawkins *et al.*, 2003），カリブ海バハマでは1980年から2000年にかけての20年間で約0.4℃（Sheppard and Rioja-Nieto, 2005）であった。本研究の海水温データが測定された宇和島市下波の沖合に位置する豊後水道南部および北に位置する斎灘では，1968年より試験船によるほぼ毎月１回の定線調査が行われている（宇野, 2004）。1964年から2002年の61ヶ月移動平均値は，1970年代後半はやや高めで，1980年代前半の低温期間を経て，1980年代後半以降上昇傾向にあった。1980年から1999年までの20年間では，豊後水道南部で1.1℃，斎灘で0.9℃であった（宇野, 2004）。また，1985年から2003年にかけて，南西諸島から日本海で0.01–0.06℃ yr^{-1}，東海沖や関東東方沖では0.1℃ yr^{-1}の上昇率を記録した（気象庁, 2004）。以上の日本沿岸の研究と比較すると，本研究では20年間で約0.66℃（１年当たり約0.033℃）の上昇率となることから（Fig. 3, Table 1），少し低い傾向が認められた。

宇和島市下波における月ごとの年代別海水温を詳しく分析すると，冬季の海水温上昇が顕著であり，その速度は0.059℃ yr^{-1}（深さ5.0 m）から0.074℃ yr^{-1}（深さ2.0 m）であり，24年間では1.4℃（深さ5.0 m）から1.8℃（深さ2.0 m）の上昇に相当する。一方，夏季における水温上昇は，0.007℃ yr^{-1}（深さ2.0 m）から0.022℃ yr^{-1}（深さ5.0 m）であったが有意差は認められず，特に８月に関しては全ての深さで低下傾向を示した。そのため，冬季の海水温上昇速度は夏季の３–９倍に相当することが明らかになった。

我々は本研究の対象である宇和島市下波の北東約５kmに位置する宇和島市遊子沖にて，2001年12月以来月２回のSTD（AST200-PK; Alec Electronics Co., Ltd.）を用いた水温・塩分の長期海洋モニタリングを実施している。2001年12月から2003年８月までの深さ１–３mの塩分は，12月から２月までの冬季の塩分は高く（34.47±0.15），６月から８月までの夏季は低い（33.94±0.27）傾向が明らかになった（Suzuki *et al.*, 2006）。黒潮の塩分は34.5であることから，このモニタリング結果は，冬季には宇和海沿岸の中部に位置する宇和島市沿岸一帯まで暖かい黒潮系水が長期間にわたり流入し続けていることを示している。また，平岡ら（2005）は高知県土佐湾沿岸における水温上昇の概要を報告している。土佐湾は本研究海域から東に約100 kmの地点に位置する極めて開放的な湾であり，黒潮の影響を強く受けている。土佐湾の年別表層水温の偏差は－0.7℃（1965年）から1.5℃（2002年）の間で変動し，70年代でやや高く，80年代で低く，90年代は高く維持されており，土佐湾における沿岸水域の水温上昇は湾内への黒潮の流入量に関連するのではないかと考察している。また，近年，黒潮が九州・四国沖に接岸傾向にあり，宇和海への黒潮系水の流入が増加していることも報告されている（兼田ら, 2002）。以上より，黒潮が九州・四国の沿岸域に接岸する傾向があることが冬季の顕著な水温上昇の要因の１つであると推察される。さらに，Sakamoto *et al.*（2005）は黒潮の流速は地球温暖化によって増加することを予測しており，今後も宇和海への黒潮系水流入の増加傾向は続く可能性が高いと考えられる。

本研究の観測地点である宇和島市下波の沖合に位置する豊後水道では，夏季には上層に海面加熱と黒潮側からの水平的な加熱による暖水層の形成と，陸棚斜面に起源をもつ冷水が下層に進入する現象（bottom intrusion）によって冷水層が形成されていることが報告されている（兼田ら, 2002; Kaneda *et al.*, 2002等）。黒潮が九州東岸から豊後水道にかけて接岸して流れているときはbottom intrusionが強く，豊後水道の水温が低下し，反対に離岸して流れているときはbottom intrusionが弱く，水温が上昇する。黒潮が離岸傾向をとった1999年はbottom intrusionが発生しなかったため，豊後水道の海水温は例年よりも約２℃高くなった。同様に，黒潮が離岸傾向を示した1974，75，77–79，86，89，94，95年も99年の海水温と同程度かそれ以上の高温であった。bottom intrusionの強度は1980年代後半から弱体化し，1990年代後半から再び強くなっている（Takeoka *et al.*, 2000）。以上の研究より，近年，黒潮が接岸傾向にあるため，夏季には水温が低いbottom intrusionの豊後水道への侵入が強くなっていることが示される。そのために黒潮の影響が増大する傾向にあるものの，宇和海沿岸域では，夏季の海水温が低下傾向またはほぼ一定となっていることが推察される。

従来，水温上昇の沿岸域生態系における影響評価は，熱帯域のサンゴ礁生態系における研究が中心であった。グレートバリアリーフ等のサンゴ礁生態系では，夏季の最高水温が１℃上昇するだけで，サンゴに共生する褐中藻類の光合成量が減水し，サンゴが白化をおこし，斃死にいたることが報告されている（Jokiel and Coles, 1990; Berkelmans and Oliver, 1999等）。また，日本沿岸では，1990年代後半より静岡県から九州西岸沿岸一帯で，アイゴやブダイ等の藻食性魚類の被食によるアラメ・カジメ群落等の藻場の消失が多数報告されるようになり（桐山ら, 1999, 2002; 中山・新井,

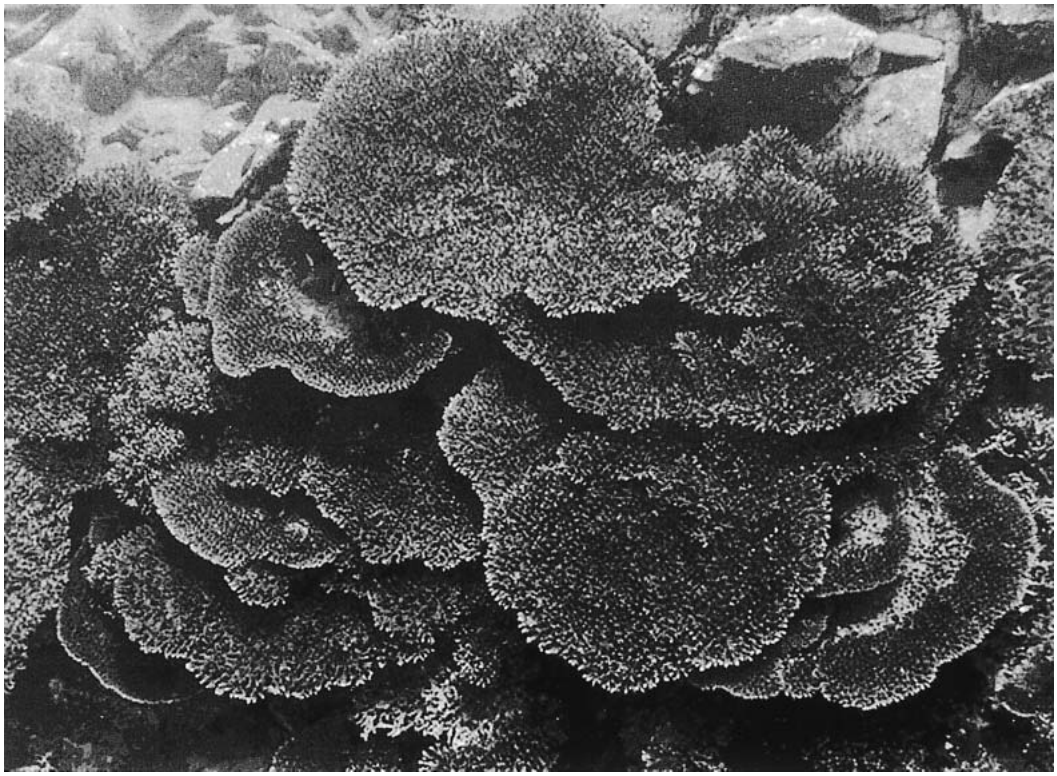

Fig. 4. Coral reef community found at the southern coast of Uwajima, the Uwa Sea (Photographed by I. Takeuchi on December, 2006).

1999; 清本ら, 2000; 長谷川ら, 2003等), 水温上昇が魚類の活動を活発化させていることが考えられる。本研究では, 宇和海沿岸では冬季における水温上昇が顕著であることが明らかになった。2004年に発刊された「日本のサンゴ礁」では, 宇和海沿岸の岩礁域にはサンゴが分布するものの, 高い被度でサンゴが分布するのは西海町（現在の愛南町）以南であると報告されている（岩瀬, 2004)。しかし, 2006年12月に実施した我々の予備的な調査では, 愛南町の北に位置する宇和島市南部でも大規模なサンゴ群落が出現していることが確認された（Fig. 8)。宇和島市遊子沖では, 2004年以降, 熱帯性のミドリイガイが出現し始めており, また, 2001–2003年にはロープ1 mあたり33–34 kg（湿重量）あった養殖コンブの生産量も2003–2005年には約1/10に減少しており, 12月から1月にかけての冬季の水温上昇の影響が考えられた（Suzuki *et al.*, MS)。よって, 宇和海沿岸では, 冬季の水温上昇により, 従来越冬できなかった熱帯あるいは亜熱帯性の海洋生物が越冬可能となり, 逆に温帯性の生物の一部は冬季の最低水温の上昇に耐えられず, 生態系を構成する生物群集の組成が大きく変動しはじめていることが考えられる。

以上の結果をまとめると, 宇和海沿岸の海水温の上昇速度は他の地域よりも低いものの, 冬季の上昇速度は0.059–0.074℃ yr^{-1}と顕著であった。冬季は黒潮系水の大幅な流入の影響を強く受けており, また, 黒潮の流速は地球温暖化によって増加することが予測されていることから（Sakamoto *et al.*, 2005), 今後も地球温暖化が続くならば宇和海に流入する黒潮系水の影響も増加し, 海水温の上昇速度が速まることが予想される。一方, 夏季は黒潮によって引き起こされる冷却効果のあるbottom intrusionの影響下にあり, もしbottom intrusionがこの海域に存在しなければ, 海水温の上昇速度は本研究で求められたものよりもさらに速くなっていた可能性がある（1.1から1.5倍程度)。即ち, 宇和海の水温上昇はbottom intrusionによって緩和されていると考えられる。2100年には地球の平均気温は1.4–5.8℃上昇することが予測されており（IPCC, 2001), 前述したように黒潮の影響も増大することが予想されることから, 宇和海沿岸域では, 海水温は冬季を中心に今後も上昇し続けることが考えられる。

謝辞

本水温データを提供していただいた愛媛県水産試験場, データ解析に関してご助言いただいた愛媛大学農

学部若松伸司教授及び同大学沿岸環境科学研究センター兼田淳史博士，本論文に関して様々な有意義な意見をいただいた2名の匿名の査読者に深くお礼申し上げる。

文献

BERKELMANS, R. and J.K. OLIVER (1999): Large-scale bleaching of corals on the Great Barrier Reef. Coral Reefs, **18**, 55–60.

COLES, S.L. and B.E. BROWN (2003): Coral bleaching-capacity for acclimatization and adaptation. Adv. Mar. Biol., **46**, 183–223.

長谷川雅俊, 小泉康二, 小長谷輝夫, 野田幹雄 (2003): 静岡県榛南海域における磯焼けの持続要因としての魚類の食害. 静岡県水産試験場研究報告, **38**, 19–25.

HAWKINS, S.J., A.J. SOWTHWARD and M.J. GENNER (2003): Detection of environmental change in a marine ecosystem - evidence from the English Channel. Sci. Total Environ., **310**, 245–256.

平岡雅規, 浦 吉徳, 原口展子 (2005): 土佐湾沿岸における水温上昇と藻場の変化. 海洋と生物, **27** (5), 485–493.

IPCC (2001): Climate Change 2001: The Scientific Basis. Cambridge University Press, 881pp.

岩崎伸一, 松浦知徳, 渡辺 勲 (2002): 地殻変動を除去した長期海水位変動と海面水温の関係―本州沿岸域―. 海の研究, **11** (5), 529–542.

岩瀬文人 (2004) 日本各地のサンゴ礁の現状 6－2－4 四国. 日本のサンゴ礁（環境省・日本サンゴ礁学会編), 財団法人 自然環境研究センター, 東京, p.266–277.

JOKIEL, P.L. and S.L. COLES (1990): Response of Hawaiian and other Indo-Pacific reef corals to elevated temperature. Coral Reefs, **8**, 155–162.

JOKIEL, P.L. and E.K. BROWN (2004): Global warming, regional trends and inshore environmental conditions influence coral bleaching in Hawaii. Glob. Chan. Biol., **10**, 1627–1641.

兼田淳史, 乗松桂輔, 渡辺浩三, 小泉喜嗣, 武岡英隆 (2002): 黒潮の離接岸が豊後水道の水温に与える影響. 沿岸海洋研究, **39** (2), 181–188.

KANEDA, A., H. TAKEOKA, E. NAGAURA and Y. KOIZUMI (2002): Periodic intrusion of cold water from the Pacific Ocean into the bottom layer of the Bungo Channel in Japan. J. Oceanogr. **58**, 547–556.

桐山隆哉, 藤井明彦, 吉村 拓, 清本節夫, 四井敏雄 (1999): 長崎県下で1998年秋に発生したアラメ類の葉状部欠損現象. 水産増殖, **47** (3), 319–323.

桐山隆哉, 藤井明彦, 四井敏雄 (2002): 長崎県下で広く認められたヒジキの生育阻害の原因. 水産増殖, **50** (3), 295–300.

気象庁 (2004): 報道発表資料 日本沿岸の海面水位の長期変化について ―海面推移変化は海洋内部に原因―. 4 pp.

気象庁 (2005): 2.4.2. 日本の海面水位の変化. 異常気象レポート2005. http://www.data.kishou.go.jp/climate/cpdinfo/climate_change/2005/2.4.2.html

気象庁 (2006): 海面水温の長期変化傾向（全球平均). http://www.data.kishou.go.jp/kaiyou/shindan/a_1/glb_warm/glb_warm.html

清本節夫, 吉村 拓, 新井章吾, 桐山隆哉, 藤井明彦, 四井敏雄 (2000): 長崎県野母崎において1998年秋に発生したクロメ葉状部欠損現象の経過観察. 西海区水産研究所研究報告, **78**, 57–65.

中山恭彦, 新井章吾 (1999): 南伊豆・中木における藻食性魚類3種によるカジメの採食. 藻類, **47**, 105–112.

SAKAMOTO, T.T., H. HASUMI, M. ISHII, S. EMORI, T. SUZUKI, T. NISHIMURA and A. SUMI (2005): Responses of the Kuroshio and the Kuroshio Extension to global warming in a high-resolution climate model. Geophys. Res. Lett., **32** (14), L14617, 10.1029/2005GL023384.

SHEPPARD, C. and R. RIOJA-NIETO (2005): Sea surface temperature 1871–2099 in 38 cells in the Caribbean region. Mar. Environ. Res., **60**, 389–396.

SUZUKI, S., K. FURUYA and I. TAKEUCHI (2006): Growth and annual production of the brown alga *Laminaria japonica* (Phaeophyta, Laminariales) introduced into the Uwa Sea in southern Japan. J. Exp. Mar. Biol. Ecol. **339**, 15–29.

SUZUKI, S., K. FURUYA, T. KAWAI and I. TAKEUCHI (MS): Effect of seawater temperature on the production of *Laminaria japonica* in the Uwa Sea, southern Japan. (Submitted)

TAKEOKA, H., Y. KOIZUMI and A. KANEDA (2000): Year-to-year variation of a *kyucho* and a bottom intrusion in the Bungo Channel, Japan. *In* Interactions between Estuaries, coastal seas and shelf seas. YANAGI, T. (ed.), Terra Scientific Publishing Company (TERRAPUB), Tokyo, p.197–215.

友定 彰 (2002): 海洋観測の継続を期待する. 月刊 海洋, **34** (11), 751–756.

宇野奈津子 (2004): 愛媛県における海洋モニタリング. 月刊 海洋, **36** (1), 31–34.

WOEHRLING, D., A. LEFEBVRE, G. LE FÈVRE-LEHOËRFF and R. DELESMONT (2005): Seasonal and longer term trends in sea temperature along the French North Sea coast, 1975 to 2002. J. Mar. Biol. Ass. U.K., **85**, 39–48.

Received November 6, 2006
Accepted May 2, 2007

La mer 45 : 47-58, 2007
Société franco-japonaise d'océanographie, Tokyo

Vertical distribution and feeding ecology of a copepod *Gaetanus variabilis* in the southern Japan Sea during winter

Atsushi YAMAGUCHI[1], Susumu OHTSUKA[2], Kazumasa HIRAKAWA[3], Tsutomu IKEDA[1]

Abstract: Vertical distribution, gut fullness and gut contents were investigated on an aetideid copepod *Gaetanus variabilis* during winter at a station in the southern Japan Sea. Most individuals of C3-C6 (adult) *G. variabilis* were distributed between 500 and 1000 m depth. While early copepodid stages resided deeper than older ones, no diel vertical migration was detected throughout the copepodid stages. Feeding activity of *G. variabilis* as judged by gut fullness scores varied with developmental stage/sex, but no diel feeding rhythm was observed. Adult males cease feeding as a reflection of degeneration of their feeding appendages. The gut content analysis showed that *G. variabilis* is a particle feeder consuming mainly upon silicoflagellates, followed by diatoms, tintinnids and fragments of metazooplankton. An estimated daily ration of *G. variabilis* population based on calculated metabolic rates was 5.03 mg C m^{-2} day^{-1}, which accounts for 4.5% of the local primary production or 54% of particulate organic carbon flux down to the 500 m depths at southern Japan Sea.

Keywords: *gut content, daily ration, mesopelagic, copepods, Japan Sea*

1. Introduction

While a large body of information about feeding of pelagic copepods has been accumulated on epipelagic and neritic species, little is known about those living in the deep-sea (cf. review of MAUCHLINE, 1998). From the viewpoint of global carbon cycle, biological mineralization of organic carbon in the mid- to deep-ocean is thought to be a key process. Since a significant portion (17–60%) of planktonic respiration is hypothesized to occur in the mesopelagic layer (BIDDANDA and BENNER, 1997; HERNÁNDEZ-LEÓN and IKEDA, 2005), accurate information about plankton feeding in the deep ocean is needed to evaluate the role of zooplankton in mineralization of organic carbon in the deep-sea.

The family Aetideidae is a medium to large-sized calanoid copepods inhabiting mesopelagic to bathypelagic zones of the world oceans. Aetideid copepods feed on both phytoplankton and zooplankton, and are characterized as mixed feeders or detritivores (MATTHEWS, 1964; ARASHKEVICH, 1969). AUEL (1999) estimated that ingestion rates of aetideid copepods to be 1.6 ± 0.1 g C m^{-2} yr^{-1} in the 500–2000 m depth in the Greenland Sea, which accounts >40% of the available carbon supply in mesopelagic layers. In the Swedish fjord, BÅMSTEDT (1981) noted that among carnivores the aetideid copepods has the highest annual mean energy requirement (43% of carnivorous energy flow). Both studies show that the aetideid copepods play a important role in material cycle and mineralization, mediating particulate matter flux in the mesopelagic zones of high latitude seas.

In the Japan Sea, the species-diversity of

1: Laboratory of Marine Biodiversity, Graduate School of Fisheries Sciences, Hokkaido University, 3-1-1 Minatomachi, Hakodate, Hokkaido 041-8611, Japan
2: Takehara Marine Science Station, Setouchi Field Science Center, Graduate School of Biosphere Science, Hiroshima University, 5-8-1 Minatomachi, Takehara, Hiroshima 725-0024, Japan
3: Hokkaido National Fishery Research Institute, 116 Katsurakoi, Kushiro, Hokkaido 085-0802, Japan

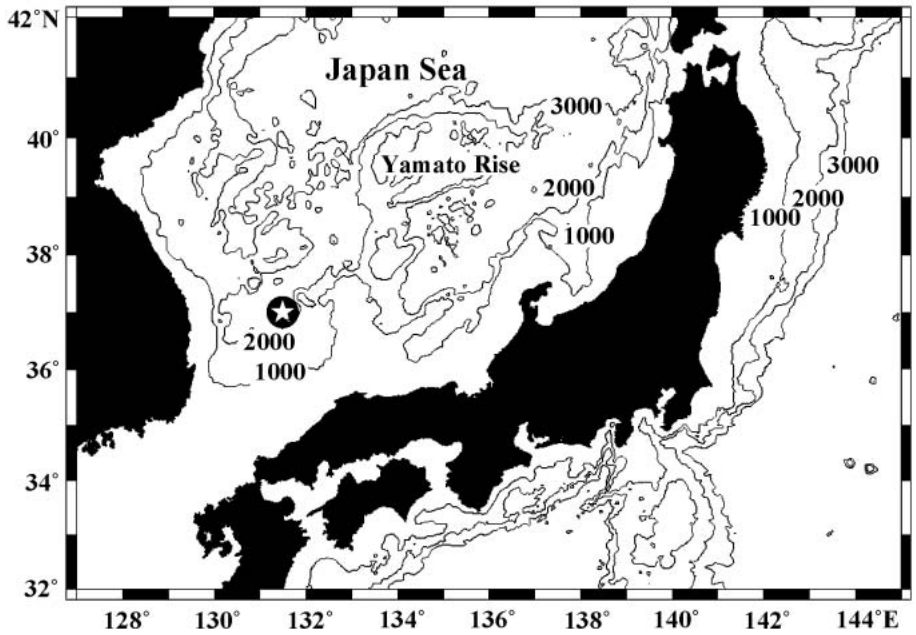

Fig. 1. Location of sampling station (circled star) in the southern Japan Sea. Depth contours (1000, 2000, and 3000 m) are superimposed.

zooplankton at depth is known to be much less than those in the adjacent regions of the North Pacific (VINOGRADOV, 1973). This is largely due to the lack of bathypelagic species in the Japan Sea, because of the connecting straits between Japan Sea and western North Pacific are shallow (<130 m) (ZENKEVITCH, 1963). In the southern Japan Sea, the number of pelagic copepod species is reported to be 62 (TAKAHASHI and HIRAKAWA, 2001) or 87 (HIRAKAWA *et al.*, 1990). Among them, only 15 species are known to occur in the mesopelagic zone of the Japan Sea (TAKAHASHI and HIRAKAWA, 2001), where characterized by near-zero temperature. Since *Gaetanus variabilis* (=*Gaidius variabilis*) is the only suspension feeding copepod inhabiting the lower mesopelagic zone (cf. HIRAKAWA *et al.,* 1990), it is of great interest to know the function of *G. variabilis* in the vertical material flux in the Japan Sea.

In the present study, we investigated the ecology of *G. variabilis* in the southern Japan Sea, including their vertical distribution, gut contents and gut fullness. We also calculate the daily ration of *G. variabilis* based on their metabolic rates (oxygen consumption) to assess their role in material flux in the mesopelagic zones of the Japan Sea.

2. Materials and Methods

2-1. Sample collection

In 26-27 January 1997, zooplankton samplings were made in the daytime and nighttime with oblique tows of IONESS (mesh size: 330 μm, mouth opening: 1 m^2) through 16 discrete depths between the surface and 1000 m at St. J7 (37°00′N, 131°30′E; 2130 m deep) in the southern Japan Sea (Fig. 1). IONESS (Intelligent Operation Net Environmental Sampling System: SEA Co. Ltd, Japan) is a version of MOCNESS (WIEBE *et al.*, 1985) and capable of collection of eight samples per cast. Consecutive two IONESS casts from 16 depth strata between 1000–900, 900–800, 800–700, 700–600, 600–500, 500–400, 400–300, 300–200, 200–150, 150–100, 100–75, 75–50, 50–30, 30–20, 20–10, and 10–0 m achieved each sampling. Daytime casts were made from 11:54–14:08 (local time) and night casts from 19:22–22:07. Sunrise and sunset of 26 January 1997 was at 07:16 and 17:32, respectively. A flow meter (Rigosha, Japan) was mounted in the mouth of the net to register the

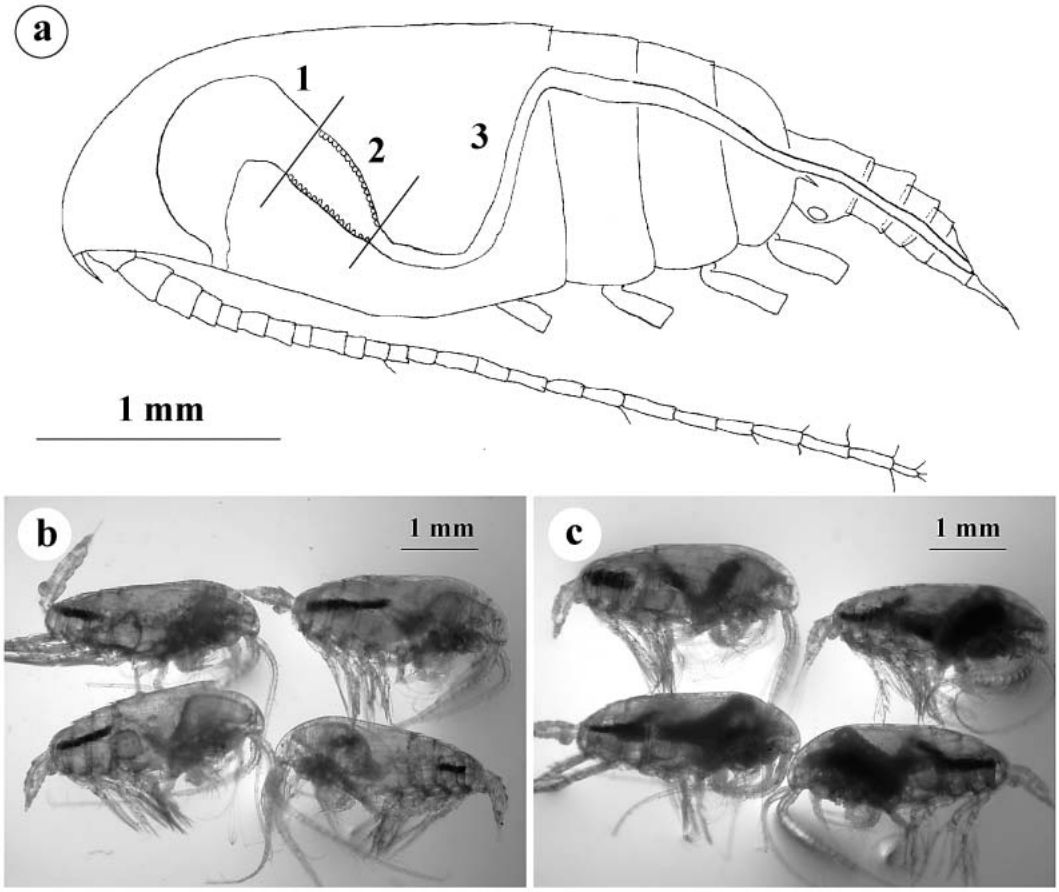

Fig. 2 *Gaetanus variabilis* C6F. (a) Diagram of digestive tract showing three principal zones (1-3). Zones 1-2 were defined as foregut and zone 3 as hindgut in this study. (b) Specimens of which only hindgut filled (gut content score: 3). (c) Specimens of which both foregut and hindgut filled (gut content score: 4). See text for details.

volume of water passing through the net. All zooplankton samples were immediately preserved in 5% borax-buffered formalin-seawater on board. Temperature and salinity data were obtained by a CTD system (SBE 911plus). Water samples were collected from 0, 20, 50, 75, 100, 125, 200, 300, and 500 m depth using water bottles, filtered through Whatman GF/F filters, and chlorophyll *a* was extracted with N, N-dimethylformamide (SUZUKI and ISHIMARU, 1990) and measured using a fluorometer (EP-777, Japan Spectroscopic Inc.). Chlorophyll *a* data were provided by Dr. H. NAGATA (Seikai National Fisheries Research Institute).

2-2. Enumeration

At the land laboratory, *Gaetanus variabilis* specimens were sorted, staged and counted from a 7/8 aliquot. Separation of females (F) from males (M) was possible from copepodid stage 4 (C4) onward (e.g. C4F or C4M). The 330 μm mesh net was considered to retain from C3 onward, as judged by diagonal size (467 μm) of the net used and the cephalosome width of each copepodid stage (mean $\pm$ 1sd, C2: 371$\pm$14; C3: 518$\pm$20; C4F: 686$\pm$57, C4M: 724$\pm$59 μm). Biomass (wet mass) of each copepodid stage was estimated from the prosome length data in YAMAGUCHI *et al.* (2005), combined with wet mass-prosome length relationships of this species (YAMAGUCHI and IKEDA, 2000).

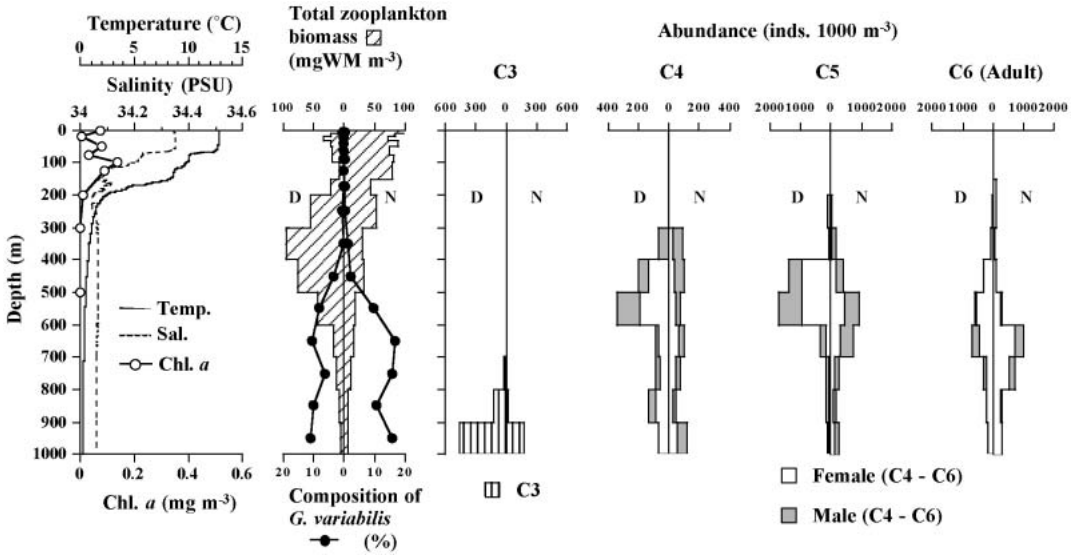

Fig. 3. Vertical distributions of temperature, salinity, and chlorophyll *a* (left), total zooplankton biomass and composition of *Gaetanus variabilis* (middle), and each copepodid stage of *G. variabilis* (middle to right). Female/male determination was done for C4 to C6. D: day, N: night.

Biomass of *G. variabilis* at each sampling stratum was computed from abundance data multiplied by individual wet mass. Percentage composition of *G. variabilis* biomass to the total zooplankton biomass was calculated from total zooplankton wet mass data provided by Dr. N. IGUCHI (Japan Sea National Fisheries Research Institute).

2-3. Gut content and gut fullness analysis

Based on the cellular structure, the gut of copepods was separated into three zones (cf. MAUCHLINE, 1998). Morphology of digestive tract of *Gaetanus variabilis* was semi-looped z-shaped (Fig. 2a), and the zones 1–2 referred as foregut and zone 3 as hindgut in this study. Under a stereomicroscope, the gut fullness of C5 and C6 (adults) was scored into 1–4 (1: gut empty, 2: only foregut filled, 3: only hindgut filled, 4: both foregut and hindgut filled; cf. Fig. 2b, c).

Nighttime samples of *Gaetanus variabilis* C6F from 600–700 m depth, where they were most numerous, were used for gut content analysis. Up to 10 individuals of which guts filled were sorted and rinsed in distilled water for overnight. Their hindguts were carefully removed from the prosome with a pair of fine needles under a dissecting microscope and then rinsed in distilled water. The specimens were placed on a deep hole glass slide filled with distilled water and dissected using fine needles. After removing all remains of the gut wall by means of a pair of tweezers, all gut contents were picked up with a fine pipette and mounted on a small area (within the diameter of a stub) of a Millipore filter with the aid of a vacuum pump. The filter was dehydrated by alcohol series (70, 90, 99 and 100%) and deposited in a decicator overnight. The totally dried filter was trimmed and mounted on a stub, and then ionsputterred. Gut contents from all individuals were mounted together on the stub and observed under a scanning electron microscope (SEM, Joel JSM-T20).

2-4. Estimation of daily ration

Daily ration was calculated from respiration data by the method described by IKEDA and MOTODA (1978). Respiration data used in this calculation were adjusted metabolic rate (*AMR;* range: 3.64–4.21 μl O_2 [body N]$^{-0.85h}$h^{-1}, mean: 3.93) at 0.5℃ (close to *in situ* temperature of the present sampling site, cf. Fig. 3) reported on *Gaetanus variabilis* in the Japan Sea by IKEDA and HIRAKAWA (1998). Dry mass (D

M, μg) of each copepodid stage of *G. variabilis* was computed from the prosome length data (YAMAGUCHI *et al.*, 2005) using an allometry equation (YAMAGUCHI and IKEDA, 2000). Assuming body N content of all *G. variabilis* copepodid stages as 9.8%DM (cf. IKEDA and HIRAKAWA, 1998), respiration rates of each copepodid stage were estimated from the mean *AMR* value. Respiration rates were then converted to carbon units assuming a respiratory quotient ($[CO_2]/[O_2]$) of 0.97 (protein metabolism, cf. GNAIGER, 1983). Carbon budget equation for copepods may be expressed as: Ingestion (*I*) = Growth (G) + Metabolism (*M*) + Egestion (*E*) + Excretion (*U*). Assuming assimilation efficiency ($[G+M]/I$) and gross growth efficiency (G/I) to be 70% and 30%, respectively (cf. IKEDA and MOTODA, 1978), ingestion rates (I: μg C individual^{-1} h^{-1}) can be calculated from M as $I = M/$ (0.7–0.3). The rates were converted to daily basis (x 24 hours), thus estimated ingestion rates were varied from 0.22 μg C ind^{-1} day^{-1} for C1 to 10.26 μg C ind^{-1} day^{-1} for C6F. Since C6M of *G. variabilis* cease feeding (cf. YAMAGUCHI *et al.*, 2005), ingestion rates were not estimated for C6M. Daily ration of individuals in a given depth stratum were summed (μg C m^{-3} day^{-1}) and integrated over 0–1000 m depth range (mg C m^{-2} day^{-1}).

3. Results

3-1. Vertical distribution and abundance

The surface temperature and salinity were 12.5℃ and 34.35PSU, respectively, and both decreased rapidly with increasing depth until 200 m (Fig. 3). Below 200 m, both temperature and salinity were stable at <1.0℃ and 34.05PSU, respectively, indicating the characters of "Japan Sea Proper Water" (cf. SUDO, 1987). Chlorophyll *a* showed a maximum (0.14 mg m^{-3}) at 100 m, then decreased rapidly with depth and was almost nil at 200 m.

Total zooplankton biomass peaked at 300–400 m during day, while at 0–10 m during night (Fig. 3). This day-night shift of total zooplankton biomass was attributed by two large diel vertical migrators: a hyperiid amphipod *Themisto japonica* (cf. IKEDA *et al.*, 1992) and a euphausiid *Euphausia pacifica* (cf. IGUCHI *et al.*, 1993). Biomass of *Gaetanus variabilis* varied between 0 and 3.5 mg WM m^{-3} with depth, and their contribution to the total zooplankton biomass was greater below 500 m depths (6.3–16.7%). In terms of standing stock, biomass of *G. variabilis* was 0.93–1.02 g WM m^{-2} that accounts 2.89-2.92% of total zooplankton biomass integrated over 1000 m (31.8–35.3 g WM m^{-2}).

Gaetanus variabilis was distributed below 150 m both day and night, and no diel changes in the vertical distribution pattern was seen across all copepodid stages (Fig. 3). C1–C3 distributed mainly below 800 m throughout the day. The depth where the 50% population resided ($D_{50\%}$, cf. Pennak, 1943) was 930 m (daytime) or 942 m (nighttime) for C3. On the other hand, C4 was concentrated at 500–600 m throughout the day ($D_{50\%}$ of C4F and C4M was 588-650 m and 537–588 m, respectively). C5 was abundant at 400–600 m extending their vertical distribution to shallower depth than C4 did ($D_{50\%}$ of C5F and C5M was 522–597 m and 537–590 m, respectively). Adult female (C6F) and male (C6M) occurred the shallowest depths (150–200 m), although their populations centered at slightly deeper depth than that of C5 ($D_{50\%}$ of C6F and C6M was 608-681 m and 664–684 m, respectively). Total abundance of C3–C6 stage *G. variabilis* integrated over the 0–1000 m water column was 675–815 individuals m^{-2}. Sex ratios (female:male) were nearly equal for C4 (1.2–1.6:1) and C5 (0.8–1.4:1), but skewed to female for C6 (3.9–5.4:1) (Fig. 3).

3-2. Gut content and daily ration

Gut fullness scores of C5 and C6 *Gaetanus variabilis* varied little between day and night but between stages (Fig. 4). All C6M exhibited empty guts throughout the day. Subsequent observations on feeding appendages of C6M revealed that their maxillae had reduced setae, suggesting that they are unable to feed. For C5F, C5M and C6F, no significant changes in gut fullness scores with depth were observed (Fig. 4). It is noted that the data 200–400 m depths are not accurate because of smaller sample size (n=1–11, cf. Fig. 3).

Observed diet components of *Gaetanus variabilis* were centric diatoms (*Thalassiosira eccentrica* and others), tintiniids (*Parafavella*

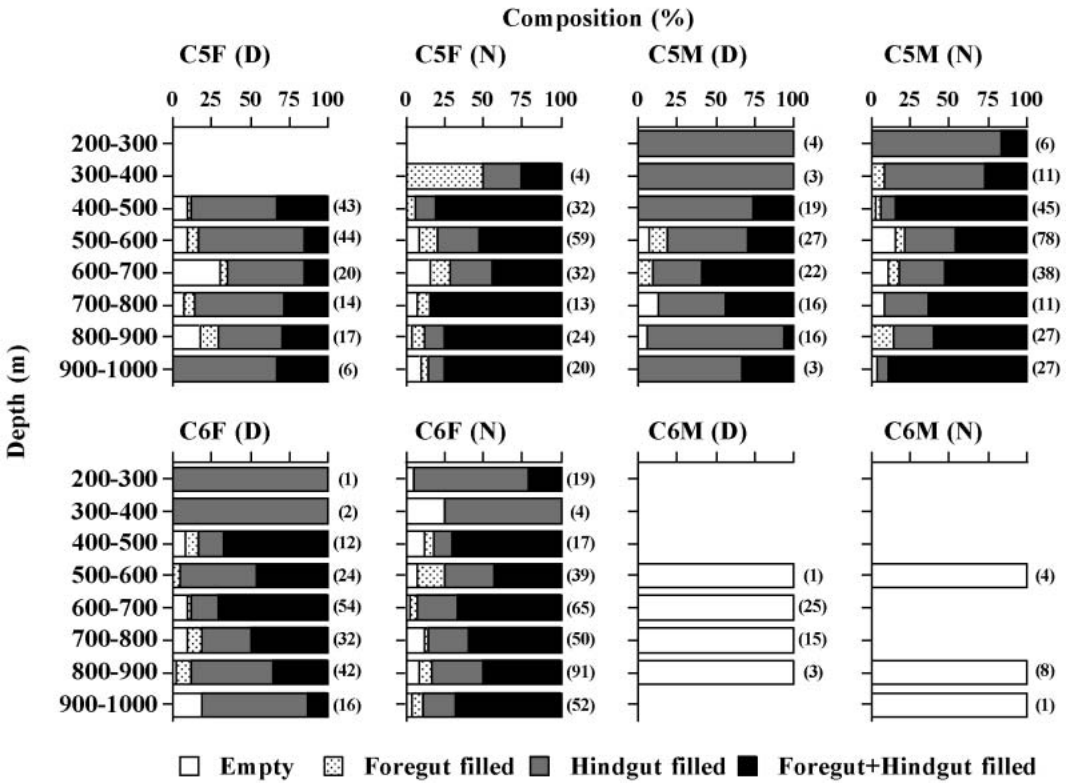

Fig. 4. Vertical distribution of percentage composition of gut content score (1: empty, 2: foregut filled, 3: hindgut filled, and 4: both foregut and hindgut filled) of C5–C6 stages of *Gaetanus variabilis*. Numbers of examined specimens were shown in the parentheses. F: female, M: male; (D): day, (N): night.

sp.), silicoflagellates (*Distephanus speculum*) and fragments of metazooplankton (hook of chaetognaths) (Fig. 5). Silicoflagellates were most numerous (more than 100 cells per stub), followed by centric diatoms (>50), tintiniids (>10) and the fragments of metazoans (<10). It is noted that most of the centric diatom and tintiniid cells were observed being damaged, but silicoflagellate cells were intact.

Vertical profiles of the estimated daily ration of the total of C3-C6 of *Gaetanus variabilis* populations showed a maximum at 500–700 m depth 14.4 μg C m^{-3} day^{-1}, Fig. 6), with an integrated value over the 0–1000 m water column of 5.03 mg C m^{-2} day^{-1}.

4. Discussion

4.1. Vertical distribution

In the Oyashio region, western subarctic Pacific, a reversed (nocturnal descent) diel vertical migration pattern of a modest degree has been reported for *Gaetanus* (=*Gaidius*) *variabilis* (YAMAGUCHI and IKEDA, 2000). However, no such the DVM was observed for the same *G. variabilis* at the station in the southern Japan Sea in this study (Fig. 3). In the northern Norwegian fjord, the vertical behavior of aetideid copepods (*Chiridus armatus*) is reported to be variable, depending on the seasonal change in day/night lengths, and the DVM ceased during the periods of summer midnight sun (no dark period) and winter darkness (no light daytime) (FALKENHAUG *et al.*, 1997). From this view, YAMAGUCHI and IKEDA's earlier study (YAMAGUCHI and IKEDA, 2000) was the compilation of data from all seasons of the year. In contrast, the present results are from January only which corresponds to the annual minimum of day length at this latitude. This difference may be attributed to this dissimilar conclusion for the DVM behavior of *G. variabilis* between these two studies.

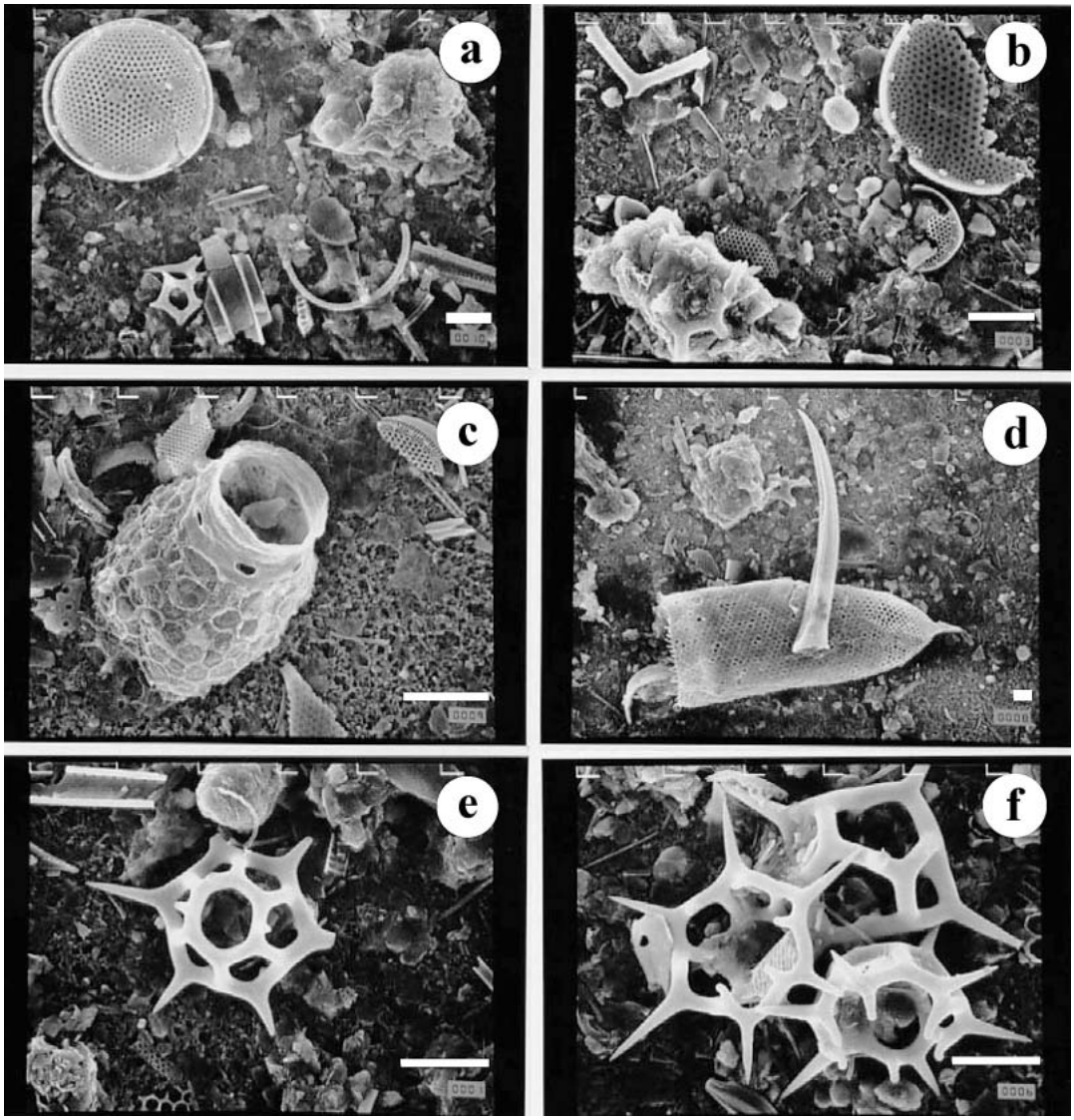

Fig. 5. SEM micrographs of gut contents of *Gaetanus variabilis* C6F. The diatom *Thalassiosira eccentrica* (a, b), tintinnids (*Parafavella* spp.) (c, d), fragment (hook) of chaetognaths (d), and the silicoflagellate *Distephanus speculum* (e, f) are seen. Scale bars indicate 10 μm.

Differential depth distribution patterns across copepodid stages of *Gaetanus variabilis* observed in this study (Fig. 3) suggest possible ontogenetic vertical migration (OVM) of this species characterized by developmental ascent. The OVM pattern and its magnitude of *G. variabilis* estimated in the present study (420 m: 942 m [$D_{50\%}$ of C3] −522 m[$D_{50\%}$ of C5F]) are consistent to those reported at Site H (41°30′N, 145°47′E) in the Oyashio region (337 m, Yamaguchi and Ikeda 2000) and St. KNOT (44°00′N, 155°00′E) in the western subarctic Pacific (543 m, Yamaguchi *et al.*, 2004). The OVM characterized by developmental ascent is a widespread phenomenon in deep-sea copepods (Weikert and Koppelmann, 1993; Richter, 1994; Falkenhaug *et al.*, 1997) and ostracods (Kaeriyama and Ikeda, 2002). The OVM pattern is interpreted as a life history trait or strategy to reduce predation risk. They spend

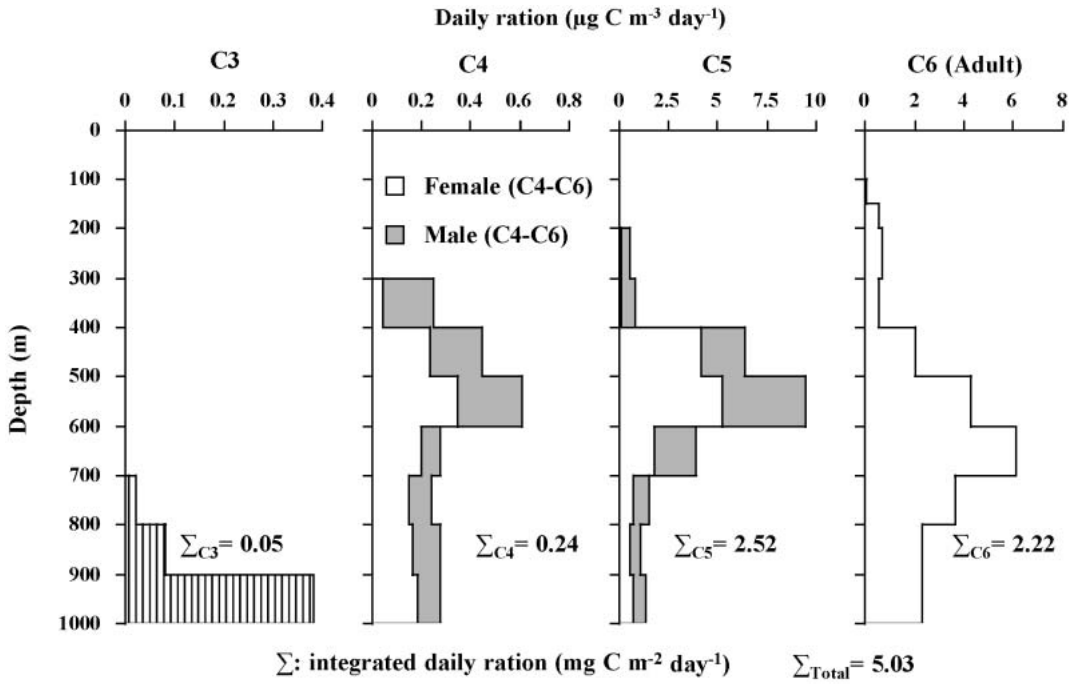

Fig. 6. Vertical distribution of daily ration of each copepodid stage of *Gaetanus variabilis*, and its total integrated over the 0-1000 m water column. Note that daily ration is based on mean abundance of day/night.

the juvenile stages in lower-predation environments (deep layer) and ascend to higher-food environments with development (YAMAGUCHI *et al.*, 2004). Since the lifetime fecundity of deep-sea zooplankton is low in general (cf. MAUCHLINE, 1991), reducing mortality at the juvenile stage is of prime importance for the maintenance of their populations.

4.2. Feeding activity

Observed degeneration of feeding appendages of C6M *Gaetanus variabilis* in this study is a common phenomenon known in aetideid copepods (MATTHEWS, 1964; MACLELLAN and SHIH, 1974). Degeneration of feeding appendages results in cease feeding (Fig. 4), then body mass of C6M becomes less than that of C5M because of its utilization for metabolism and production of spermatophores at C6M. The decrease in the body mass (i.e. negative growth) from C5M to C6M of *G. variabilis* has already been reported by YAMAGUCHI and IKEDA (2000). Longevity of C6M of aetideids is known to be shorter than that of C6F (MATTHEWS, 1964), which is reflected in the skewed sex ratios to females in C6 (Fig. 3).

Diel feeding rhythms characterized by a marked peak at night is a common phenomenon for epipelagic copepods (ATKINSON *et al.*, 1996; SAITO and TAGUCHI, 1996; BESIKTEPE, 2001). Day and night differences in gut fullness of *Gaetanus variabilis* were less marked (Fig. 4). The depth where *G. variabilis* distributed throughout the day (400–800 m, Fig. 3) corresponds to the light intensity of 10^{-3} to 10^{-7} μW cm^{-2} in clearest oceanic water, or the thresholds for daytime predation by fish (10^{-6} μW cm^{-2}) and for phototaxis of copepods (10^{-4} μW cm^{-2}) (MACKIE, 1985). Since feeding copepods are more vulnerable to visual predation than non-feeding copepods, TSUDA *et al.* (1998) hypothesized that the copepods' nocturnal feeding without DVM is advantageous in reducing visual predation by fish. From this view, absence of diel feeding rhythm of *G. variabilis* of this study may be related to the dim light conditions in their habitat depth throughout the day where visual predation risk is considered to be low.

Recently, SCHØYEN and KAARTVEDT (2004)

have revealed spatial and temporal variations of various scales of feeding activities of an another aetideid copepod *Chiridius armatus* by measuring fecal pellet production rates. According to their results, fecal pellet production by adult female *C. armatus* increased at nighttime during the day, in spring season of the year and for those living in shallower depths. Assuming that gut fullness is comparable to fecal pellet production, presence of clear diel feeding rhythm and the effect of depth distribution seen in *C. armatus* may be interpreted by their shallower habitats (<200 m depth) than those of *G. variabilis* (500–1000 m) in this study.

4-3. Gut contents

From the morphology of mouthpart appendages, aetideid copepods are classified to mixed feeders on both animals and plants (ARASHKEVICH, 1969). In the laboratory experiment, OLSEN *et al.* (2000) observed that the aetideid copepod *Chiridius armatus* foraged heavily on dead, non-moving prey, suggesting the use of chemoreceptors in the search for food. Microscopic observation (SEM or TEM) on gut contents of aetideid copepods revealed that "pigmented cells", diatoms, dinoflagellates, coccoliths, cysts and eggs, silicoflagellates, radiolarians and fragments of copepods (HARDING, 1974), or bacteria, olive-green materials, olive-green body/minipellets, siliceous fragments, amorphous materials, and crustacean cuticles (GOWING and WISHNER, 1986; 1992) are major components. HOPKINS and TORRES (1989) examined the gut contents of aetideid copepods (*Gaetanus tenuispinus* and *Euchirella rostromagna*) in the Southern Ocean, and found diatoms, silicoflagellates, dinoflagellates, tintinnids and radiolarians in it. Relative contribution of phytoplankton, protozoans and metazoans in the total diet components of aetideids is reported to be 52, 31 and 18%, respectively (HOPKINS and TORRES, 1989). Gut contents of *Gaetanus variabilis* in this study (Fig. 5) are consistent to that of HOPKINS and TORRES (1989) in that the most numerous components were silicoflagellates, followed by centric diatoms, tintiniids, and the fragments of metazoans.

LAMPITT *et al.* (1993) observed that *Gaetanus pileatus* ingested marine snow aggregates. Since the marine snow aggregates consist of cyanobacteria and picoplankton, each of which are too small to ingest by these classes of crustaceans, such the feeding mediated by marine snow could be a significant short cut in the food chain pathways (cf. GOWING and WISHNER, 1992). In the present study, non- or little damaged silicoflagellate cells were observed frequently in the gut contents of *Gaetanus variabilis* (Fig. 5). According to TAKAHASHI (1987), the sinking of silicoflagellates is in the form of large aggregates which sink faster than discrete cells, and silicoflagellates generally sink faster than marine snow mediated diatom assemblages. This faster sinking of silicoflagellates is a possible cause for its dominance in the gut content of mesopelagic *G. variabilis*.

4-4. Implications for carbon flux

In our calculation of carbon ingestion by *Gaetanus variabilis* from respiration rates, we assumed assimilation efficiency as 70% (cf. IKEDA and MOTODA, 1978). The assimilation efficiency may be underestimated, since ALVAREZ and MATTHEWS (1975) determined assimilation efficiency of aetideid copepod *Chiridius armatus* to be 90% on *Artemia* and 95% on mixed zooplankton in laboratory experiments. These high assimilation efficiency values are on animal food which contains high organic matter (=low ash). CONOVER (1966) reported a negative relationship between assimilation efficiency and ash contents for copepods fed various types of food. Since we found no evidence of carnivorous feeding in *G. variabilis* from gut content analysis in this study (Fig. 5), the assimilation efficiency of *G. variabilis* cannot be so high as observed for *C. armatus* by ALVAREZ and MATTHEWS (1975).

Primary production (NAGATA, 1998) and CZCS chlorophyll concentrations (KIM *et al.*, 2000) in the Japan Sea have been reported to peak in spring, and the former reaches as high as ca. 1000 mg C m^{-2} day^{-1} (calculated from Table 1 of NAGATA, 1998). Primary production has been estimated in the waters around Yamato Rise, central Japan Sea, in winter is 112 mg C m^{-2} day^{-1} (calculated from Table 1 of

NAGATA, 1998). If we apply the flux-primary production relationship established by SUESS (1980) ; $C_{flux} = C_{prod} / (0.0238 z + 0.212)$, where C_{prod} is primary production (112 mg C m^{-2} day^{-1}) and C_{flux} is carbon flux (mg C m^{-2} day^{-1}) at a given depth (z, m), POC fluxes down to the 500 m depth was estimated to be 9.25 mg C m^{-2} day^{-1}. Compared with the winter primary production data or fluxes at 500 m depth presently available, calculated POC ingestion by *Gaetanus variabilis* (5.03 mg C m^{-2} day^{-1}, Fig. 6) accounts to 4.5% of primary production or 54.4% of POC fluxes at 500 m depth. In the 500–1000 m water column of the southern Japan Sea, the biomass of *G. variabilis* is a small fraction (6–17%) of the total zooplankton (Fig. 3). Nevertheless, this species is only component of suspension feeding copepods (HIRAKAWA *et al.*, 1990; TAKAHASHI and HIRAKAWA, 2001), and provides a significant impact on POC flux in this zone (>500 m) (Fig. 6).

In Greenland Sea, the POC consumption by euchaetid and aetideid copepods in the mesopelagic zones has been calculated as 4–28% of the local primary production (AUEL, 1999). AUEL (1999) has noted that aetideid copepods alone consume more than 40% of carbon supply to the mesopelagic zone. In Swedish fjords, the population of an aetideid copepod *Chiridius armatus* has been evaluated to have the greatest annual mean energy requirement (43% of carnivorous energy flow) among other carnivorous zooplankton (BÅMSTEDT, 1981). Thus, the feeding of the aetideid copepods is estimated to influence the carbon flux in the high latitude seas.

Acknowledgements

Dr. J. M. NAPP kindly reviewed our manuscript. We gratefully acknowledge the officers and crews of R.V. *Kaiyo-Maru* and colleagues of Japan Sea National Fisheries Research Institute for their kind help in field sampling. We thank Dr. H. NAGATA and Dr. N. IGUCHI for providing chlorophyll *a* data and total zooplankton wet mass data, respectively.

References

ALVAREZ, V. and J. B. L. MATTHEWS (1975): Experimental studies on the deep-water pelagic community of Korsfjorden, western Norway. Feeding and assimilation by *Chiridius armatus* (Crustacea, Copepoda). Sarsia, **58**, 67–78.

ARASHKEVICH, Ye. G. (1969): The food and feeding of copepods in the northwestern Pacific. Oceanology, **9**, 695–709.

ATKINSON, A., P. WARD and E. J. MURPHY (1996): Diel periodicity of subantarctic copepods: Relationships between vertical migration, gut fullness and gut evacuation rate. J. Plankton Res., **18**, 1387–1405.

AUEL, H. (1999): The ecology of arctic deep-sea copepods (Euchaetidae and Aetideidae). Aspects of their distribution, trophodynamics and effect on the carbon flux. Ber. Polarforsch., **319**, 1–97.

BÅMSTEDT, U. (1981): Seasonal energy requirements of macrozooplankton from Kosterfjorden, western Sweden. Kieler Meeresforsch. Sonderh., **5**, 140–152.

BESIKTEPE, S. (2001): Diel vertical distribution, and herbivory of copepods in the southwestern part of the Black Sea. J. Mar. Sys., **28**, 281–301.

BIDDANDA, B. and R. BENNER (1997): Major contribution from mesopelagic plankton to heterotrophic metabolism in the upper ocean. Deep-Sea Res. I, **44**, 2069–2085.

CONOVER, R. J. (1966): Factors affecting the assimilation of organic matter by zooplankton and the question of superfluous feeding. Limnol. Oceanogr., **11**, 346–354.

FALKENHAUG, T., K. S. TANDE and T. SEMENOVA (1997): Diel, seasonal and ontogenetic variations in the vertical distributions of four marine copepods. Mar. Ecol. Prog. Ser., **149**, 105–119.

GNAIGER, E. (1983): Calculation of energetic and biochemical equivalents of respiratory oxygen consumption. *In* Polarographic Oxygen Sensors, Gnaiger, E. and H. FORSTNER (eds.), Springer-Verlag, Berlin, pp. 337–345.

GOWING, M. M. and K. F. WISHNER (1986): Trophic relationships of deep-sea calanoid copepods from the benthic boundary layer of the Santa Catalina Basin, California. Deep-Sea Res., **33A**, 939–961.

GOWING, M. M. and K. F. WISHNER (1992): Feeding ecology of benthopelagic zooplankton on an eastern tropical seamount. Mar. Biol., **112**, 451–467.

HARDING, G. C. H. (1974): The food of deep-sea copepods. J. Mar. Biol. Ass. U.K., **54**, 141–155.

HERNÁNDEZ-LEÓN, S. and T. IKEDA (2005): A global assessment of mesozooplankton respiration in the ocean. J. Plankton Res., **27**, 153–158.

HIRAKAWA, K., T. IKEDA and N. KAJIWARA (1990): Vertical distribution of zooplankton in Toyama Bay, southern Japan Sea, with special reference to Copepoda. Bull. Plankton Soc. Japan, **37**, 111–126.

HOPKINS, T. L. and J. J. TORRES (1989): Midwater food webs in the vicinity of a marginal ice zone in the western Weddell Sea. Deep-Sea Res., **36A**, 543–560.

IGUCHI, N., T. IKEDA and A. IMAMURA (1993): Growth and life cycle of a euphausiid crustacean (*Euphausia pacifica* Hansen) in Toyama Bay, southern Japan Sea. Bull. Japan Sea Natl. Fish. Res. Inst., **43**, 69–81 (in Japanese with English abstract).

IKEDA, T. and K. HIRAKAWA (1998): Metabolism and body composition of zooplankton in the cold mesopelagic zone of the southern Japan Sea. Plankton Biol. Ecol., **45**, 31–44.

IKEDA, T. and S. MOTODA (1978): Estimated zooplankton production and their ammonia excretion in the Kuroshio and adjacent seas. Fish. Bull., **76**, 357–367.

IKEDA, T., K. HIRAKAWA and A. IMAMURA (1992): Abundance, population structure and life cycle of a hyperiid amphipod *Themisto japonica* (Bovallius) in Toyama Bay, southern Japan Sea. Bull. Plankton Soc. Japan, **39**, 1–16.

KAERIYAMA, H. and T. IKEDA (2002): Vertical distribution and population structure of the three dominant planktonic ostracods (*Discoconchoecia pseudodiscophora, Orthoconchoecia haddoni* and *Metaconchoecia skogsbergi*) in the Oyashio region, western North Pacific. Plankton Biol. Ecol., **49**, 66–74.

KIM, S. W., S. SAITOH, J. ISHIZAKA, Y. ISODA and M. K ISHINO (2000): Temporal and spatial variability of phytoplankton pigment concentrations in the Japan Sea derived from CZCS images. J. Oceanogr., **56**, 527–538.

LAMPITT, R. S., K. F. WISHNER, C. M. TURLEY and M. V. ANGEL (1993): Marine snow studies in the Northeast Atlantic Ocean: distribution, composition and role as a food source for migrating plankton. Mar. Biol., **116**, 689–702.

MACKIE, G. O. (1985): Midwater macroplankton of British Columbia studied by submersible Pisces IV. J. Plankton Res., **7**, 753–777.

MACLELLAN, D. C. and C. SHIH (1974): Descriptions of copepodite stages of *Chiridius gracilis* Farran, 1908 (Crustacea: Copepoda). J. Fish. Res. Bd. Can., **31**, 13371349.

MATTHEWS, J. B. L. (1964): On the biology of some bottom-living copepods (Aetideidae and Phaennidae) from western Norway. Sarsia, **16**, 1–46.

MAUCHLINE, J. (1991): Some modern concepts in deep-sea pelagic studies: patterns of growth in the different horizons. *In* Marine Biology, Its Accomplishment and Future Prospect, MAUCHLINE, J. and T. NEMOTO (eds.), Hokusen-sha, Tokyo, pp. 107–130.

MAUCHLINE, J. (1998): Advances in Marine Biology Vol. 33, The Biology of Calanoid Copepods. Academic Press, San Diego, 710 pp.

NAGATA, H. (1998): Seasonal changes and vertical distributions of chlorophyll a and primary productivity at the Yamato Rise, central Japan Sea. Plankton Biol. Ecol., **45**, 159–170.

OLSEN, E. M., T. JØRSTAD and S. KAARTVEDT (2000): The feeding strategies of two large marine copepods. J. Plankton Res., **22**, 1513–1528.

PENNAK, R. W. (1943): An effective method of diagramming diurnal movements of zooplankton organisms. Ecology, **24**, 405–407.

RICHTER, C. (1994): Regional and seasonal variability in the vertical distribution of mesozooplankton in the Greenland Sea. Ber. Polarforsch., **154**, 1–87.

SAITO, H. and S. TAGUCHI (1996): Diel feeding behavior of neritic copepods during spring and fall blooms in Akkeshi Bay, eastern coast of Hokkaido, Japan. Mar. Biol., **125**, 97–107.

SCHØYEN, M. and S. KAARTVEDT (2004): Vertical distribution and feeding of the copepod *Chiridius armatus*. Mar. Biol., **145**, 159–165.

SUDO, H. (1987): A note on the Japan Sea Proper Water. Prog. Oceanogr., **17**, 313–336.

SUESS, E. (1980): Particulate organic carbon flux in the oceans-surface productivity and oxygen utilization. Nature, **288**, 260–263.

SUZUKI, R. and T. ISHIMARU (1990): An improved method for the determination of phytoplankton chlorophyll using N,N-dimethyl-formamide. J. Oceanogr. Soc. Japan, **46**, 190–194.

TAKAHASHI, K. (1987): Seasonal fluxes of silicoflagellates and *Actiniscus* in the subarctic Pacific during 1982–1984. J. Mar. Res., **45**, 397–425.

TAKAHASHI, T. and K. HIRAKAWA (2001): Day-night vertical distributions of the winter and spring copepod assemblage in Toyama Bay, southern Japan Sea, with special reference to *Metridia pacifica* and *Oithona atlantica*. Bull. Plankton Soc. Japan, **48**, 1–13 (in Japanese with English abstract).

TSUDA, A., H. SAITO and T. HIROSE (1998): Effect of gut content on the vulnerability of copepods to visual predation. Limnol. Oceanogr., **43**, 1944–1947.

VINOGRADOV, M. E. (1973): New data on the quantitative distribution of plankton in the deep layers of the Sea of Japan. Oceanology, **13**, 904–907.

WEIKERT, H. and R. KOPPELMANN (1993): Vertical structural patterns of deep-living zooplankton in the NE Atlantic, the Levantine Sea and Red Sea: a comparison. Oceanologica Acta, **16**, 163–177.

WIEBE, P. H., A. W. MORTON, A. M. BRADLEY, R. H. BACKUS, J. H. CRADDOCK, V. BARBER, T. J.

COWLES and G. R. FLIERL (1985): New developments in the MOCNESS, an apparatus for sampling zooplankton and micronekton. Mar. Biol., **87**, 313–323.

YAMAGUCHI, A. and T. IKEDA (2000): Vertical distribution, life cycle, and developmental characteristics of the mesopelagic calanoid copepod *Gaidius variabilis* (Aetideidae) in the Oyashio region, western North Pacific Ocean. Mar. Biol., **137**, 99–109.

YAMAGUCHI, A., T. IKEDA, Y. WATANABE and J. ISHIZAKA (2004): Vertical distribution patterns of pelagic copepods as viewed from the predation pressure hypothesis. Zool. Stud., **43**, 475–485.

YAMAGUCHI, A., S. TACHIBANA, K. HIRAKAWA and T. IKEDA (2005): Descriptions of the copepodid stages of the mesopelagic copepod, *Gaetanus variabilis* (Brodsky-1950) (Calanoida, Aetideidae) from the Japan Sea. Crustaceana, **78,** 819–838.

ZENKEVITCH, L. (1963): Biology of the Seas of the U.S.S.R. George Allen and Unwin, London, 955 pp.

Received September 25, 2006
Accepted June 13, 2007

La mer 45 : 59-60, 2007
Société franco-japonaise d'océanographie, Tokyo

資　料

第 45 巻第 1 号掲載欧文論文の和文要旨

Aida Sartimbul[1]・中田英昭[2]・林育夫[3]：対馬暖流沿岸域における最近年の水温変化とその底刺網漁獲量への影響

対馬暖流沿岸域（新潟県粟島）において測定した水温データと粟島付近の底刺網（目合120mm）による漁獲量データ（いずれも1995～2005年）をもとに、最近年の水温変化とその漁獲生物への影響を調べた。粟島沿岸の水温の変化は太平洋振動指数（PDO）と有意な負の相関を示し、1995～1997年と2003年は相対的に低温、1998～2002年と2004年は高温で推移した。1997/1998年の低温から高温への変化は、ENSOなど大規模の気候変化と関連している可能性があるものと推察された。底刺網の漁獲量組成は上記の水温変化に対応して大きく変化し、1995–1998年にはサザエ（*Turbo cornutus*）、1998–2001年にはブリ（*Seriola quiqueradiata*）、続いて2001–2005年にはマダラ（*Gadidae* spp.）が最も卓越した。また、ヒラメ（*Paralichthys olivaceus*）の漁獲量はブリと対照的に低水温年に増加する傾向を示した。最近のサザエ漁獲量の急激な減少は、粟島周辺の個体群が60mm以下の小型を主体としたものに変化していることとよく一致しており、採藻による海藻の漁獲量が同様に減少していることから、利用可能な餌料の減少や岩礁への固着力が低下する冬季の風速（波浪）の増加に起因する可能性が高い。

（[1]長崎大学生産科学研究科（〒852–8521長崎市文教町1–14）[2]長崎大学水産学部（〒852–8521長崎市文教町1–14）[3]水産総合研究センター日本海区水産研究所（〒951–8121新潟市水道町1–5939–22））

小牧加奈絵・川辺正樹：西部北太平洋のメラネシア海盆における上部深層流の構造

降下式音響ドップラー流速計で測定した流速と反射強度のデータを使い、メラネシア海盆ソロモン海膨の北東斜面における2000～3500m深の上部深層流の構造を調べた。この海流は、南極周極流から分岐し、高酸素の上部南極周極水を運びながら北上する深層流である。ソロモン海膨での上部深層流は二つのコアに分かれ、西側と東側の流速コアはそれぞれ水深約3000mと4000mの斜面上に位置していた。東西の流速コアの間に大きな厚みをもつ反流があり、その幅は100km以上に及んでいた。この反流は、水深約3500mの斜面上を流れ、反射強度の非常に高い海水を運んでいた。これらの観測結果は、東カロリン海盆の南端で観測されたことのある東向きの赤道深層流が、反射強度の高い赤道域の海水を運びながら海底斜面に導かれてメラネシア海盆の反流につながることを示唆している。

（東京大学海洋研究所　〒164–8639　東京都中野区南台1–15–1　TEL 03–5351–6420　Fax 03–5351–6418　e-mail kanae@nenv.k.u–tokyo.ac.jp（小牧））

荒川久幸，中山裕美子，森永勤：三宅島周辺浅海域における高濁度水の分布と挙動

三宅島周辺浅海域では，島の南西および北東方向に高濁度水が，その他に黒潮の濁度と同等な清澄海水が，それぞれ分布していた。高濁度水の分布の偏在は島を包含する黒潮の流路の方角，すなわち北東流に起因し，島影効果といえる。また，北東海域の高濁度水の分布形状はパッチ状をしており，2つに分離していた。さらに，パッチの中心部では濁度の値は水深が深くなるほど増大し，水深30－50mで最大値の光束消散係数1.1–1.2m^{-1}を示した。そこに懸濁する粒子は無機含有率が76%と高く，三宅島に由来する陸起源と考えられる。陸上の火山灰は粒径 1–2000 μmの広範囲のサイズの粒子からなる。一方，沿岸近くの海底堆積物は火山物質由来の粘土鉱物smectiteやchloriteなどを含有した。また，粒径60 μm以下のサイズの微細な粒子はほとんど存在しなかった。

以上から，降雨によって火山灰を含む泥濁水が岸から海水中へ流出すると，粒径60 μm以上のサイズの粒子は直ちに沈降かつ海底へ堆積し，それ以下のサイズの粒子は移流により拡散・沈降する。さらに，沖合へ分散した微小懸濁粒子は密度躍層付近で停滞し，高濁度層を形成していると考えられた。

（東京海洋大学海洋科学部海洋環境学科　〒108–8477　東京都港区港南4–5–7）

山口篤[1]*・大塚攻[2]・平川和正[3]・池田勉[1]：冬季の日本海南部における中層性かいあし類*Gaetanus variabilis*の鉛直分布、腸内容物および餌要求量

日本海南部の中層域（200～1000m層）における主要動物プランクトンであるアエティデウス科かいあし類*Gaetanus variabilis*の鉛直分布と腸内容物を1997 年冬季に調査した。*G. variabilis*の大半は水深500～1000mに分布していた。初期発育段階は後期発育段階に比べて深い層に分布していたが、いずれの発育段階においても昼夜の鉛直移動は見られなかった。腸内容物量から判断した摂餌強度は発育段階によって異なったが、昼夜の差は見られなかっ

た。雄成体には終日腸内容物が見られず、これは口器付属肢が雄成体では退化することの反映であると考えられた。腸内容物の観察から*G. variabilis*は主に珪質鞭毛藻、珪藻、有鐘繊毛虫や多細胞動物の破片などを餌とする、粒子食性種であることが明らかになった。呼吸量から*G. variabilis*の餌要求量を推定したところ、本種は0〜1000m水柱内において5.03mg C m^{-2} day^{-1}を摂餌していると考えられた。これは冬季の日本海南部における一次生産量の4.5%、また水深500 m に到達する粒状有機炭素輸送量の54%に相当する値で、日本海南部中層域の物質循環における*G. variabilis*の重要性が明らかになった。

（1: 北海道大学大学院水産科学研究院 2: 広島大学大学院生物圏科学研究科 3: 北海道区水産研究所 *連絡先：〒041−8611 函館市港町3−1−1 北海道大学大学院水産科学研究院海洋生物学講座（プランクトン） e-mail: a-yama@fish.hokudai.ac.jp）

La mer 45: 61, 2007
Société franco-japonaise d'océanographie, Tokyo

学 会 記 事

1. 新入会員

氏名	所属	紹介者
平田　貴文	Plymouth Marine Laboratory Prospect Place, the Hoe, Plymouth, Devon, pL13DH UK	吉田次郎
小林　　豊	千葉県水産総合研究センター 東京湾漁業研究所 千葉県富津市小久保3091	荒川久幸
謝　旭　曜	漁業情報サービスセンター 東京都中央区豊海町4–5 豊海振興ビル6F	長島秀樹
佐川　龍之	東京都中野区南台1–15–1 東京大学海洋研究所	小松輝久

2. 退会・（逝去者含む）
大塚一志　橋詰和慶　山田昌郎　岩田静夫
川名吉一郎

3. 住所変更
長谷川（旧姓石黒）直子
〒522–0002　滋賀県彦根市松原町3612
かんどりニューハイツ103

日仏海洋学会会則

昭和35年4月7日 制定
昭和60年4月27日 改正
平成4年6月1日 改正

第1条 本会は日仏海洋学会と称する。

第2条 本会の目的は日仏海洋および水産学者の連絡を密にし，両国のこの分野の科学の協力を促進するものとする。

第3条 上記の目的を実現するため本会は次の事業を行なう。

⑴ 講演会の開催
⑵ 両国の海洋学および水産学に関する著書，論文等の相互の翻訳，出版および普及
⑶ 両国の海洋，水産機器の技術の導入および普及
⑷ 日仏海洋，水産学者共同の研究およびその成果の論文，映画などによる発表
⑸ 両国間の学者の交流促進
⑹ 日仏海洋，水産学者の相互の親睦のために集会を開くこと
⑺ 会報の発行および出版
⑻ その他本会の目的を達するために必要な事業

第4条 本会には，海洋，水産学の分野に応じて分科会を設けることができる。
分科会は評議員会の決議によって作るものとする。

第5条 本会の事務所は日仏会館（〒150 東京都渋谷区恵比寿3丁目9番25号）に置く。

第6条 本会に地方支部を置くことができる。

第7条 本会会員は本会の目的に賛成し，所定の会費を納めるものとする。
会員は正会員，学生会員および賛助会員とする。

第8条 正会員会費は年額6,000円，学生会員会費は年額4,000円，賛助会員会費は一口年額10,000円とする。

第9条 本会は評議員会によって運営される。
評議員の定数は50名とし，正会員の投票によって選出される。選挙事務は別に定める選出規定による。
会長は評議員会の同意を得て5名までの評議員を追加することができる。
評議員の任期は2年とする。ただし，重任を妨げない。

第10条 評議員はその内より次の役員を選ぶ。ただし，監事は評議員以外からも選ぶことができる。
会長 1名，副会長 2名，幹事 10名，
監事 2名
役員の任期は2年とする。ただし，重任を妨げない。
役員の選出方法は別に定める選出規定による。

第11条 本会に名誉会長，顧問および名誉会員を置くことができる。名誉会長，顧問および名誉会員は評議員会の決議により会長これを委嘱または推薦する。
日仏会館フランス人学長を本会の名誉会長に推薦する。

第12条 会長は本会を代表し，総会および評議員会の議長となる。会長事故あるときは副会長がこれに代わる。
会長，副会長および幹事は幹事会を構成し，本会の庶務，会計，編集，研究発表，渉外などの会務を行う。
監事は本会の会計を監督する。

第13条 年に1回総会を開く。総会では評議員会の報告を開き，会の重要問題を審議する。会員は委任状または通信によって決議に参加することができる。
会長は必要に応じて評議員会の決議を経て臨時総会を招集することができる。

第14条 本会則の変更は総会の決議による。

日仏海洋学会評議員・役員選出規定

1．本規定は日仏海洋学会会則第9条および第10条に基づき本会の評議員および役員の選出方法について規定するものである。

2．評議員は正会員の50名連記無記名投票により選出する。
評議員の選挙事務は庶務幹事が行う。ただし，開票にあたっては本会役員以外の会員2名に立会人を委嘱するものとする。

3．会長は評議員の単記無記名投票により選出する。
会員選挙の事務は庶務幹事が行う。ただし，開票にあたっては本会役員以外の会員2名に立会人を委嘱するものとする。

4．副会長，幹事，および監事は，会長の推薦に基づき評議員会で決定する。

5．本規定の改正は評議員会の議を経て行う。

日仏海洋学会賞規定

1．日仏海洋学会賞（以下「学会賞」という）および日仏海洋学会論文賞（以下「論文賞」という）を本学会に設ける。学会賞は本学会員で，海洋学および水産学において顕著な学術業績を挙げた者のなかから，以下に述べる選考を経て選ばれた者に授ける。
論文賞は若手研究者や大学院生を筆頭著者とする論文を対象とする。原則として選考年度を含む3年（暦年）の間に，本学会誌に発表された論文のなかから，優秀な論文2編以内を選び，その著者（共著者を含む）に，以下に述べる選考を経て授ける。

2．学会賞および論文賞候補者を選考するため学会賞および論文賞受賞候補者推薦委員会（以下「委員会」という）を設ける。

3．委員会の委員は13名とする。
委員は毎年春の評議員会で選出し，委員長は委員の互選により定める。
会長は委員会が必要と認めた場合，評議員の同意を得て2名まで委員を追加委嘱することができる。

4．委員会は学会賞受賞候補者1件および論文賞受賞候補者2件以内を選び，12月末までに選定理由書をつけて会長に報告する。

5．会長は委員会が推薦した各候補者につき無記名投票の形式により評議員会にはかる。
投票数は評議員総数の3分の2以上を必要とし，有効投票のうち4分の3以上の賛成がある場合，これらを各賞受賞者として決定する。

6．授賞式は翌年春の総会において行い，学会賞受賞者には賞状およびメダルを，論文賞受賞者には賞状をそれぞれ贈呈する。

7．本規定の改正は評議員会の議を経て行う。

覚書

1　委員は各専門分野から選出されるように十分配慮すること。

2　受賞者は原則として順次各専門分野にわたるよう十分配慮すること。

3　平成14年度より適用する。

日仏海洋学会誌「うみ」投稿規定

1.「うみ」（欧文誌名 La mer）は日仏海洋学会の機関誌として，和文または欧文により，海洋学および水産学ならびにそれらの関連分野の研究成果を発表する学術雑誌であり，同時に研究者間の情報交換の役割をもつことを目的としている。

2.「うみ」は，原則として年 4 回発行され，投稿（依頼原稿を含む）による原著論文，原著短報，総説，学術資料，書評その他を，編集委員会の審査により掲載する。これらの著作権は日仏海洋学会に帰属する。

3. 投稿は日仏海洋学会会員，および日仏海洋学会正会員に準ずる非会員からとする。共著者に会員を含む場合は会員からの投稿とみなす。

4. 用語は日，仏，英 3 カ国語のいずれかとする。ただし，表および図の説明の用語は仏文または英文に限る。原著論文には約200語の英文または仏文の要旨を別紙として必ず添える。なお，欧文論文には約500字の和文要旨も添える。ただし，日本語圏外からの投稿の和文要旨については編集委員会の責任とする。

5. 原稿はすべてワードプロセッサを用いて作成し，本文・原図とも 2 通（正，副各 1 通）ずつとする。副本は複写でよい。本文原稿はすべてA4判とし，白紙にダブル・スペース（和文ワープロでは相当間隔）で記入する。表原稿および図の説明原稿は本文原稿とは別紙とする。

6. 投稿原稿の体裁形式は「うみ」最近号掲載論文のそれに従う。著者名は略記しない。記号略号の表記は編集委員会の基準に従う。引用文献の表示形式は，雑誌論文，単行本分載論文（単行本の一部引用も含む），単行本などの別による基準に従う。

7. 原図は版下用として鮮明で，縮尺（版幅または1/2版幅）に耐えられるものとする。

8. 初稿に限り著者の校正を受ける。

9. すべての投稿原稿について，1 編あたり 5 万円の論文掲載料を申し受けます。

10. 会員に対しては10印刷ページまでの掲載を無料とする。会員の投稿で上記限度を超える分および非会員投稿（依頼原稿を除く）の印刷実費はすべて著者負担（1 万円/ページ）とする。ただし，カラー印刷を含む場合には，別に所定の費用（1 ページあたり9万円）を著者（会員，非会員とも）負担とする。

11. すべての投稿原稿について，1 編あたり別刷り50部を無料で請求できる。50部を超える分は請求により50部単位で有料で作製される。別刷り請求用紙は初稿校正と同時に送付される。

12. 原稿の送り先は下記の通りとする。なお著者（共著の場合は代表者）連絡先のe-mailアドレス並びにFAX番号を付けることとする。

〒108–8477 東京都港区港南4–5–7
東京海洋大学海洋科学部海洋環境学科（吉田 次郎気付）
日仏海洋学会編集委員会
e-mail：jiroy@s.kaiyodai.ac.jp

執 筆 要 領

1. 原稿

⑴ 和文原稿の場合：ワードプロセッサを使用し，A4版の用紙におよそ横30字，縦25行を目安に作成すること。

⑵ 欧文原稿の場合：ワードプロセッサを使用し，A4版の用紙にダブルスペース25行でタイプし，十分な英文添削または仏文添削を経て提出すること。

⑶ 和文原稿，欧文原稿いずれの場合も，要旨，表原稿および図版説明原稿はそれぞれ本文原稿とは別紙とする。

⑷ 最終原稿提出の際に，印刷原稿とともに原稿，表，図版が保存されたフロッピーディスク，CD-R/RW，MO等での提出を依頼する。この場合，原稿はMicrosoft WORD，Just System 一太郎，PDFの原稿のみに限る。また，表，図版はこれら原稿ファイルの中に取り込むか，bmp，jpg等の一般的な画像ファイルに保存したものに限る。なお，電子媒体は返却しない。

2. 原稿記載の順序

⑴ 原著（和文原稿）：原稿の第１ページ目に表題，著者名，研究の行われた所属機関，所在地，郵便番号を和文と英文で記載する。研究終了後所属機関が変わった場合は現所属機関も記載する。連絡先（共著の場合は連絡先とする著者を明示する）の住所，電話番号，ファックス番号，E-mailアドレスも記す。最後にキーワード（４語以内），ランニングヘッドを英文で記載すること。第２ページ目に欧文要旨（欧文表題，著者名を含む）を200語以内で記す。本文は第３ページ目から，「緒言」「資料」「結果」「考察」「謝辞」「文献」「図版の説明」などの章立てあるいは項目で順に記載する。基本的には最近号掲載論文の体裁形式を参考にして投稿原稿を作成すること。原稿には通しのページ番号を記入すること。

⑵ 原著（欧文原稿）：原稿の第１ページ目に表題，著者名，研究の行われた所属機関，所在地，郵便番号を記載する。研究終了後所属機関が変わった場合は現所属機関も記載する。最後にキーワード（４語以内），ランニングヘッドを記載すること。第2ページ目に欧文要旨（欧文表題，著者名を含む）を200語以内で記す。本文は第３ページ目からとする。「Introduction」「Data」「Results」「Discussion」「Acknowledgement」「References」「Figure Caption」などの章立てで順に記載する。基本的には投稿原稿の体裁形式は最近号掲載論文を参考にして作成すること。最終ページに和文の表題，著者名，連絡先著者住所，電話番号，ファックス番号，E-mailアドレスおよび約500字以内の和文要旨を添える。原稿には通しのページ番号を記入すること。

⑶ 原著短報，総説：和文ならびに欧文原稿とも原著論文に準ずる。

⑷ 学術資料，書評：特に記載に関する規定はないが，すでに掲載されたものを参考にすること。

3. 活字の指定

原稿での活字は10.5pt～12ptを目安に設定し，英数字は半角フォントを用いること。学名はイタリック，和文原稿での動植物名はカタカナとすること。句読点は（。）および（,）とするが，文献リストでは（.）および（,）を用いること。章節の題目，謝辞，文献などの項目はボールドまたはゴシックとする。

4. 文献

文献は本文および図表に引用されたもののすべてを記載しなければならない。和文論文，欧文論文共に筆頭著者のアルファベット順（同一著者については，単著，共著の順とし，それぞれ発表年の古い順）にまとめ，以下の例に従って記載する。

⑴ 論文の場合

有賀祐勝,前川行幸,横浜康継（1996）：下田湾におけるアラメ群落構造の経年変化.うみ，**34**，45–52.

YANAGI, T. T. TAKAO and A. MORIMOTO (1997): Co-tidal and co-range charts in the South China Sea derived from satellite altimetry data. La mer, **35**, 85–93.

⑵ 単行本分載論文（単行本の一部引用の場合）

村野正昭（1974）：あみ類と近底層プランクトン.海洋学講座10　海洋プランクトン（丸茂隆三編），東京大学出版会，東京，p.111–128.

WYNNE, M. J. (1981): Pheaophyta: Morphology and classification. *In* the Biology of Seaweeds. LOBBAN, C. S. and M. J. WYNNE (eds.), Blackwell Science, Oxford, p.52–85.

⑶ 単行本の場合

柳　哲雄（1989）：岸海洋学―海の中でものはどう動くか―. 恒星社厚生閣，東京，154pp.

SVERDRUP, H. U., M. W. JOHNSON and R. H. FLEMING (1942): The Oceans: Their Physics, Chemistry and General Biology. Prentice-Hall, Englewood Cliffs, New York, 1087pp.

⑷ 本文中での文献の引用

本文中での文献の引用方法はすでに発行された雑誌を参考にするが，基本的には次の形式に従う。

①GREVE and PARSONS(1977)

②（AVIAN and SANDRIN, 1988），

③YANAGI *et al.*（1997）は……（３名以上の共著の場合）

④……示されている（例えば，YANAGI *et al.*, 1997）（３名以上の共著の場合）

5. 図，表および写真

⑴ 図，表および写真とその説明はすべて英文または仏文を用いる。

⑵ 図，表はそのまま写真製版用の草稿となるような明瞭なもので，A4版の上質紙に作製したもの（写真は，正原稿についてもオリジナルとは別にA4版の用紙にコピーしておくことが望ましい）のみを受け付ける。カラー図を希望する場合はその旨明記する。この場合，別に所定の費用を著者負担とする。

⑶ 写真は光沢平滑印画紙に鮮明に焼き付けたものを受け付ける。カラー写真の印刷を希望する場合はその旨明記する。この場合，別に所定の費用を著者負担とする。

⑷ 図，表および写真は刷り上がり時に最大横が14cm，縦が20cm（説明文を含む）以内であることを考慮して作製すること。

⑸ 図（写真を含む）には，Fig. 1, Fig. 2, ……のように通し番号をつけ，一つの図中に複数の図を含む場合はFig. 3（a), Fig. 3（b), ……のように指定する。本文中での引用は和文原稿の場合も 「Fig. 1にみられるように……」のようにすること。

⑹ 表には，表題の次（表の上のスペース）に説明をつけ，表ごとに別紙とし，Table 1, Table 2,.....のように通し番号をつけること。

⑺ 図，表および写真は1枚ごとに著者名，通し番号をつけること。また，本文中での挿入箇所を最終提出原稿の該当箇所右欄外に朱書きすること。

⑻ 図，写真の説明は別紙にまとめること。

⑼ 地図にはかならず方位と縮尺または緯度，経度を入れること。

6. 単位系

原則としてSI単位を用いること。塩分は実用塩分単位（Practical Salinity Unit： psuまたは PSU）を用いる場合は単位なしとする。

Information for Contributors

1. The scientific journal,"La mer," the official organ of Japanese-French Oceanographic Society (JFOS), is published quarterly. "La mer" is open to all researchers in oceanography, fisheries and related sciences in the world. The journal is devoted to the publication of original articles, short contributions, reviews, book reviews, and information in oceanography, fisheries and related fields. Submission of a manuscript will imply that it has not been published or accepted for publication elsewhere. The editorial board decides the acceptance of the manuscript on the basis of peer-reviews and is responsible for its final editing. The Society reserves the copyright of all articles in the Journal.
2. *Submission*: Manuscripts must be written in French, English or Japanese. Authors are requested to submit their original manuscript and figures with one copy to the Editor in chief.
3. *Publication charges*: Each accepted article is charged 50,000 yen for publication. For members, there will be no page charge for less than ten printed pages, and 10,000 yen will be charged per page for the excess, except for color pages. For nonmembers there is a publication charge of 10,000 yen per printed page except for color pages. Color illustrations will be provided at cost.
4. *Proofs and reprints*: Fifty reprints of each article will be provided free of charge. Additional reprints can be provided in blocks of 50 copies. Proofs will be sent to the corresponding author. A reprint order form will be sent with the proofs.
5. Manuscripts should be sent to

   Editor in Chief of "La mer"
   Jiro Yoshida
   Department of Ocean Sciences
   Tokyo University of Marine Science and Technology
   Konan, Minato-Ku, Tokyo, Japan 108–8477.
   jiroy@s.kaiyodai.ac.jp

Manuscript Preparation

1. General
   1) Manuscripts must be typed with double-spacing on one side of A4 size white paper with wide margins.
   2) Figures, tables, and figure captions should be prepared separate from the main text.
   3) Authors should submit an electronic copy of their paper with the final version of the manuscript. The electronic copy should match the hardcopy exactly and should be stored in CD-R/W or FD. MS-WORD (Windows) and PDF formats are accepted.
2. Details
   1) The first page of the manuscript should include the title, author's full names and affiliations including Fax numbers and E-mail addresses. The corresponding author should be designated. Key words (up to four words) and running head should be written at the bottom of the page.
   2) An abstract of 200 words or less in English or French should be on the second page.
   3) The main text should start on the third page. Please adhere to the following order of presentation: main text, acknowledgements, appendices, references, figure captions, tables. All pages except the first page must be numbered in sequence.
   4) Mathematical formulae should be written with a wide space above and below each line. Syst e me International (SI) units and symbols are preferred.
   5) All references quoted in the text should be listed separately in alphabetical order according to the first author's last name. Citations must be complete according to the following examples:

   Article: YANAGI, T. T. TAKAO and A.MORIMOTO (1997): Co-tidal and co-range charts in the South China Sea

derived from satellite altimetry data. La mer, **35**, 85–93.

Chapter: WYNNE, M.J. (1981): Pheaophyta: Morphology and classification. *In* the Biology of Seaweeds. LOBBAN, C.S. and M. J. WYNNE (eds.), Blackwell Science, Oxford, p. 52–85.

Book: SVERDRUP, H. U., M. W. JOHNSON and R. H. FLEMING (1942): The Oceans: Their Physics, Chemistry and General Biology. Prentice-Hall, Englewood Cliffs, New York, 1087pp.

6) *Illustrations*: All illustrations should be provided in camera-ready form, suitable for reproduction (which may include reduction) without retouching. Photographs, charts and diagrams are all to be referred to as "Fig(s)." and should be numbered consecutively in the order to which they are referred. They should accompany the manuscript, but should not be included within the text. All figures should be clearly marked on the back with the figure number and the author's name. All figures are to have a caption. Captions should be supplied on a separate sheet.

7) *Photographs*: Original photographs must be supplied as they are to be reproduced (e.g. black and white or color). If necessary, a scale should be marked on the photograph. Please note that photocopies of photographs are not acceptable. Half-tone illustrations should be kept to a minimum.

8) *Color illustrations*: The printing cost of color illustrations must be borne by authors or their institution. Authors will receive information about the cost on acceptance of the manuscript.

9) *Tables*: Tables should be numbered consecutively and given a suitable caption on top and each table typed on a separate sheet.

賛 助 会 員

アレック電子株式会社	神戸市西区井吹台東町７－２－３
株式会社 イーエムエス	神戸市中央区東川崎町１－３－３ 神戸ハーバランドセンタービル　13F
有限会社 英和出版印刷	文京区千駄木４－20－６
株式会社 内田老鶴圃 内田　悟	文京区大塚３－34－３
財団法人 海洋生物環境研究所	千代田区神田神保町３－29　帝国書院ビル５Ｆ
株式会社 川合海苔店	大田区大森本町２－31－８
ケー・エンジニアリング株式会社	台東区浅草橋５－14－10
いであ株式会社	世田谷区駒沢３－15－１
三洋測器株式会社	渋谷区恵比須南１－２－８
株式会社高岡屋	台東区上野６－７－22
テラ株式会社	文京区湯島４－１－13－402
渡邊機開工業株式会社	愛知県渥美郡田原町神戸大坪230

IDEA Consultants, Inc.

社会基盤の形成と環境保全の総合コンサルタント

当社は、新しい総合コンサルタントとして、社会基盤整備や環境保全にかかわる企画、調査、分析、予測評価から計画・設計、維持・管理に至るすべての段階において、お客様のニーズに常に最適で付加価値の高いサービスを提供しております。
社名の「いであ」(I-D-E-A)は、
「**I**nfrastructure(社会基盤整備)」
「**D**isaster(災害)」
「**E**nvironment(環境)」
「**A**menity(快適性)」
の頭文字を合わせたもので、業務分野を表現しており、安全・安心で快適な社会の持続的発展と、健全で恵み豊かな環境の保全と継承を支えることを象徴しています。

国土環境(株)と日本建設コンサルタント(株)は2006年6月1日に合併しました。

業務内容

■河川・海岸の整備・保全計画及び構造物の設計・管理
■道路・交通・都市の計画・設計・管理
■橋梁の設計・管理
■自然及び人工災害に係る事前・事後対策調査、計画・設計
■環境に関する現況調査、予測、解析
■環境アセスメント(環境影響評価)、環境保全対策
■環境に関する生物の調査、分類、同定、実験、解析、育成
■生物生息環境の保全、再生、創造
■理化学分析・試験(環境質)、環境リスクの評価・管理
■気象情報配信とバイオウェザーサービス
■海外での環境協力事業


フクジュソウ(絶滅危惧種)【植物調査】


信濃川やすらぎ堤(新潟県)【親水型堤防護岸設計】


せせらぎの道(神奈川県)【景観道路計画・設計】


周南大橋(錦ニールセンローゼ橋)【臨港道路設計】


クマタカ(絶滅危惧種)【猛禽類調査】


ヒヌマイトトンボ(絶滅危惧種)【生息環境の研究・保全対策】

人と地球の未来のために ──

いであ株式会社

http://ideacon.jp/

本社	〒154-8585	東京都世田谷区駒沢 3-15-1	電話:03-4544-7600
東京本部	〒105-0004	東京都港区新橋 6-17-19(新御成門ビル)	電話:03-5405-3700
環境創造研究所	〒421-0212	静岡県志太郡大井川町利右衛門 1334-5	電話:054-622-9551
国土環境研究所	〒224-0025	神奈川県横浜市都筑区早渕 2-2-2	電話:045-593-7600
東京支社	〒105-0004	東京都港区新橋 6-17-19(新御成門ビル)	電話:03-5405-8150
大阪支社	〒553-0003	大阪府大阪市福島区福島 7-20-1(KM西梅田ビル)	電話:06-6453-3033
大阪支社 環境コンサルタント事業部	〒550-0002	大阪府大阪市西区江戸堀 3-2-23	電話:06-6448-2551
札幌支店	〒060-0062	北海道札幌市中央区南二条西 9-1-2(サンケン札幌ビル)	電話:011-272-2882
東北支店	〒980-6016	宮城県仙台市青葉区中央 4-6-1(仙台中央ビル)	電話:022-263-6744
名古屋支店	〒460-0002	愛知県名古屋市中区丸の内 1-4-12(アレックスビル)	電話:052-211-4884
名古屋支店 環境コンサルタント事業部	〒455-0032	愛知県名古屋市港区入船 1-7-15	電話:052-654-2551
広島支店	〒730-0051	広島県広島市中区大手町 2-1-1(広島商中日生ビル7F)	電話:082-545-8500
九州支店	〒812-0055	福岡県福岡市東区東浜 1-5-12	電話:092-641-7878
沖縄支店	〒900-0003	沖縄県那覇市安謝 2-6-19	電話:098-868-8884
事務所	北陸,四国		

青森,盛岡,秋田,山形,福島,新潟,茨城,千葉,北関東,相模原,神奈川,静岡,長野,富山,金沢,岐阜,三重,福井,滋賀,奈良,

日仏海洋学会入会申込書

（正会員・学生会員）

	年度より入会	年　月　日申込
氏　名 ローマ字		年　月　日　生
住　所　〒 勤務先　機関名 電　話　E-mail:		
自　宅　住　所　〒 電　話　E-mail:		
紹介会員氏名		
送付金額　円	送金方法	
会誌の送り先（希望する方に○をつける）	勤務先　自　宅	

（以下は学会事務局用）

受付	名簿 原簿	会費 原簿	あて名 カード	学会 記事

入会申込書送付先：〒150-0013 東京都渋谷区恵比寿 3-9-25

（財）日仏会館内

日 仏 海 洋 学 会

郵便振替番号：00150−7−96503